Master's thesis

NTNU
Norwegian University of Science and Technology
Faculty of Engineering
Department of Structural Engineering

Herman Hagen Horvei

Analysis of Bolted Beam-to-Column Joints Subjected to Major and Minor Axis Bending

Master's thesis in Civil and Environmental Engineering
Supervisor: Arild Holm Clausen
Co-supervisor: Arne Aalberg
June 2022

NTNU
Kunnskap for en bedre verden

Herman Hagen Horvei

Analysis of Bolted Beam-to-Column Joints Subjected to Major and Minor Axis Bending

Master's thesis in Civil and Environmental Engineering
Supervisor: Arild Holm Clausen
Co-supervisor: Arne Aalberg
June 2022

Norwegian University of Science and Technology
Faculty of Engineering
Department of Structural Engineering

NTNU
Norwegian University of
Science and Technology

Department of Structural Engineering
Faculty of Engineering
NTNU- Norwegian University of Science and Technology

ACCESSIBILITY

OPEN

MASTER THESIS 2022

SUBJECT AREA:	DATE:	NO. OF PAGES:
Steel Structures	11.06.2022	26+57

TITLE:

Analysis of Bolted Beam-to-Column Joints Subjected to Major and Minor Axis Bending

Analyse av boltede bjelke-søyle knutepunkt påkjent av bøyning om sterk og svak akse

BY:

Herman Hagen Horvei

SUMMARY:
Applying finite element analysis in the design of steel structures has emerged as a faster, simpler, and more accurate alternative than designing according to Eurocode 3. IDEA StatiCa is an example of software dedicated to the design of steel members and joints. It employs finite element analysis combined with design checks according to Eurocode 3 to analyze and verify structures. To offer short computation time, the software has adopted some simplifications, which might affect its accuracy. This thesis aims to explore IDEA StatiCa's possibilities and limitations for the design of steel joints.

Three different types of bolted beam-to-column joints with open I and H-sections are investigated. Most of the thesis focus on major axis joints, where the beam is subjected to a combination of bending moment (about the major axis) and axial force. Additionally, minor axis joints are explored, where either the beam or the column is subjected to bending moment about its weak axis. Finite element models of the joints were assembled in Abaqus and validated against experimental results before models in IDEA StatiCa were verified against the Abaqus models and manual calculations based on Eurocode 3 and relevant literature. Parametric studies were carried out to explore different geometric configurations and load conditions.

It was found that IDEA StatiCa predicts a lower moment resistance than Abaqus for all cases considered. However, in general, it predicted a higher resistance than Eurocode 3. The cause for the discrepancies can, to a large extent, be attributed to IDEA StatiCa's neglect of geometric imperfections and geometric nonlinearity. The calculated rotational stiffness also shows some discrepancies, which can mainly be ascribed to the way IDEA StatiCa defines the initial stiffness (the secant stiffness at 2/3 of the moment resistance). Despite these discrepancies, it was found that IDEA StatiCa is a reliable and convenient design tool, that facilitates simple design of steel joints.

RESPONSIBLE TEACHER: Arild Holm Clausen

SUPERVISOR(S): Arild Holm Clausen, Arne Aalberg

CARRIED OUT AT: The Department of Structural Engineering, NTNU

Preface

This master thesis is the final work of my Master's degree at the Norwegian University of Science and Technology (NTNU). The thesis is written for the Department of Structural Engineering in the spring of 2022.

I want to extend sincere gratitude towards my supervisor Arild H. Clausen at NTNU, and my co-supervisor Erik L. Grimsmo at Aas-Jakobsen. Thank you for all the valuable expertise and discussions. I also want to thank Arne Aalberg for occasionally joining my guidance meetings and providing insight and wisdom. Lastly, I want to thank Torodd Berstad, who assisted me with technical support throughout the semester.

Herman Hagen Horvei

Oslo, June 2022

Abstract

Applying finite element analysis in the design of steel structures has emerged as a faster, simpler, and more accurate alternative than designing according to Eurocode 3. IDEA StatiCa is an example of software dedicated to the design of steel members and joints. It employs finite element analysis combined with design checks according to Eurocode 3 to analyze and verify structures. To offer short computation time, the software has adopted some simplifications, which might affect its accuracy. This thesis aims to explore IDEA StatiCa's possibilities and limitations for the design of steel joints.

Three different types of bolted beam-to-column joints with open I and H-sections are investigated. Most of the thesis focus on major axis joints, where the beam is subjected to a combination of bending moment (about the major axis) and axial force. Additionally, minor axis joints are explored, where either the beam or the column is subjected to bending moment about its weak axis. Finite element models of the joints were assembled in Abaqus and validated against experimental results before models in IDEA StatiCa were verified against the Abaqus models and manual calculations based on Eurocode 3 and relevant literature. Parametric studies were carried out to explore different geometric configurations and load conditions.

It was found that IDEA StatiCa predicts a lower moment resistance than Abaqus for all cases considered. However, in general, it predicted a higher resistance than Eurocode 3. The cause for the discrepancies can, to a large extent, be attributed to IDEA StatiCa's neglect of geometric imperfections and geometric nonlinearity. The calculated rotational stiffness also shows some discrepancies, which can mainly be ascribed to the way IDEA StatiCa defines the initial stiffness (the secant stiffness at 2/3 of the moment resistance). Despite these discrepancies, it was found that IDEA StatiCa is a reliable and convenient design tool, that facilitates simple design of steel joints.

Sammendrag

Anvendelse av elementmetoden for dimensjonering av stålkonstruksjoner har vokst frem som et raskere, enklere og mer nøyaktig alternativ enn å dimensjonere i henhold til Eurocode 3. IDEA StatiCa er et eksempel på programvare dedikert til dimensjonering av stålkonstruksjoner. Den anvender elementmetoden for å analysere konstruksjonen, og kontrollerer resultatene opp mot Eurocode 3. For å tilby raske beregninger har programvaren implementert forenklinger som kan påvirke nøyaktigheten. Målet med denne oppgaven er å utforske IDEA StatiCas muligheter og begrensninger for dimensjonering av knutepunkter i stål.

Tre forskjellige typer av boltede bjelke-søyle knutepunkter med åpne I- og H-tverrsnitt undersøkes. Mesteparten av oppgaven fokuserer på knutepunkt der bjelken utsettes for en kombinasjon av bøyemoment om bjelkens sterke akse og aksialkraft. Knutepunkt der enten bjelken eller søylen utsettes for bøyemoment om sin svake akse blir også undersøkt. Elementmodeller av knutepunktene i Abaqus ble først validert mot eksperimentelle resultater, før modeller i IDEA StatiCa ble verifisert mot Abaqus-modellene og håndberegninger basert på Eurocode 3 og relevant litteratur. I tillegg til dette ble det utført parameterstudier for å utforske flere geometrikonfigurasjoner og lastbetingelser.

Resultatene viser at IDEA StatiCa beregner en lavere momentkapasitet enn Abaqus for alle betraktede tilfeller, men generelt sett en høyere kapasitet enn Eurocode 3. Årsaken til avvikene kan i stor grad tilskrives neglisjeringen av geometriske imperfeksjoner og geometrisk ikke-linearitet. Beregnet rotasjonsstivhet viser også avvik, men dette kan i hovedsak tilskrives måten IDEA StatiCa definerer rotasjonsstivheten på (sekantstivheten ved 2/3 av momentkapasitet). Til tross for avvikene, konkluderes det med at IDEA StatiCa er et pålitelig og praktisk dimensjoneringsverktøy, som fasiliter ukomplisert dimensjonering av knutepunkt i stål.

Table of contents

1 Introduction

Steel has been a popular building material for decades due to its high strength and stiffness, low weight to strength ratio, high ductility, fair price, and easy assembly. Most steel structures generally consist of beams and columns joined together with different types of connections, and the main categories for steel joints are bolted and welded joints. Where welded joints offer higher stiffness and strength due to the members being more rigidly connected, bolted joints are easier to assemble and generally offer higher ductility and rotational capacity. The latter is an important aspect when designing for earthquakes and the collapse of structures.

The design of steel structures is governed by Eurocode 3, which is divided into several parts covering different topics. The most relevant for this thesis are NS-EN 1993-1-1 [1], which covers the general rules for the design of steel structures in buildings; NS-EN 1993-1-5 [2], which covers plated steel structures; and NS-EN 1993-1-8 [3], which covers the design of joints. As Eurocode 3 is based on simplified analytical models, the standard is in many cases shown to be highly conservative when designing joints [4, 5]. This can result in an underestimation of the ultimate capacity of up to 45 % [4]. Applying Eurocode 3 as a basis for design can, in many cases, result in uneconomical structures with relatively low utilization. Furthermore, the process of designing joints based on Eurocode 3 can be quite cumbersome and time-consuming, and more complex geometries are not covered by the standard. Using finite element analysis (FEA) software has therefore become popular among structural engineers, as it in many cases offers a better prediction of structural behavior and is significantly less time-consuming.

1.1 Problem description

IDEA StatiCa is an engineering software dedicated to the design of structural components, including steel joints. The software allows for the calculation of stresses and strains for a user-defined steel joint and checks stresses, strains, and forces according to Eurocode 3. It offers a simple interface, relatively fast calculations, as well as documentation of the design process. The developer of the software has conducted several numerical experiments, and the software coincides well with calculations according to Eurocode 3 [6]. To enable fast calculations, some simplifications are adopted, which might limit the software's accuracy compared to more complex finite element models and physical experiments.

This thesis aims to explore the limitations of the software IDEA StatiCa, and its ability to accurately predict the behavior of steel joints subjected to external forces. The software is verified numerically against a wide variety of benchmark tests, but it is uncertain how accurately it predicts the behavior of more complex geometries and load situations. As the software is developed for design of structures, it is expected that the results will show discrepancies compared to physical experiments. However, it is of high interest to determine if the results are on the safe

side of Eurocode 3 - and if not, if it is on the safe side of real-world behavior and more complex finite element models. Abaqus is an example of a more complex general-purpose FEA software, which will be utilized in this thesis. It has very few limitations and is highly suitable to use in the verification process of IDEA StatiCa.

1.1.1 Joint configurations

The thesis is delimited to explore how IDEA StatiCa predicts the behavior of three different types of bolted beam-to-column joint configurations composed of open I and H-sections. These three joint configurations are shown in Figure 1.1. The first joint (Figure 1.1a) is a typical strong axis joint, where both the column and the beam are subjected to bending about its strong/major axis. This joint configuration is typical in frame structures, where it may be subjected to a combination of bending moment and axial force. Joints subjected to bending moment and axial force is a topic that is only briefly covered by Eurocode 3, which makes it a highly relevant problem to be analyzed by IDEA StatiCa. Major axis joints subjected to combined bending and axial force will therefore be the main focus in this thesis. Other joint configurations not covered by Eurocode 3 are minor axis bolted beam-to-column joints, where either the beam or the column is subjected to bending about its weak axis, as shown in Figure 1.1b and 1.1c, respectively. These joint configurations are also relevant problems to be analyzed in IDEA StatiCa, and will therefore be briefly investigated in this thesis. The nomenclature *Major axis joint*, *Beam minor axis joint*, and *Column minor axis joint*, with reference to Figure 1.1a, 1.1b and 1.1c, respectively, will be adopted in this thesis.

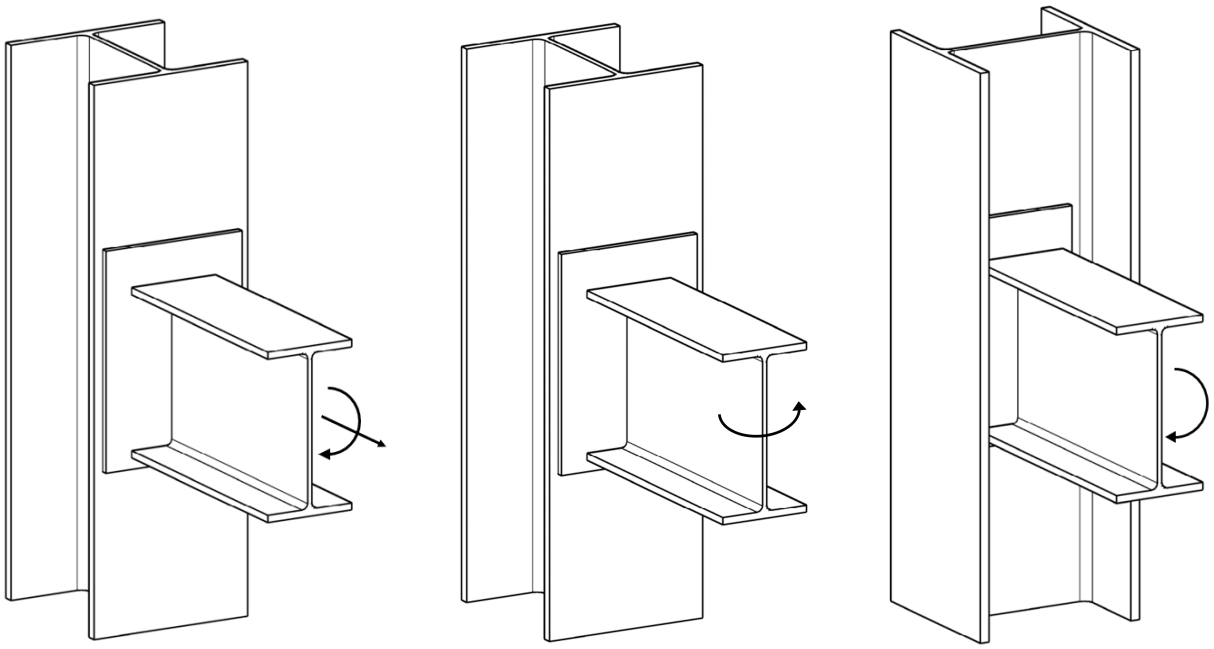

(a) Major axis joint **(b)** Beam minor axis joint **(c)** Column minor axis joint

Figure 1.1: Different bolted beam-to-column joint configurations

1.1.2 Validation and verification

As the software is intended for design purposes, where the exact material data is unknown, the software has adopted a simplified material model based on characteristic values of the material. Hence, the results of the analysis conducted in IDEA StatiCa will possibly show large

discrepancies compared to experimental data where the material behavior is more complex. For this reason, it is of lesser interest to compare the results from IDEA StatiCa directly to experimental data, as the results are not expected to be identical. Therefore, the thesis will include both *verification* and *validation* to evaluate the software. *Model verification* is the process of determining the degree to which a computerized model accurately represents a conceptual or analytical model, while *model validation* is the process of determining the degree to which a computerized model accurately represents real-world behavior, i.e. experimental results [7, 8]. Or stated simpler: verification determines if the model *solves the equations correctly*, while validation determines if the model *solves the correct equations* [9].

In this thesis, more complex numerical models in the finite element software Abaqus will be validated against physical experiments, to generate robust and accurate models of physical problems. The models generated in Abaqus will be moderately simplified, before being used to verify the models in IDEA StatiCa. This ensures that the results are comparable, and it is possible to determine to what extent IDEA StatiCa's simplifications affect its accuracy. The main characteristics of a beam-to-column joint, and the characteristics that will be considered in this thesis, are:

- *Ultimate moment resistance*, which is used to control the joint in the ultimate limit state. This is probably the most important characteristic to determine in an analysis.
- *Initial rotational stiffness*, which is used to determine whether a joint is to be considered rigid, semi-rigid, or pinned in a global analysis.
- *Rotational capacity*, which is relevant for collapse analysis, plastic analysis, and earthquake exposed structures.

Considering that IDEA StatiCa is a design software intended to replace manual calculations based on design codes, such as Eurocode 3, the results from IDEA StatiCa will also be compared to Eurocode 3 calculations. In this way, it is possible to establish how the software compares to governing design codes.

1.1.3 Organization

The remainder of the thesis is organized into four chapters. Chapter 2 includes relevant theory and information about IDEA StatiCa and finite element analysis in Abaqus in general. Additionally, relevant parts of Eurocode 3, and literature on topics not covered by Eurocode 3, will be discussed. Chapter 3 covers major axis joints, and will be the main chapter of this thesis. Chapter 4 covers beam and column minor axis joints and is a continuation of the previous chapter. Chapter 3 and 4 are organized similarly, and both include validation of numerical models, verification of IDEA StatiCa against Abaqus and Eurocode 3/component method, and a parametric study. Chapter 5 concludes the thesis and suggests topics for further work.

2 Theory

This chapter will cover the theoretical background of IDEA StatiCa, as well as selected topics on finite element analysis with Abaqus, to better understand how the verification and validation are carried out. Furthermore, the relevant topics from NS-EN 1993-1-8 [3] will be briefly discussed. However, since not all topics needed for the determination of capacity and stiffness are covered by the standard, relevant theory from literature that compliments Eurocode 3 will be addressed.

2.1 IDEA StatiCa

The concept of *Component-based finite element method* (CBFEM) was introduced by the developers of IDEA StatiCa [10, 11]. CBFEM is a method for design of steel joints and members with incorporated design checks according to relevant design codes. It is intended to replace *component method* calculations, which are manual calculations based on design codes and other literature. An example of analysis in IDEA StatiCa is shown in Figure 2.1

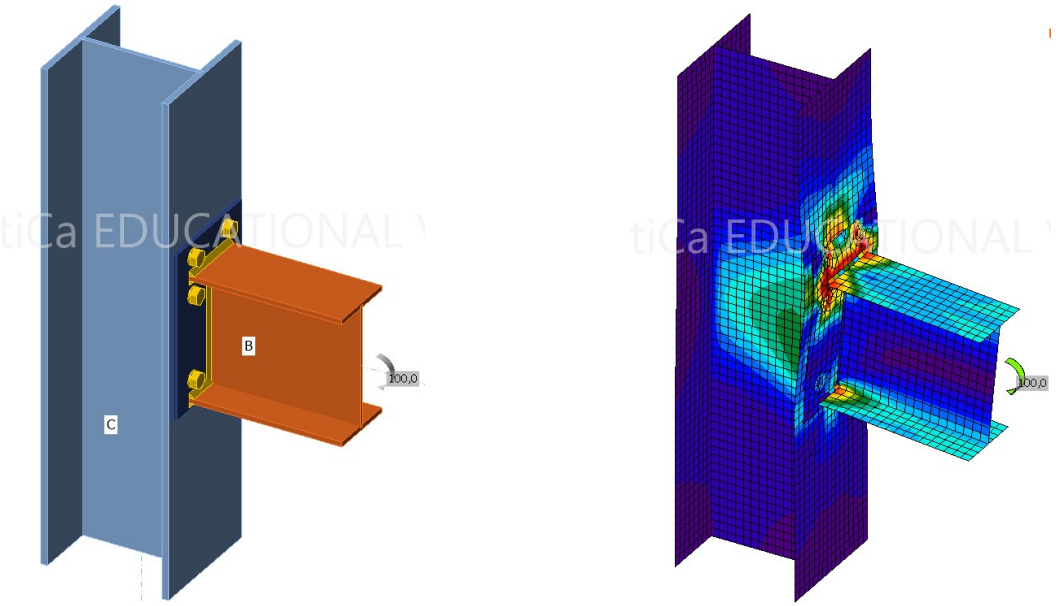

(a) Geometric model

(b) Contour plot of equivalent stresses on the deformed shape

Figure 2.1: Design in IDEA StatiCa

2.1.1 Element type

The software employs the finite element method to analyze the structure. The finite element model is discretized using four-node shell elements with six degrees of freedom per node. The

element's membrane behavior is based on the work of Ibrahimbegovic et al. [12]. They proposed a quadrilateral element with independent rotation and displacement fields interpolated linearly, resulting in an element with drilling degrees of freedom. The out-of-plane flexural behavior is based on the works of Dvorkin et al. [13], who proposed a shear flexible plate element based on the Reissner-Mindlin plate theory [14].

2.1.2 Modeling of welds and bolts

The welds in the joint are modeled using special solid elements that take into consideration weld dimensions and position relative to the plate. Instead of modeling the bolt with physical elements, IDEA StatiCa has implemented springs to simulate the bearing and tensile behavior of bolts. These springs are assumed to be coupled to the plates with multi-point constraints (MPC), which constrains the degrees of freedom of a set of slave nodes to the motion of a control point. In this case, the control points are the ends of the springs, and the slave nodes are the nodes in the plate assumed to be in contact with the bolt. The springs exhibit a bilinear force-displacement relationship, with an elastic part followed by an inelastic hardening part. The tensile stiffness is based on the analytical derivation in the guideline VDI 2230 [15], and the tensile capacity is in accordance with NS-EN 1993-1-8 [3]. The shear stiffness and resistance are based on EN 1993-1-8, with deformation capacity determined by experiments conducted by the developer [6]. The contact between plates is enforced with the penalty method, where the contact is imposed by augmenting the potential energy of the system by a penalty term [16], which can be interpreted as adding a spring stiffness on the contact surface [17].

2.1.3 Material model

As mentioned, IDEA StatiCa employs a simplified material model. The steel is assumed to be elastic-plastic with a yielding plateau slope equal to E/1000, as seen in Figure 2.2 [15]. Similar to other FEA softwares, IDEA StatiCa operates with true stresses and strains, which are related to the engineering (or nominal) stress-strain-curve through the following equations:

$$\sigma_{true} = \sigma_{eng}(1 + \varepsilon_{eng}) \tag{2.1}$$

$$\varepsilon_{true} = ln(1 + \varepsilon_{eng}) \tag{2.2}$$

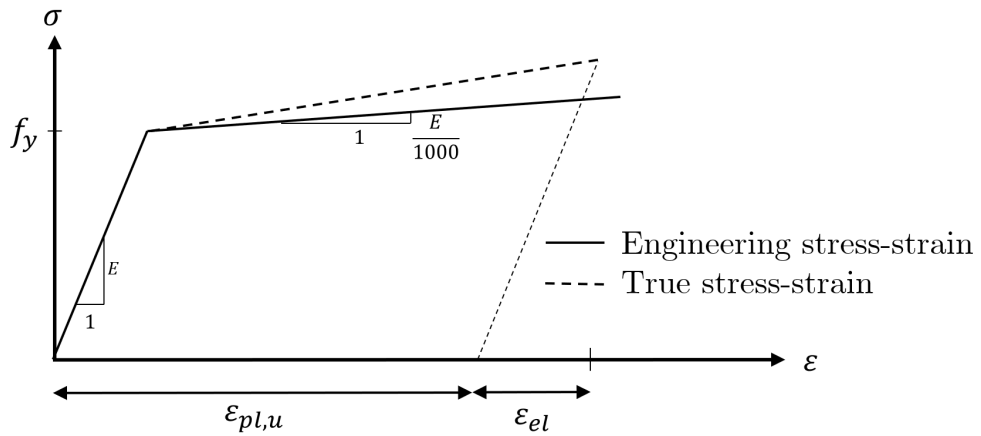

Figure 2.2: Material model in IDEA StatiCa

2.1.4 Determination of resistance

The capacity of the joint is limited by either the capacity of the bolts, the capacity of the welds, or the plastic strain in the plates. The capacity of bolts and welds is calculated according to NS-EN 1993-1-8 [3], while the limit of plastic strain in the plate can be chosen by the designer. NS-EN 1993-1-5 [2] recommends that a limit of 5 % for tensile membrane strains is applied in analyses. However, this is a highly conservative limit with little rationalization from experiments. The limit of plastic strain has a modest effect on the ultimate moment resistance of a joint [6], but has a considerable effect on the rotational capacity. The limit strain of the steel is therefore an important parameter for certain analyses.

2.1.5 Solution method

IDEA StatiCa employs a geometrically linear analysis with a nonlinear material model. This implies that the equilibrium equation is established for the undeformed system, and is not updated when the geometry deforms. The stiffness matrix, $\mathbf{K}$, and load vector, $\mathbf{R}$, in the equilibrium equation is therefore not a function of the deformations, as seen in the system equation:

$$\mathbf{K}\mathbf{D}(\bar{t}) = \mathbf{R} \tag{2.3}$$

where the $\bar{t}$ is the *pseudo-time* of the system.

Geometrically nonlinear analysis is also available in the software, but only for joints with hollow section members. According to the theory manual [15], the behavior of such members will not accurately be captured by geometrically linear analysis. IDEA StatiCa solves the nonlinear system using Newton-Raphson iterations, with the option of applying the external load in increments. This enables the possibility of producing load-displacement curves - or more relevant for this thesis: moment-rotation curves. In this way, it is also possible to derive the initial stiffness of a moment connection and use this to characterize the connection as pinned, rigid, or semi-rigid according to NS-EN 1993-1-8 [3]. This characterization can subsequently be used in an analysis of the global structure.

2.2 Abaqus

Abaqus is a powerful general-purpose FEA software suite applicable for analyzing a wide range of structural problems. The software suite consists of five packages, where the ones relevant for this thesis are: Abaqus/CAE (Complete Abaqus Environment), which allows for modeling and visualization of components; and Abaqus/Standard and Abaqus/Explicit, which employ implicit and explicit integration schemes, respectively, to solve the modeled problem. Abaqus has much higher functionality than IDEA StatiCa, and will, if employed correctly, offer a more accurate solution. For this reason, Abaqus will be used in the verification of IDEA StatiCa.

2.2.1 Element type

Structural problems can be discretized using different types of elements, depending on the requirement of accuracy and type of analysis. For more complicated structures, such as beam-to-column joints, 3D solid elements are preferred since they capture the physical geometry explicitly

without substantial simplification. Therefore, a finite element analysis with solid elements allows for the most accurate simulation, but with a cost of higher computation time. In the simulations in this thesis, the eight-node brick element with reduced integration (C3D8R) will mainly be employed. The six-node wedge element (C3D6) will be used for discretizing welds and bolts. Reduced integration means that the strains are sampled with a quadrature rule of one order lower than full integration when assembling the stiffness matrix, thus greatly reducing the computational cost [18]. Abaqus automatically implements hourglass stiffness to prevent the hourglass modes that otherwise might occur when using reduced integration [19].

2.2.2 Material model

When validating the finite element model in Abaqus to experimental results, it is necessary to apply a material model that resembles the behavior of the actual material used in the experiment. However, the complete stress-strain curves of materials used in an experiment are often not available. Instead, only yield stress, ultimate stress, and occasionally fracture strain are reported. To approximate the stress-strain curve of the material, the material model proposed in the upcoming standard prEN 1993-1-14 [20] can be utilized. This is a piecewise linear material model relevant for the simulation of hot rolled steel, where only the yield stress, f_y, and the ultimate stress, f_u, must be known. This material model is the illustrated in Figure 2.3.

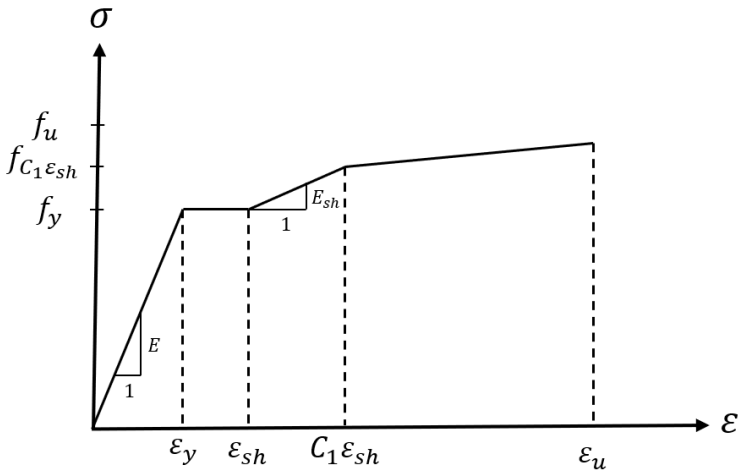

Figure 2.3: Material model for hot rolled steel from prEN 1993-1-14

$$f(\varepsilon) = \begin{cases} E\varepsilon & \text{for } \varepsilon \leq \varepsilon_y \\ f_y & \text{for } \varepsilon_y < \varepsilon \leq \varepsilon_{sh} \\ f_y + E_{sh}(\varepsilon - \varepsilon_{sh}) & \text{for } \varepsilon_{sh} < \varepsilon \leq C_1\varepsilon_u \\ f_{C_1\varepsilon_u} + \dfrac{f_u - f_{C_1\varepsilon_u}}{\varepsilon_u - C_1\varepsilon_u} & \text{for } C_1\varepsilon_u < \varepsilon \leq \varepsilon_u \end{cases} \tag{2.4}$$

$$\varepsilon_y = \frac{f_y}{E} \tag{2.5}$$

$$\varepsilon_{sh} = 0.1\frac{f_y}{f_u} - 0.055, \quad \text{but} \quad 0.015 < \varepsilon_{sh} \leq 0.03 \tag{2.6}$$

$$\varepsilon_u = 0.6(1 - \frac{f_y}{f_u}), \quad \text{but} \quad 0.06 < \varepsilon_u \leq \text{elongation at fracture} \tag{2.7}$$

$$C_1 = \frac{\varepsilon_{sh} + 0.25(\varepsilon_u - \varepsilon_{sh})}{\varepsilon_u} \tag{2.8}$$

$$C_2 = \frac{\varepsilon_{sh} + 0.4(\varepsilon_u - \varepsilon_{sh})}{\varepsilon_u} \tag{2.9}$$

$$E_{sh} = \frac{f_u - f_y}{C_2\varepsilon_u - \varepsilon_{sh}} \tag{2.10}$$

The post-yield behavior of the material is modeled by defining data points with true stress and corresponding true plastic strain. True stress and strain are related to nominal stress and strain through equations 2.1 and 2.2, and the true plastic strain, $\varepsilon_{true,pl}$, is defined by:

$$\varepsilon_{true,pl} = \varepsilon_{true} - \varepsilon_{true,elastic} = \varepsilon_{true,total} - \frac{\sigma_{true}}{E} \tag{2.11}$$

Material failure

prEN 1993-1-14 [20] proposes that the structural resistance of a joint should be determined by evaluating the load-deformation path. The resistance should be set equal to the lesser of the maximum load level of the computed load-deformation path and the force level where the maximum tolerable deformation or strain occurs. For joints with a load-deformation curve with a distinct extreme point, the first criterion is the most relevant. However, some joints exhibit a curve with a constant increase in load level, and the second criterion is therefore governing in analysis. prEN 1993-1-14 refers to NS-EN 1993-1-5 [2] for the limit of acceptable strain that should be applied in analyses. Applying the recommended limit of 5 % strain in a finite element analysis with solid elements will greatly underestimate both the moment resistance and the rotational capacity compared to experimental results. This is because finite element analyses with solid elements and an idealized geometry will generate local stress and strain concentrations. In reality, the stresses will be redistributed, and strain concentrations with absolute values well above 5 % will not result in failure of the joint.

To overcome this problem, and to obtain a numerical model true to real-world behavior, a material model with progressive damage will be applied in Abaqus. This enables simulation of joint failure, and a clear quantity for the moment resistance can thus be obtained. Progressive damage implies that the stresses in the elements are reduced compared to elements without damage, which is formulated mathematically as:

$$\boldsymbol{\sigma} = (1 - D)\bar{\boldsymbol{\sigma}} \tag{2.12}$$

where $\boldsymbol{\sigma}$ and $\bar{\boldsymbol{\sigma}}$ are the stresses in an element with and without damage, respectively, and D is the damage parameter ranging from 0 to 1. The damage initiation is defined by a strain where the stress reduction will initiate, and the damage parameter, D, is a function of the subsequent plastic strain. After damage initiation, the stresses are instantly or gradually reduced as D approaches 1, where the element exhibits zero capacity. This approach aims to capture the physical behavior of steel and is applicable for simulating the failure of steel joints.

2.2.3 Solution method

When analyzing structures in Abaqus, two main solution methods are available: Abaqus/Standard with a static, general procedure, and Abaqus/Explicit, with an explicit integration scheme. The static solution method does not take into account inertia forces or other dynamic effects, as the system is purely represented by the stiffness matrix. In Abaqus, it is possible to include geometric nonlinearity. This means that the stiffness matrix, $\mathbf{K}$, and the load vector, $\mathbf{R}$, are a function of the deformation vector, $\mathbf{D}$, and the stiffness matrix and the load vector are updated throughout the load application. This is formulated mathematically in the following equation:

$$\mathbf{K}(\mathbf{D}(\bar{t}))\mathbf{D}(\bar{t}) = \mathbf{R}(\mathbf{D}(\bar{t})) \tag{2.13}$$

By contrast, the explicit solution method includes dynamic effects. An explicit integration scheme (central difference method) is implemented to solve the equation of motion, which is formulated as:

$$\mathbf{K}(\mathbf{D}(t))\mathbf{D}(t) + \mathbf{M}\ddot{\mathbf{D}}(t) = \mathbf{R}(\mathbf{D}(t)) \tag{2.14}$$

where $\mathbf{M}$ is the mass matrix of the system, $\ddot{\mathbf{D}}$ is the acceleration vector, and t is the real-time of the system.

Many quasi-static structural problems can be analyzed using both of these methods, as the dynamic effects will be insignificant. In general, a static procedure will be more accurate as the solution at increment 'n+1' is a function of the solution at increment 'n+1'. This requires a nonlinear solution algorithm to solve the system. On the other hand, the explicit solution method calculates the solution at time 't+1' *explicitly* from the solution at time 't'. The explicit solution method therefore requires smaller time steps, or load increments, to converge to the correct solution. However, for certain problems with a high degree of nonlinearity, the explicit solution method is preferred, as it in general offers a higher degree of convergence. To reduce the computation time, load scaling can be applied. This implies that the velocities are increased in such a way that a specified deformation is achieved faster. The problem with load scaling is that inertia forces become more prominent, and possibly influence the solution of the system. To ensure that no significant dynamic effects occur, an energy balance check should be performed to confirm that the kinetic energy is small compared to the internal strain energy. In this thesis, both the static and the explicit solution methods will be applied.

2.3 Component method

The component method is a method for manually calculating the resistance and stiffness of a joint based on the capacity and stiffness of the different joint components. This calculation method is implemented in NS-EN 1993-1-8 [3] and is based on numerous research programs with considerable amounts of experimental tests. Among these are the works of Zoetemeijer [21] and Witteveen et al. [22], who proposed analytical models for the resistance of the T-stub in tension, which is a key component in bolted beam-to-column joints. Other significant contributions are the works of Chen and Newlin [23], who addressed the resistance of the column web. The current stiffness model was proposed by Weynand et al. [24]. Their work has since been revised, and

new key components added. The most important components in a bolted beam-to-column joint are shown in Figure 2.4, with reference to their respective capacity and stiffness coefficient in NS-EN 1993-1-8 listed in Table 2.1.

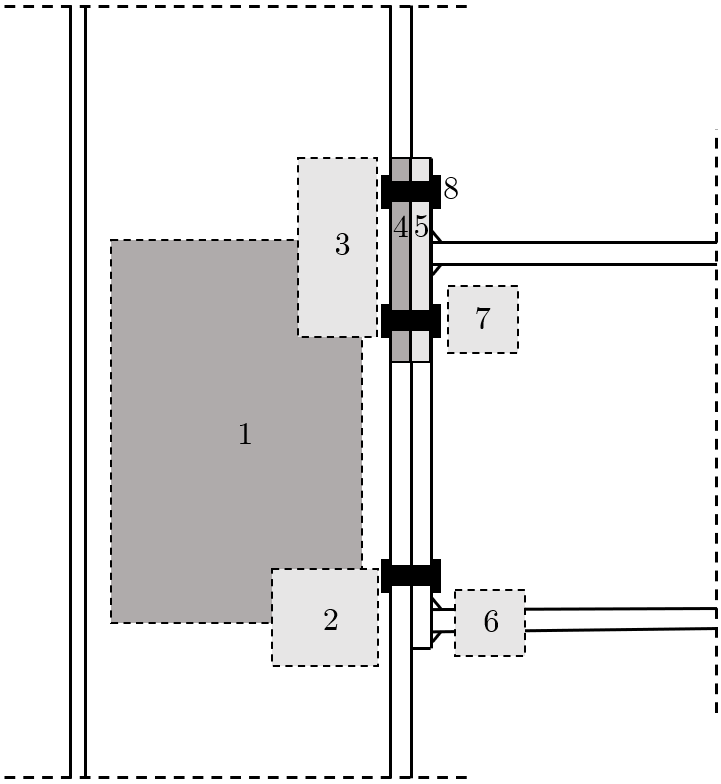

Figure 2.4: Components in NS-EN 1993-1-8

Table 2.1: Components in NS-EN 1993-1-8

Number	**Component**	**Capacity in EN 1993-1-8 [3]**	**Stiffness coefficient**
1	Column web in shear	§6.2.6.1	k_1
2	Column web in compression	§6.2.6.2	k_2
3	Column web in tension	§6.2.6.3	k_3
4	Column flange in bending	§6.2.6.4	k_4
5	End-plate in bending	§6.2.6.5	k_5
6	Beam flange in compression	§6.2.6.7	-
7	Beam web in tension	§6.2.6.8	-
8	Bolts in tension	§6.2.6.4/§6.2.6.5	k_{10}

The moment resistance of the joint is controlled by the component(s) with the lowest capacity. The resulting moment resistance can be calculated by the following expression:

$$M_{j,rd} = \sum_r h_r \cdot F_{tr,Rd} \tag{2.15}$$

where $M_{j,Rd}$ is the ultimate resistance of the joint, $F_{tr,Rd}$ is the capacity of bolt row r in tension, and h_r is the distance from the bolt row to the center of compression. However, the total force in the bolts cannot exceed the capacity of other components in the joint.

The rotational stiffness of the joint can similarly be calculated using the individual stiffnesses of the components in the joint:

$$S_j = \frac{Ez^2}{\mu \sum_i \frac{1}{k_i}} \tag{2.16}$$

where k_i is the stiffness coefficient of component i, and μ is the relationship between initial stiffness and tangent stiffness; $\mu = S_{j,ini}/S_j$. This parameter is defined by the following equation:

$$\mu = \begin{cases} 1 & for \quad M_{j,Ed} \leq 2/3 M_{j,Rd} \\ \left(\frac{1.5 M_{j,Ed}}{M_{j,Rd}}\right)^{\psi} & for \quad 2/3 M_{j,Rd} < M_{j,Ed} \leq M_{j,Rd} \end{cases} \tag{2.17}$$

where $M_{j,Ed}$ is the design moment of the joint. The parameter ψ is given as 2.7 for welded and bolted end-plate joints. This equation implies that the moment-rotation curve of a joint can be considered linear up to 2/3 of the moment resistance.

2.3.1 Joints subjected to a combination of moment and axial force

As NS-EN 1993-1-8 only briefly covers joints subjected to a combination of moment and axial force, calculation methods from relevant literature on the topic will be applied. In the following sections, the relevant expressions for calculating the moment resistance, initial rotational stiffness, and rotational capacity will be presented.

Ultimate moment resistance

NS-EN 1993-1-8 states that axial forces in the attached part of a joint can be neglected if the force is lower than 5 % of the plastic capacity for axial force, $N_{pl,Rd}$. If the axial force exceeds this limit, the following equation should be used to verify the capacity of the joint:

$$\frac{M_{j,Ed}}{M_{j,Rd}} + \frac{N_{j,Ed}}{N_{j,Rd}} \leq 1 \tag{2.18}$$

where $M_{j,Ed}$ and $N_{j,Ed}$ are the design moment and axial force, respectively. $M_{j,Rd}$ and $N_{j,Rd}$ are the design moment resistance and axial force resistance calculated without simultaneously acting axial force and bending moment, respectively. These two criteria result in an interaction diagram as shown in Figure 2.5. Another approach is to consider the resulting forces in the beam flanges from axial force and moment, and compare these to the capacity of the components in the joint. This method was described by Sokol et al. [25], and the method will result in a

higher resistance for most combinations of bending moment and axial force. An example of an interaction diagram applying this method is also shown in Figure 2.5.

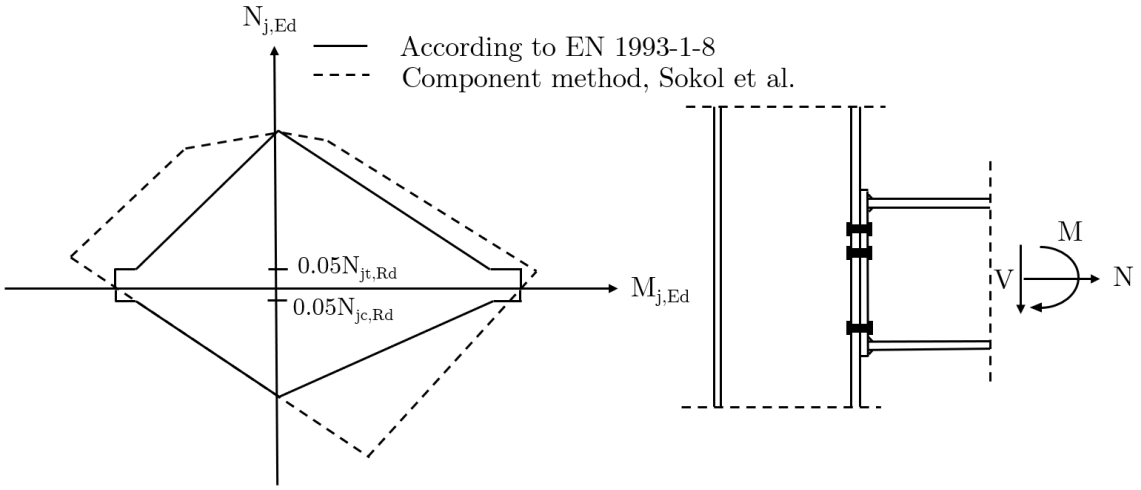

Figure 2.5: Interaction between moment and axial force [25]

The method proposed by Sokol et al. [25] is derived for proportional loading, i.e. assuming that the eccentricity, $e = M_{j,Ed}/N_{j,Ed}$, is kept constant during loading. Resistance formulas for combined bending moment and axial force can be derived by considering the moment equilibrium about the compressive and the tensile resultant while ensuring that the resulting forces does not exceed the capacity, as illustrated in Figure 2.6. The bending moment is assumed to give tension in the upper flange of the beam.

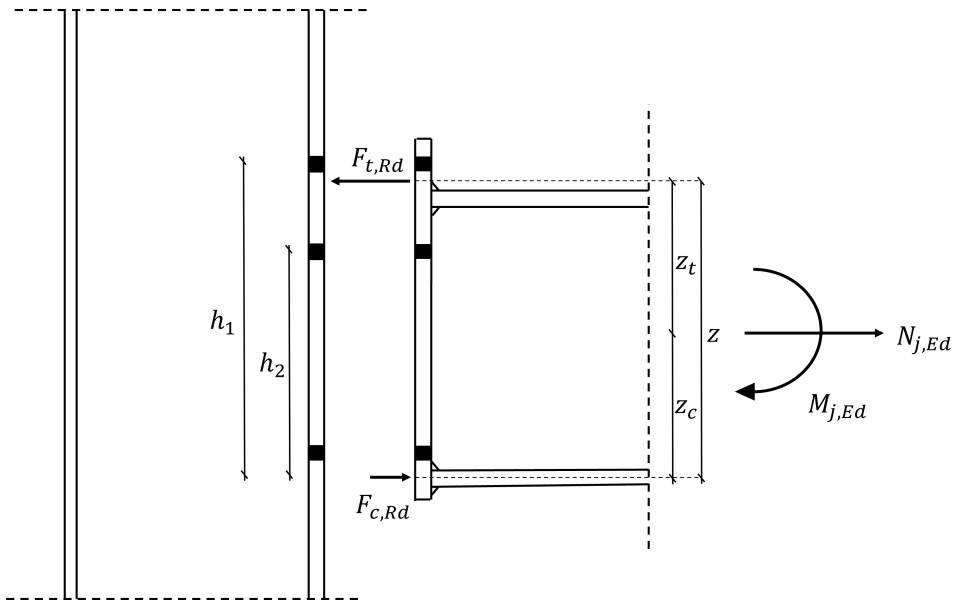

Figure 2.6: Combined axial force and moment

The moment equilibrium gives the following sets of equations:

$$M_{j,Ed} + N_{j,Ed} \cdot z_c \leq F_{t,Rd} \cdot z \tag{2.19}$$

$$M_{j,Ed} - N_{j,Ed} \cdot z_t \leq F_{c,Rd} \cdot z \tag{2.20}$$

where $F_{c,Rd}$ and $F_{t,Rd}$ are the capacity of the compression and tension zone, respectively. With more than one bolt row in tension, the capacity of the tensile zone can be calculated as the resultant force of the bolts in tension, with the assumption of plastic distribution of forces. The internal moment arm, z, can then be calculated:

$$z = \frac{h_r \sum_i F_{t,r,Rd}}{\sum_i F_{t,r,Rd}} \tag{2.21}$$

where $F_{t,r,Rd}$ is the capacity of bolt row r with distance h_r from the compressive resultant. Rewriting equation 2.19 and 2.20 while assuming constant eccentricity, e, gives the following expression for moment resistance:

$$M_{j,Rd} = min \begin{cases} \dfrac{F_{t,Rd} \cdot z}{1 + \dfrac{z_c}{e}} \\ \dfrac{F_{c,Rd} \cdot z}{1 - \dfrac{z_t}{e}} \end{cases} \tag{2.22}$$

In this equation, it is assumed that $e > z_t$ or $e < -z_c$. For large magnitudes of axial force, there will be tension or compression in both beam flanges, as illustrated in Figure 2.7, and the expressions for resistance must be modified. The capacity of the components must be recalculated, as they behave differently in compression and in tension. However, this is not relevant for the cases considered in this thesis, as the eccentricity is within the assumed limits.

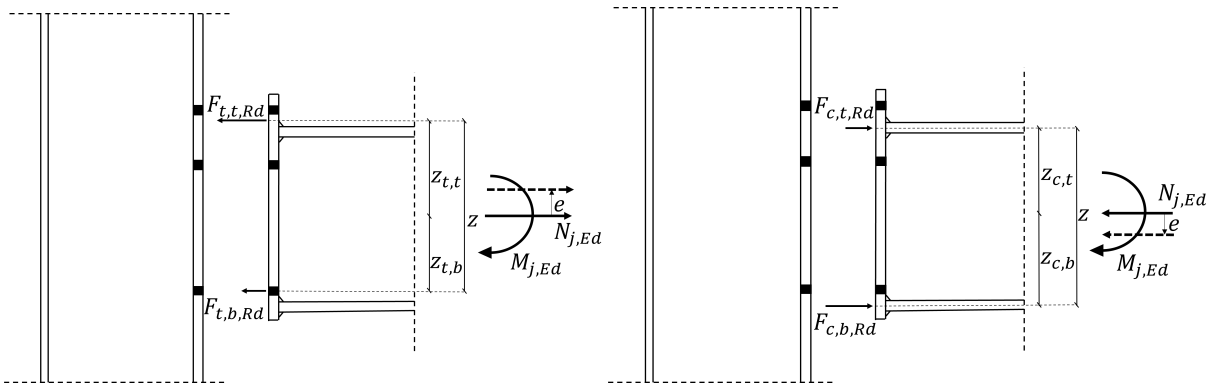

(a) Tension **(b)** Compression

Figure 2.7: Component method with high axial force-to-moment ratio

With non-proportional loading, i.e. moment or axial force applied independently, the resistance of the joint remains unchanged. This presupposes that the joint does not fail from axial force or moment acting alone.

Stiffness

The presence of axial force implies that certain joint components are activated more than when the bending moment acts alone. As a consequence, the initial rotational stiffness of the joint is altered. An expression for the modified stiffness was also described by Sokol et al. [25], and the derivation will be presented briefly. Considering Figure 2.8, the deformation of the top and bottom flange can be expressed as:

$$\delta_t = \frac{M + N \cdot z_c}{z \cdot E \cdot k_t} \tag{2.23}$$

$$\delta_c = \frac{M - N \cdot z_t}{z \cdot E \cdot k_c} \tag{2.24}$$

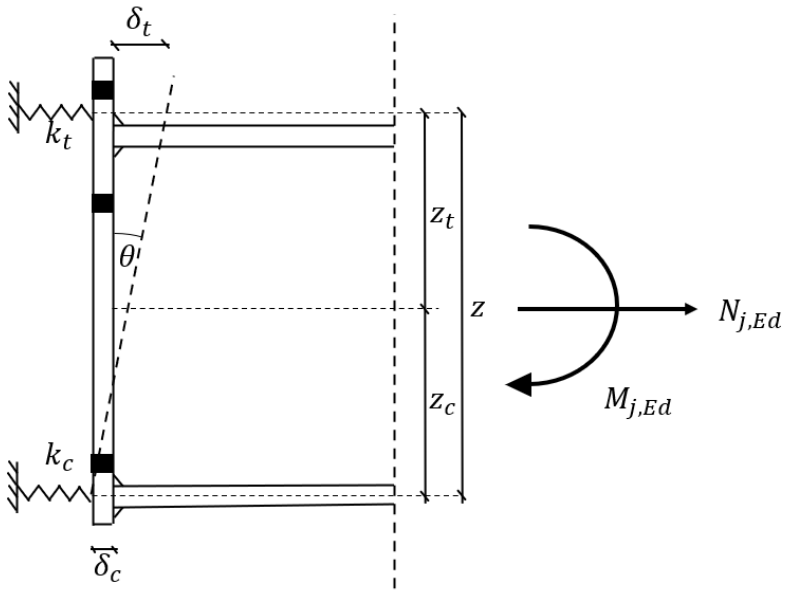

Figure 2.8: Stiffness model

From this, the total rotation, θ, can be expressed as:

$$\theta = \frac{\delta_t + \delta_c}{z} = \frac{1}{Ez^2}\left(\frac{M + N \cdot z_c}{k_t} + \frac{M - N \cdot z_t}{k_c}\right) \tag{2.25}$$

Finally, the initial stiffness, $S_{j,ini}$, can be expressed by the following equation:

$$S_{j,ini} = \frac{M}{\theta} = \frac{N \cdot e \cdot E \cdot z^2}{\frac{N \cdot e + N \cdot z_c}{k_t} + \frac{N \cdot e - N \cdot z_t}{k_c}} = \frac{e}{e + e_0}\frac{E \cdot z^2}{\sum \frac{1}{k}} \tag{2.26}$$

where e_0 is defined as:

$$e_0 = \frac{z_c \cdot k_c - z_t k_t}{k_c + k_t} \tag{2.27}$$

With more than one bolt row in tension, the equivalent stiffness of the tensile zone, k_t, is defined in NS-EN 1993-1-8 [3] as:

$$k_{eq} = \frac{\sum_r k_{eff,r} \cdot h_r}{z_{eq}} \tag{2.28}$$

where the stiffness coefficient for bolt row r is given by:

$$k_{eff,r} = \frac{1}{\sum_i k_{i,r}} \tag{2.29}$$

and equivalent moment arm is given by the following equation:

$$z_{eq} = \frac{\sum_r k_{eff,r} \cdot h_r^2}{\sum_r k_{eff,r} \cdot h_r} \tag{2.30}$$

Contrary to the moment resistance, the initial stiffness of the joint is affected by whether the axial force and bending moment are applied proportionally or not. Compressive axial force applied before the bending moment increases the stiffness and vice versa. This is because the components, in general, behave stiffer when loaded in compression than in tension.

Rotational capacity

Rotational capacity is the last main characteristic of a steel joint. NS-EN 1993-1-8 [3] states that a joint has sufficient rotational capacity for plastic analysis if both of these criteria are satisfied:

(a) Design moment resistance of the joint is governed by the resistance of either the column flange in bending or the end-plate in bending.

(b) The thickness of either the column flange or the end-plate satisfies the following condition: $t \leq 0,36d\sqrt{f_{ub}/f_y}$, where d is the diameter of the bolt, f_y is the yield strength of the relevant basis component, and f_{ub} is the ultimate strength of the bolt.

If the joint's moment resistance is limited by the shear capacity of the column web, the rotational capacity can be assumed sufficient for plastic analysis if $d_{wc}/t_w \leq 69\sqrt{235/f_y}$, where d_{wc} and t_w are the depth and thickness of the column web, respectively.

For most design purposes, it is sufficient to determine whether plastic analysis is applicable or not. However, in case the above criteria are not satisfied, or if a progressive collapse analysis is to be carried out, the actual rotational capacity of the joint might be of interest. Beg et al. [26] developed a simplified calculation method for determining the rotational capacity of bolted beam-to-column joints. The deformation capacities of the different components are derived from a mix of simplified analytical considerations and empirical data. The derivation can be found in [26], and the resulting deformation capacities for the relevant components are listed below:

1. **Column web in compression**:

$$\delta_{u1} = \frac{\varepsilon_u}{d} \tag{2.31}$$

   where d is the depth of the column web, and ε_u is determined from Figure 2.9a as a function of axial force in column; $n = N/N_{pl}$

2. **Column web in tension**:

$$\delta_{u2} = \varepsilon_u d \tag{2.32}$$

   where $\varepsilon_u = 0.1\left(\frac{\sqrt{4-3n^2}-n}{2}\right)^2$

3. **Column flange and end-plate in bending**: Deformation capacity dependent on failure mode (according to NS-EN 1993-1-8 [3]):

   (i) Mode 1:

   $$\delta_{u3} = 0.4m \tag{2.33}$$

   where m is the distance from center of bolt to weld (see Figure 6.2 in NS-EN 1993-1-8).

   (ii) Mode 2:

   $$\delta_{u3} = 0.1l_b(1 + k\frac{m}{n}) \tag{2.34}$$

   where l_b is the clamping length of the bolt, n is the distance from center of bolt to edge of plate, and k is an empirical factor; $k \in [1, 5]$.

   (iii) Mode 3:

   $$\delta_{u3} = 0.1l_b \tag{2.35}$$

4. **Column web in shear**: γ_u is a function of the depth-to-thickness ratio, and can be taken from Figure 2.9b

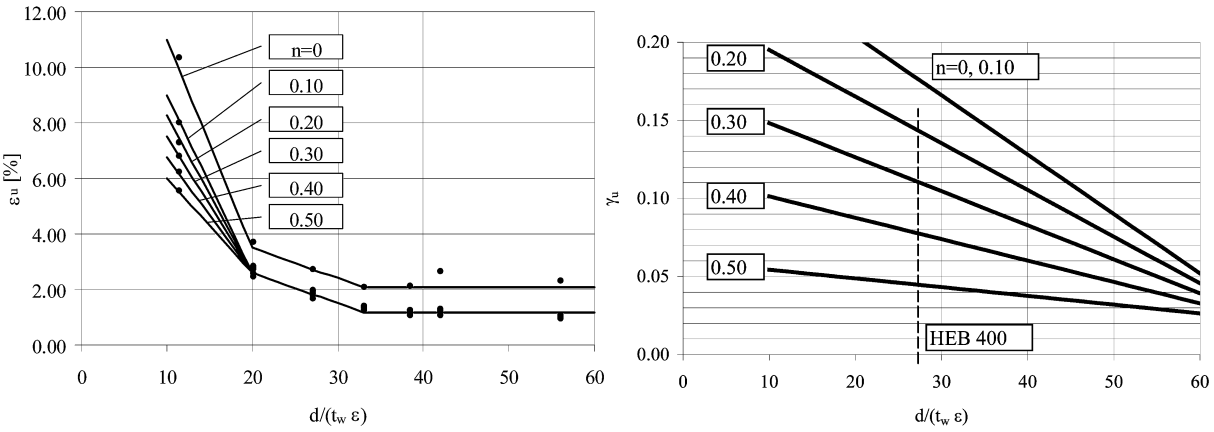

(a) Column web in compression **(b)** Column web in shear

Figure 2.9: Deformation capacity [26]

The total rotational capacity is then given as:

$$\theta_u = \frac{\delta_1 + \delta_2 + \delta_{3,ep} + \delta_{3,cf} + \gamma h_f}{h_f} \tag{2.36}$$

where $\delta_{3,ep}$ and $\delta_{3,cf}$ are the deformations from the end-plate and the column flange (including bolts), respectively, and h_f is the distance between the center of the flanges.

The component with the lowest strength contributes with its full deformation capacity. The other components contribute with deformations corresponding to that force level. The behavior of the components is assumed to be trilinear, with stiffness coefficient k_i up til 2/3 of the component's resistance, before the stiffness is reduced to $k_i/7$. This is similar to the nonlinear part of the moment-rotation curve defined in NS-EN 1993-1-8 (equation 2.16 and 2.17), except that the behavior is assumed linear after the force surpasses 2/3 of the resistance. Determination of initial stiffness and resistance of the individual components is therefore necessary in order to determine the rotational capacity of the joint. However, applying the design formulas from NS-EN 1993-1-8 directly will be overly conservative, as the formulas reflect the strength at the onset of plasticity and not the ultimate resistance [26]. A remedy for this problem is to use

the ultimate strength, instead of the yield strength, in the design formulas for the end-plate and the column flange in bending. An example of the determination of rotational capacity is demonstrated in Figure 2.10.

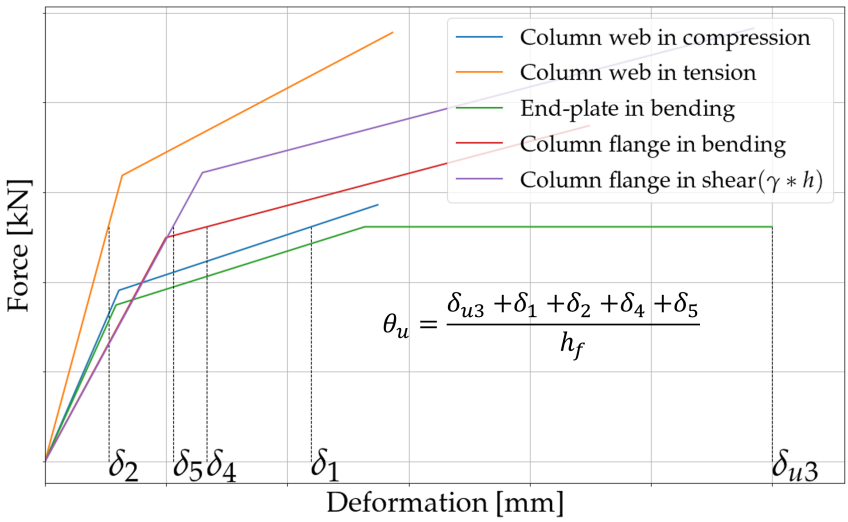

Figure 2.10: Example of calculation of rotational capacity

2.3.2 Beam minor axis joint

A bolted beam-to-column joint designed to be a major axis joint will often also be subjected to bending moment about the weak axis of the beam. In addition to carrying gravitational loads, the joint can also contribute to the horizontal brazing of the structure, where bending about the beam minor axis is expected to occur. Even though this load effect is considerably less prominent than the major axis moment, it will still be an important factor to take into consideration. Additionally, determining the minor axis stiffness of the joint might be necessary prior to a global analysis if the joint is a part of the bracing system. However, Eurocode 3 does not cover this type of joint configuration. Yield line theory might be applied to estimate the resistance, but this approach is very uncertain, and will therefore not be attempted in this thesis. The lack of available design formulas for this joint configuration makes it a problem highly relevant to be analyzed in IDEA StatiCa.

2.3.3 Column minor axis joint

The last joint configuration considered in this thesis is the column minor axis joint. This type of joint is relevant where beams from two perpendicular directions are bolted to the same open cross-section column. However, this type of joint is not covered by Eurocode 3, and analytical expressions from literature must therefore be considered to predict the resistance and the stiffness of the joint. With this type of configuration, a new component must be considered: out-of-plane bending of the column web. Gomes et al. [27] and Neves et al. [28] established expressions for the resistance and the stiffness, respectively, of this component. As these formulas are rather cumbersome, they are presented in Appendix A.

3 Major axis bending of bolted beam-to-column joints

In this chapter, major axis bolted beam-to-column joints will be analyzed, calculated, and compared to the results of analyses in IDEA StatiCa. This chapter is divided and organized into five sections. Section 3.1 presents the physical experiment used as basis for the validation. Section 3.2 provides an explanation of how the numerical models in IDEA StatiCa and Abaqus are assembled, and what assumptions are adopted in the manual calculations. Section 3.3 contains the results of the validation process, i.e. the comparison between the results obtained from the finite element analysis in Abaqus, and the results obtained from the physical experiment used for validation purposes. Section 3.4 compares the results from the analysis in IDEA StatiCa to the manual calculations based on Eurocode 3, and to the results from analyses carried out in Abaqus. Section 3.5 presents a parametric study where joints with different load conditions and geometries are analyzed and calculated. Sections 3.3, 3.4, and 3.5 all conclude with a discussion of the key findings.

3.1 Experiment

There have been conducted numerous experiments on bolted beam-to-column joints. In this thesis, the works of Zhu et al. [29], who carried out a series of full-range experiments on bolted joints, will be considered. This series of experiments is chosen as the test setup and the material data of the experiment is thoroughly described in the article. The geometry and the method of load application are illustrated in Figures 3.1a and 3.1b, respectively. The beam was welded to an end-plate with a thickness of either 10 mm or 20 mm. In some experiments, a backing plate was placed on the column flange on the opposite side of the end-plate, as shown in Figure 3.1a. The beam and the column were hot rolled with a characteristic yield strength of 350 N/mm^2, and the bolts were M24 grade 8.8. However, tensile tests of the profiles were performed, and measured values were adopted in the analyses. For bolts, tensile tests were not performed, and the characteristic material properties were adopted in the analyses.

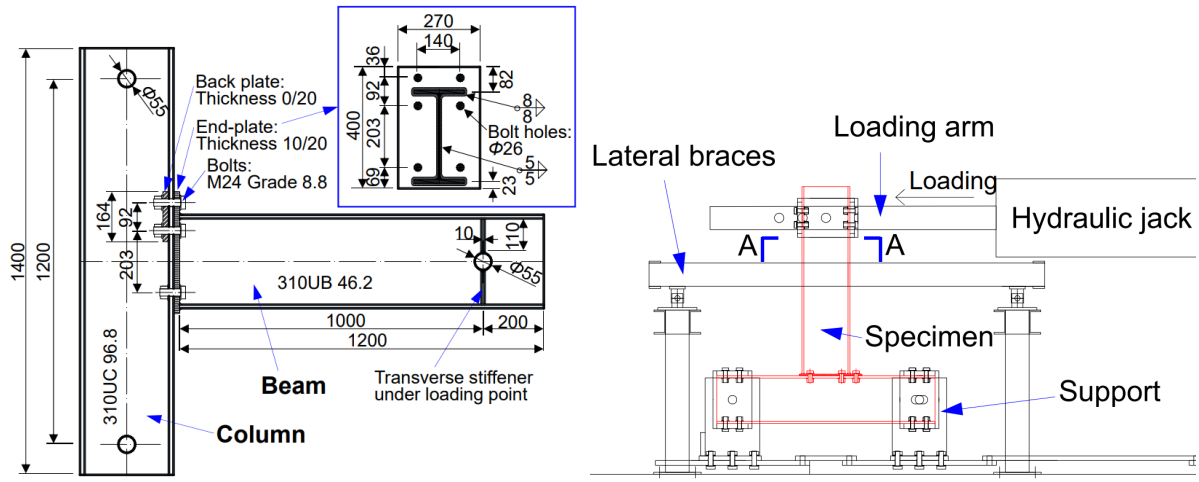

(a) Geometry **(b)** Load application

Figure 3.1: Major axis joint experimental setup [29]

3.2 Calculation models

In this section, the different assumptions and simplifications implemented in the finite element analyses and manual calculations will be explained.

3.2.1 IDEA StatiCa

IDEA StatiCa does not allow the user to specify the length of members directly. The length is instead specified as a factor multiplied by the height of the members and was therefore only approximately the same as in the experiment. The boundary conditions of the experiment can also not be replicated exactly. However, both the length of members and boundary conditions have a negligible effect on the results of the calculation.

IDEA StatiCa is primarily a design software, and it is intended that load effects extracted from a global analysis can be directly applied to joints. The loads are therefore applied to the end of members in such a way that the resulting force in the intersection between the column and the beam centerline are the loads specified by the user. In the experiment, the shear load was applied at a distance of 1164-1174 mm from the centerline of the column. To imitate the experiment, the loads in IDEA StatiCa were applied so that the ratio M/V is the same as in the experiment. When performing stiffness analysis in IDEA StatiCa, the loads applied to the analyzed member are scaled proportionally up til failure, thus reproducing the experimental load application. The IDEA StatiCa model with assumed boundary conditions is shown in Figure 3.2.

As mentioned, IDEA StatiCa employs an elastic-plastic material model, with hardening independent of the ultimate stress. Therefore, only the yield strength from tensile tests was relevant for the analysis. The limit of plastic strain was varied, with the intent to explore how this parameter influences the capacity of the joint.

IDEA StatiCa allows the user to specify the maximum size of elements in the finite element model. A simplified mesh convergence study was carried out, and it was chosen to employ an element size of 6 mm in the subsequent analyses, as this resulted in acceptable accuracy and computation time. The result of the mesh convergence study can be found in Appendix B, and the resulting mesh used in analyses can be seen in Figure 3.3.

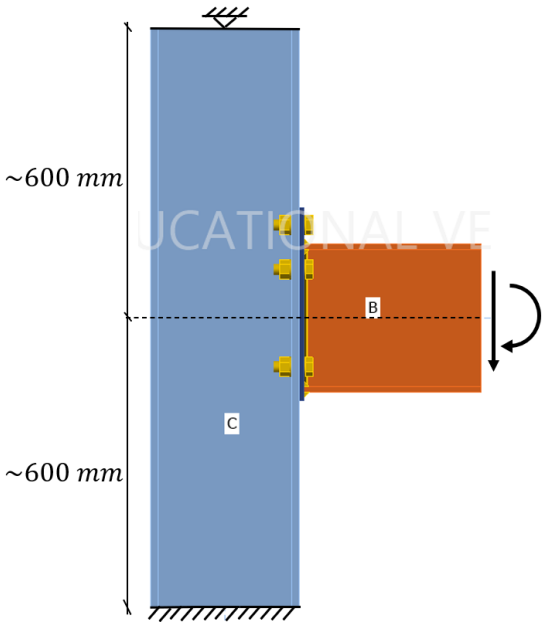

Figure 3.2: IDEA StatiCa model

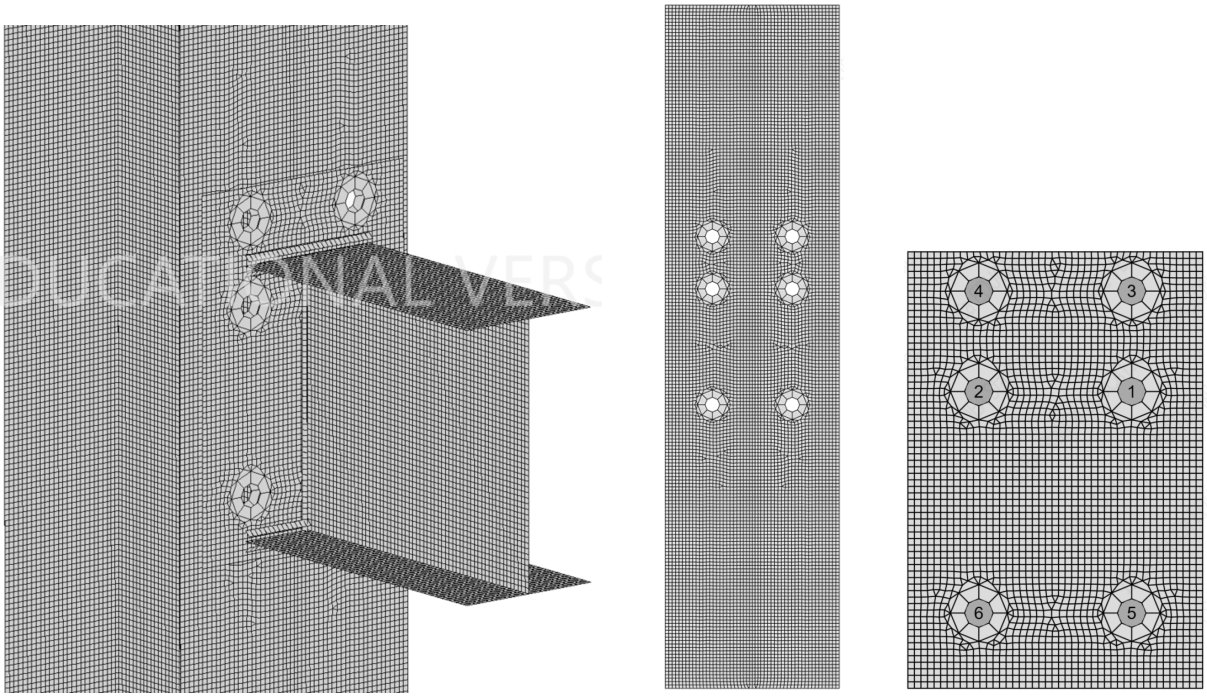

(a) Overview **(b)** Column flange **(c)** End-plate

Figure 3.3: Mesh in IDEA StatiCa

3.2.2 Abaqus model

Solution method

Simulation of a bolted beam-to-column joint loaded until failure involves a high degree of geometric and material nonlinearity, especially since a material failure model is implemented. Preliminary analyses showed that static analyses encountered convergence issues, and it was therefore required to analyze the problem using an explicit solution method. Instead of load control, deformation control was applied, as this results in fewer convergence issues. The loading

rate was increased, and the load velocity that resulted in the best balance of computation time and accuracy was determined to be 600 mm/s. The velocity was ramped up linearly from zero during the first 10 % of the simulation time. This was done to prevent artificial stress waves that might else be introduced into the system due to abrupt changes in velocity. To verify that no significant dynamic effects occurred, the kinetic energy was compared to the internal energy. For all analyses, the kinetic energy was found to be ≤ 1 % of the internal energy. Dynamic effects are therefore assumed to be negligible. To verify that the accuracy of the explicit solution method was acceptable compared to the more accurate static solution method, static analyses were performed on models without a progressive damage model

Geometry, interaction, and boundary conditions

When modeling the geometry, the different parts were modeled and meshed separately, before the complete structure was assembled. The symmetry of the problem was utilized, and only half the structure was modeled. The boundary condition on the symmetry plane prevented deformations normal to the plane, as shown in Figure 3.4. For joint configurations where buckling of the column web is the governing failure mode, it is not possible to utilize the symmetry. This is because buckling of the web includes deformations normal to the symmetry plane, which is restricted when utilizing the symmetry. In these cases, the whole joint had to be modeled, which implied a higher computational cost. The in-plane boundary conditions were applied using a rigid body constraint, where reference points in the center of the openings on the web were specified as control points for the slave nodes on the web, as shown in Figure 3.5. This implies that the nodes in the opening behave as a rigid body governed by the deformation of the control points [19]. Boundary conditions were subsequently applied to the reference points, as shown in Figure 3.6.

The welds were modeled as triangular prisms and connected to the end-plate and the beam with tie constraints. The tie constraint joins separate surfaces and prohibits relative motion [19], and is ideal for joining regions with different mesh densities. The surfaces on the end-plate and the beam were chosen as slave surfaces, while the surfaces on the welds were chosen as master surfaces, as shown in Figure 3.7. Contact between the parts was accounted for by including a “general contact” interaction, with a “hard” normal behavior. The friction coefficient for tangential behavior was chosen as 0.3. This corresponds to a “cleaned and wire-brushed surface” [30], and is a commonly used friction factor.

To take into account the threaded part of the bolts, the bolt shanks were modeled with a constant diameter consistent with the tensile area of the bolts (diameter=21.2 mm for M24 bolts). The bolt shank, nut, head, and washer were modeled in one part. This simplification is acceptable as the local behavior of the bolt is not of importance. The moment-rotation curve was obtained similarly as in the experiment. The rotation of the joint was obtained as $\theta = tan^{-1}(\delta/L) - \theta_{elastic}$, where δ and L are illustrated in Figures 3.6, and $\theta_{elastic}$ is the rotation due to elastic deformation of the beam. The rotation due to elastic deformation of the column was found to be negligible. The moment was determined using “integrated output sections” in Abaqus, which sums up the nodal forces over a section and calculates the moment about a defined point in the section.

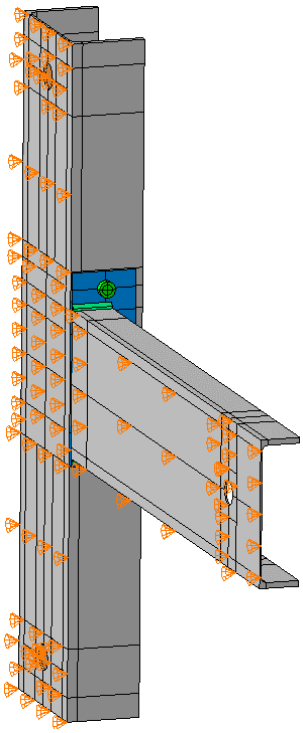

Figure 3.4: Symmetry boundary condition

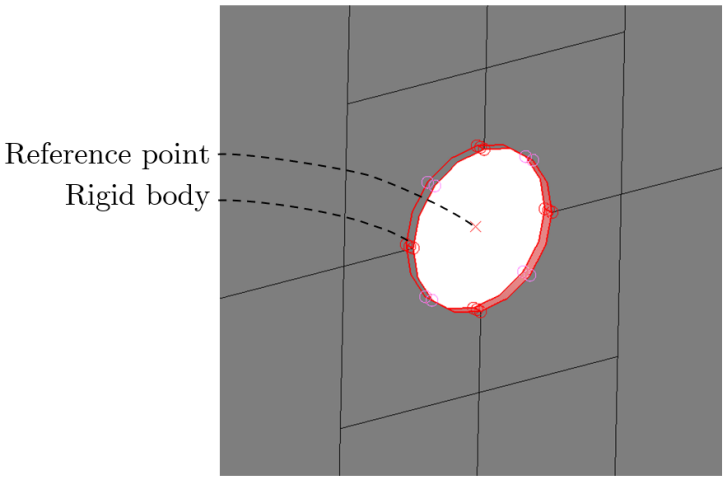

Figure 3.5: Rigid body constraint

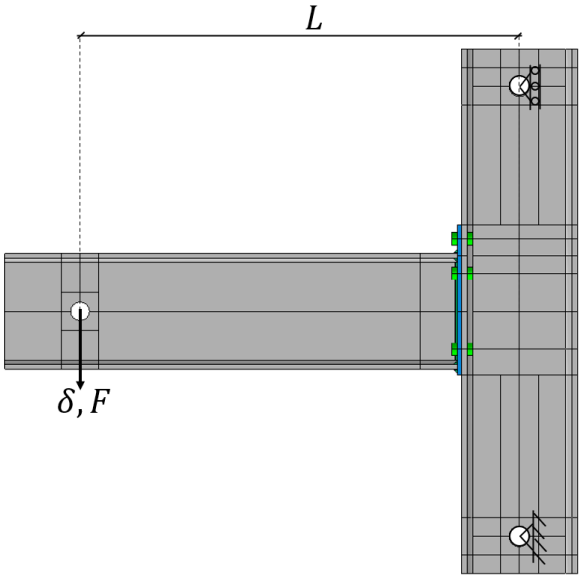

Figure 3.6: Boundary conditions and load application in Abaqus

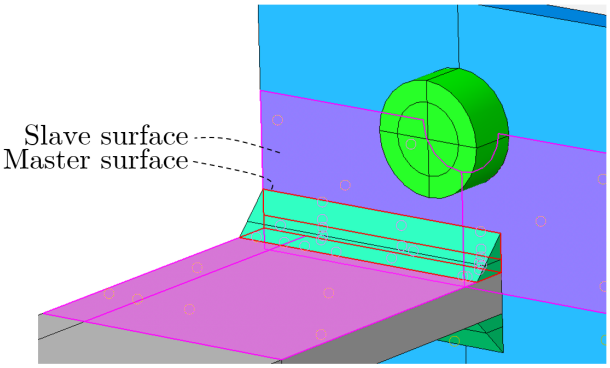

Figure 3.7: Tie constraint applied to welds

Material properties and progressive damage

The provided material properties of the steel in the experiment include yield stress, tensile strength, ultimate strain, and measured Young's modulus. The Poisson's ratio, ν was set equal to 0.3. However, to simulate the rotational capacity of the joint, preliminary analyses showed that it was necessary to include a progressive damage material model. In Abaqus, "ductile damage" and "damage evolution" can be included in the material model. This implies that for a given strain, the material failure is activated, and the stresses in the elements are immediately or gradually reduced. As the material data from the experiment is limited, an approach similar

to the one proposed by Pavlovic et al. [31] was utilized in this thesis. It is important to acknowledge that this is only an approximation, and the validity and accuracy of this approach are uncertain. To obtain accurate predictions of material failure, material calibrations should be carried out. However, to evaluate IDEA StatiCa's ability to calculate rotational capacity, and to obtain a clearly defined moment resistance, this method was deemed to be the most convenient.

Previous research has shown that the fracture strain is a function of the *stress triaxiality*, which is the ratio between hydrostatic stress and equivalent von Mises stress, as defined in the following equation:

$$\eta = \frac{\sigma_m}{\sigma_{eq}} = \frac{\frac{1}{3}(\sigma_1 + \sigma_2 + \sigma_3)}{\sqrt{\frac{1}{2}[(\sigma_1 - \sigma_2)^2 + (\sigma_2 - \sigma_3)^2 + (\sigma_3 - \sigma_1)^2]}} \tag{3.1}$$

For uniaxial tension, $\eta = 1/3$. The well-known research by Rice and Tracey [32] showed that fracture strain could be defined by an exponential function of the stress triaxiality:

$$\bar{\varepsilon}_f^{pl} = \alpha \cdot e^{-\beta\eta} \tag{3.2}$$

where $\bar{\varepsilon}_f^{pl}$ is the equivalent plastic strain at fracture, and α and β are material factors. β is often assumed to be 1.5 for most steels [31, 32, 33], while α is calibrated from material testing. If the fracture strain from a uniaxial tensile test ($\eta = 1/3$), ε_f^{pl}, is determined, the fracture strain as a function of stress triaxiality can be expressed as:

$$\bar{\varepsilon}_f^{pl} = \varepsilon_f^{pl} \cdot e^{-1.5(\eta - 1/3)} \tag{3.3}$$

In the article by Pavlovic et al. [31], it was assumed that the ratio of equivalent and uniaxial plastic strain at fracture and at the onset of material failure are the same. From this, the equivalent plastic strain at the onset of damage, $\bar{\varepsilon}_u^{pl}$, can be expressed by the uniaxial plastic strain at the onset of damage, ε_u^{pl}. In this thesis, it was further assumed that the uniaxial strain at the onset of damage is the same ε_u as defined by prEN 1993-1-14 [20] (Equation 2.7). The equivalent plastic strain at the onset of damage, $\bar{\varepsilon}_u^{pl}$, as a function of stress triaxiality, can then be expressed as:

$$\bar{\varepsilon}_u^{pl} = \varepsilon_u^{pl} \cdot e^{-1.5(\eta - 1/3)} \tag{3.4}$$

The nominal/average strain at failure for the materials in the experiment is available in the article by Zhu et al. [29]. However, a nominal strain measure does not take into account the necking and the strain concentration in the necking zone. In reality, the local strain after necking is much higher than the nominal strain. Pavlovic et al. [31] accounted for this in their material model and found that the ratio between local strain and nominal strain at failure was approximately 1.9 for S235 steel. This assumption was adopted in the simulations.

After the onset of damage, the "damage evolution" must be specified in Abaqus. The state at which an element is deleted from the mesh is defined by *plastic displacement at failure*, $\bar{u}_f^{pl}$. This is the product of characteristic element length, L_{char}, and *effective plastic strain*, as defined by [33]:

$$\bar{u}_f^{pl} = L_{char} \cdot (\bar{\varepsilon}_f^{pl} - \bar{\varepsilon}_u^{pl}) \tag{3.5}$$

The element's characteristic length for a solid element was taken as the cube root of the integration point volume [34] (which is the same as the element volume for reduced integrated elements). Since the parts in the assembly might have a mesh with varying element size, the characteristic element length was calculated based on the element volume in regions expected to experience material failure. The material failure can be immediate, but this is not recommended, as a sudden drop in stress can result in dynamic instabilities [19]. Tabulating the damage as a function of plastic displacement is therefore more appropriate. The plastic displacement vs. damage variable curve from Pavlovic was adopted for both the bolts and the plates but adjusted for mesh size and relevant plastic strain at failure. An illustration of the stress-strain curve of the material model where "ductile damage" is included, is shown in Figure 3.8.

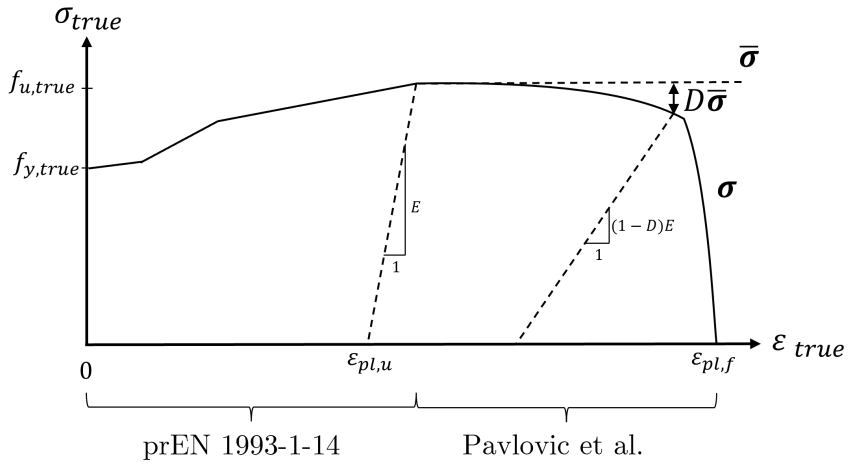

Figure 3.8: Material model with material failure

Finite element mesh

Several factors need to be considered when establishing a finite element model. Primarily, the finite element mesh needs to be able to accurately reproduce the exact solution. A mesh convergence study was therefore carried out before the actual analyses. This consists of a series of analyses where the mesh is gradually refined until a converged solution is obtained. For every analysis, an energy balance check was carried out. This involves comparing the kinetic energy and the artificial strain energy to the internal energy. Artificial strain energy is the energy used to control hourglass deformation (hourglass stiffness is added to reduced integrated elements in Abaqus) [19]. Large values of artificial strain energy indicate that the mesh is too coarse, and changes might be necessary [34]. A rule of thumb is to confirm that the artificial strain energy is ≤ 5 % of the internal energy [35]. If this criterion is satisfied, which it was for all analyses carried out, the mesh can be assumed to be suitable.

Including a "ductile damage" material model has some implications on the choice of mesh. Since the displacement at failure is proportional to characteristic element length, the material input

must be chosen in accordance with element size. Considering that not all elements in a mesh have the same size and aspect ratio, the model becomes slightly mesh sensitive. To reduce the mesh dependency, it is recommended that the aspect ratio of the element is close to one [19]. Another factor to consider when executing an explicit analysis is the length of the time step. To prevent the solution from diverging, Abaqus employs a time step smaller than the critical time step, which is defined by the following equation:

$$\Delta t \leq L_e \sqrt{\frac{\rho}{\hat{\lambda} + 2\hat{\mu}}} \approx L_e \sqrt{\frac{\rho}{E}} \tag{3.6}$$

where $\hat{\lambda}$ and $\hat{\mu}$ are the effective Lamé's constants [19], and ρ is the density of the material. This implies that the characteristic element length, L_e, of the smallest element determines the time step for the whole model throughout the analysis. It is therefore advantageous to avoid elements that are smaller than necessary and to employ elements in regions of interest that are of similar size. In this way, the required computation time of the analysis can be limited to an acceptable level.

Based on the mesh convergence study, acceptable computation time, and common practice [36], it was chosen to discretize the model with four elements over the thickness of all parts and regions expected to be dominated by bending stresses. Two elements over the thickness were applied in regions expected to mainly experience axial stresses. The mesh was created with intent of achieving element aspect ratios close to one in regions expected to experience material failure. The bolts were meshed with a combination of wedge and brick elements, as this allows the elements in the bolt shank to be of similar volume. The mesh used in the analysis is shown in Figure 3.9. Note that mesh density was reduced in areas where high density is not required.

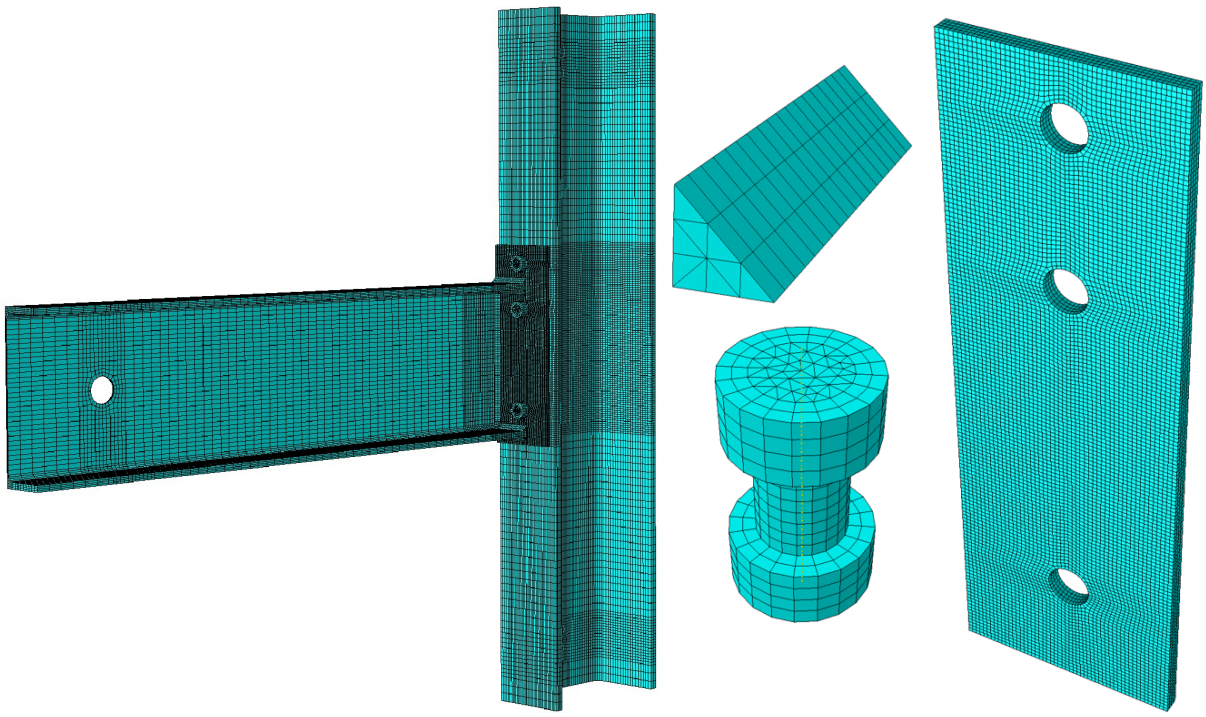

(a) Overview **(b)** Detail of weld, bolt and end-plate

Figure 3.9: Mesh in Abaqus

3.2.3 Component method

The results from the analyses carried out in IDEA StatiCa and Abaqus will be compared to the moment resistance and the initial stiffness calculated according to NS-EN 1993-1-8 [3], and the rotational capacity calculated according to Beg et al. [26]. In the calculations, all material factors for steel were set equal to 1.0, and partial factors for loads were neglected. Instead of applying characteristic values of yield stress for the sections, measured values were employed. For bolts, characteristic material properties were employed. According to Beg et al. [26], it is overly conservative to calculate the capacity of the end-plate and the column flange in bending directly according to NS-EN 1993-1-8 when calculating the rotational capacity. Therefore, it was proposed to replace f_y with $0.9f_u$ in the capacity expressions for end-plate and column flange in bending. This approach was adopted in the subsequent calculations.

3.3 Validation

Three different experimental setups, all conducted by Zhu et al. [29], were chosen as the basis for validation. This includes an experiment with a joint subjected to pure bending and two experiments with joints subjected to a combination of bending and axial force. The experimental characteristics that differ between the setups are listed in Table 3.1.

Table 3.1: Experimental setups [29]

Name	**End-plate thickness [mm]**	**Backing plate thickness [mm]**	**Loading condition**
EP10	10	-	Bending
EP10-T	10	-	Bending and tension
EP20BP20-C	20	20	Bending and compression

3.3.1 Pure bending

The first joint configuration chosen as the basis for validation is the joint with a 10 mm end-plate subjected to pure bending. Figure 3.10 shows the resulting moment-rotation curves from the experiment and the numerical simulation. Additionally, the result from a numerical simulation of a model where progressive damage was not applied is plotted in the same figure. When comparing the numerical curves, it can be seen that the curve corresponding to the model with material failure exhibits some fluctuations. This is caused by material failure and subsequent element removal. In reality, bending-induced cracks form in the extreme fibers and gradually grow in the thickness direction towards the center. In the simulation, the end-plate was discretized with four elements over the thickness, which implies that the cracks will form and grow less gradually. A finer mesh would reduce these fluctuations, as the impact of single elements on the global solution would decrease. Another remedy would be a more accurately defined damage evolution based on material calibrations, as this might reduce the abrupt change in element stresses. However, the overall solution shows good agreement with the physical experiment, and the chosen mesh and damage evolution were therefore not altered in the subsequent analyses.

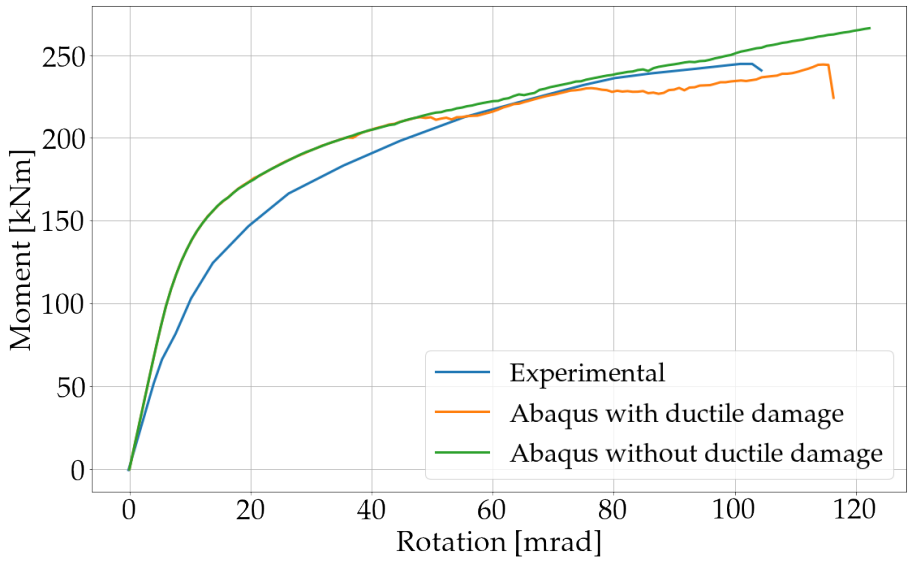

Figure 3.10: Moment-rotation curves for validation of EP10

Figure 3.11 shows contour plots of the von-Mises stresses on the deformed shape of the joint for three points on the moment-rotation curve.

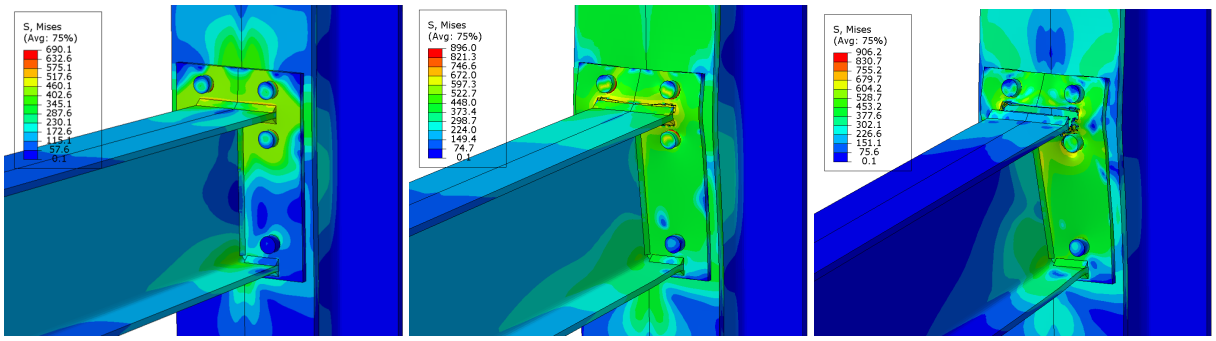

(a) M=163 kNm ($2/3M_{Rd}$) **(b)** M=244 kNm (Maximum moment) **(c)** Post-failure

Figure 3.11: Contour plot of von-Mises stresses on the deformed shape of EP10 (with progressive damage)

3.3.2 Combined bending and tension

The second joint configuration that was chosen is the joint with a 10 mm end-plate subjected to a combination of axial tensile force and bending. In the physical experiment, applying a combination of bending and axial force was done by tilting the column to an angle of $\theta_1 = 34$ °, as shown in Figure 3.12a. In this way, the force applied to the beam consisted of a shear component and an axial component. In an attempt to replicate this experimental setup, the deformation was applied in an external reference point connected to the model using a spring element, as illustrated in Figure 3.12b. This is analogous to applying the force through a rigid bar, pinned and free to rotate on both ends. The length of the load arm was assumed to be 700 mm, based on figures in [29]. Determining the axial force in the beam in the analysis was not straightforward, and the approach for the determination of axial force is explained in Appendix C.

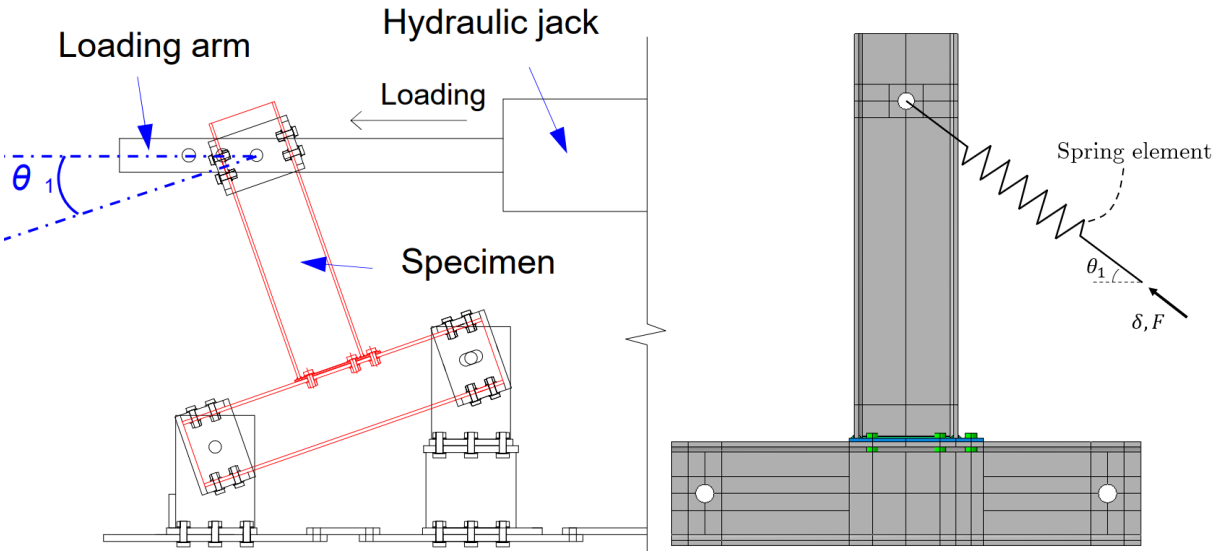

(a) Physical experiment [29] **(b)** Abaqus

Figure 3.12: Combined tensile and bending application

The resulting moment-rotation curves can be seen in Figure 3.13a. Additionally, Figure 3.13b shows the axial force-rotation curves from both the experiment and the simulation.

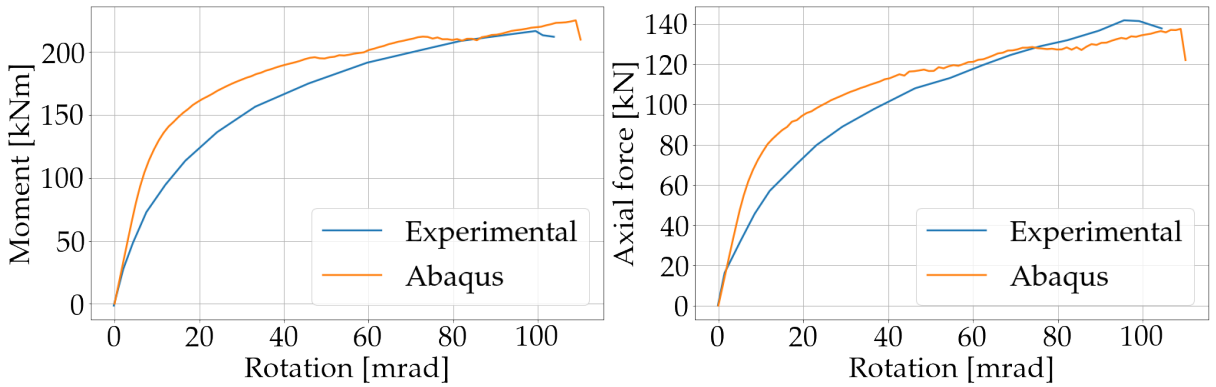

(a) Moment-rotation curve **(b)** Axial force-rotation curve

Figure 3.13: Validation of EP10-T

3.3.3 Combined bending and compression

The last joint configuration chosen as the basis for validation is the joint with a 20 mm thick end-plate and backing plate, subjected to a combination of bending and compressive axial force. As in the case of tensile axial force, the column was rotated to achieve axial force in the beam, but this time to an angle of $\theta_1 = -34°$. In the numerical simulation, the deformation was applied through a spring element to reproduce the combination of axial compressive force and bending. For this joint, the failure mode was buckling of the column web. In a physical experiment, buckling of the column web is initiated by imperfections in the steel section. In Eurocode 3, this is taken care of by introducing a reduction factor for buckling, ρ. However, in a numerical simulation that discretizes the geometry without imperfections, the resistance of the column web is unrealistically high. To overcome this problem, geometric imperfections must be introduced in the numerical simulation. A common approach is to superimpose the buckling shapes as

geometric imperfections on the perfect geometry. This is achieved by first performing a linearized buckling analysis to determine the eigenmodes/buckling shapes, and then applying the buckling shapes as geometric imperfections in the post-buckling analysis. This approach was adopted in the analysis. The amplitude of the imperfection was chosen in accordance with NS-EN 1993-1-5 [2], which states that the amplitude of the imperfection for a plate should be assumed equal to L/200, where L is the shortest span of the plate. For this joint, the amplitude was therefore assumed to be 1.4 mm. With this approach, the resulting resistance will be closer to the resistance achieved in the experiment. In Figure 3.14a the deformed joint from the experiment is shown. The buckling shape from the buckling analysis that resembles this failure mode is displayed in Figure 3.14b. After introducing this buckling shape as geometric imperfection in the analysis, the deformed shape from the post-buckling analysis in Abaqus was obtained, and is shown in Figure 3.14c.

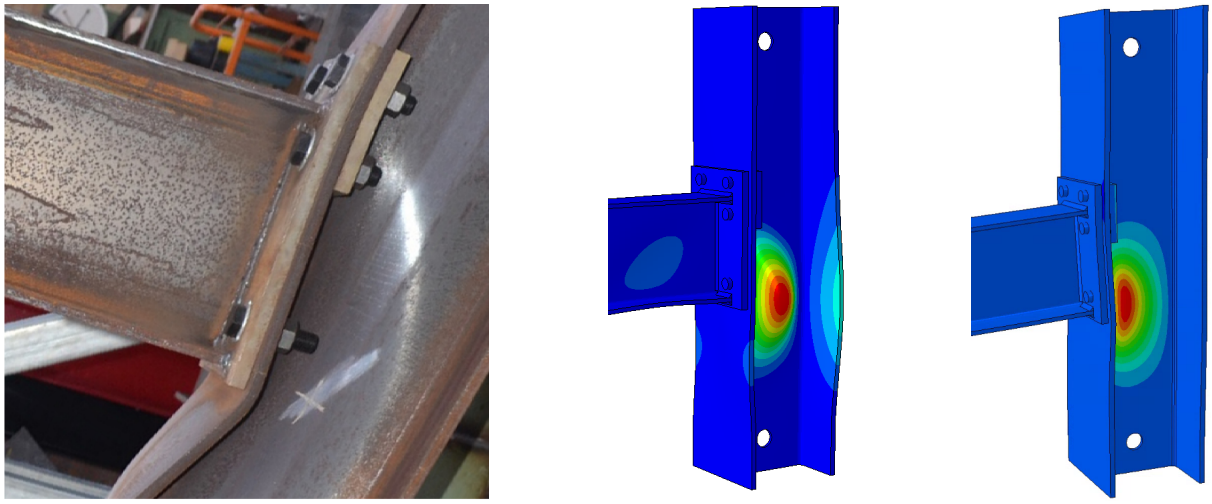

(a) Physical experiment

(b) Eigenmode from Abaqus

(c) Contour plot of out-of-plane deformation at failue

Figure 3.14: Failure of EP20BP-C

The resulting moment-rotation curves and axial force-rotation curves can be seen in Figures 3.15a and 3.15a, respectively. The moment-rotation curve from a simulation of a model without geometric imperfections is plotted in the same figure. This is done to highlight the effect of geometric imperfections in a numerical analysis where buckling is the main failure mode.

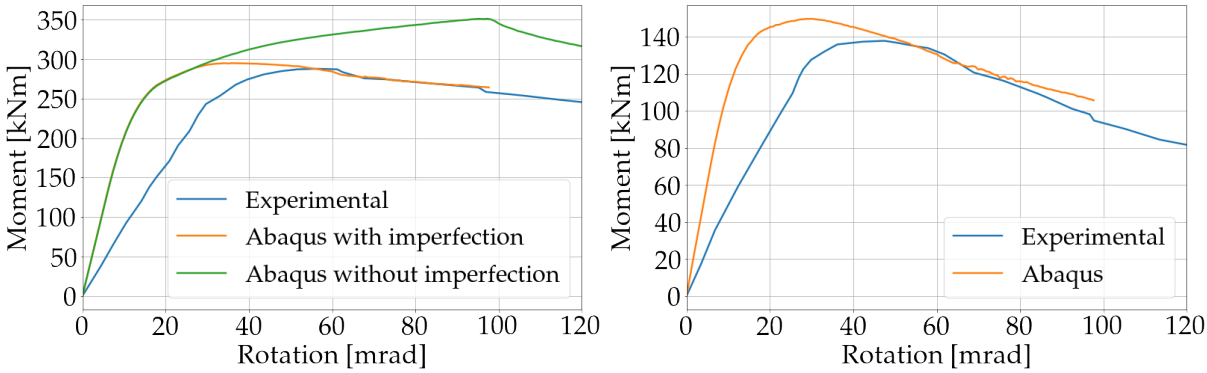

(a) Moment-rotation curve

(b) Axial force-rotation curve

Figure 3.15: Validation of EP20BP-C

3.3.4 Discussion of validation

From the moment-rotation curves, it can be seen that the moment resistance from the simulation agrees very well with the experimental results. The failure mode of joint EP10 and EP10-T was bending of the end-plate, while buckling of the column web was the failure mode in joint EP20BP20-C. The correct failure mode was captured in the numerical simulations. However, there are some discrepancies that will be discussed in the remainder of this section.

Initial stiffness

In opposition to the moment resistance, the initial stiffness exhibits considerable discrepancy between simulation and physical experiment. This can be caused by several factors, which are listed below:

- Measurement error: The measure of displacement and force level in a physical experiment will always contain some error.
- Residual stresses: Hot rolled sections will, due to the uneven cooling rates after rolling, show residual stresses of up to 50 % of the yield stress of the section [37]. Additionally, the welding of plates introduces local residual stresses as large as the section's yield stress. Residual stresses do not affect the capacity of the steel section, but the deformations will be greater for the same force level, than if no residual stresses were present [38]. Due to the residual stresses, parts of the section will yield at low levels of deformation, which causes the effective stiffness of the section to be reduced.
- Experimental setup: The load application in the experiment was not replicated exactly. When the load arm in the experiment pushed the beam, the angle of the load arm, and therefore the load direction, changed. The length of the load arm is uncertain and might influence the joint behavior. Another aspect is the boundary conditions in the experiment. In the simulation, the pinned boundary condition allowed for zero movement, but in the physical experiment, there was possibly some initial movement due to slack in the experimental setup. It is therefore common to include an unloading phase early to accurately capture the rotational stiffness of the joint. However, this was not done in this experiment.

Similar discrepancy in initial stiffness was also experienced in simulations of this experiment carried out by other authors [39]. In Section 3.4, it can be seen that the prediction of initial stiffness according to NS-EN 1993-1-8 and IDEA StatiCa is closer to the initial stiffness obtained

from Abaqus, than to the initial stiffness in the physical experiment. Based on this, it can be assumed that the discrepancy in initial stiffness stems from the nature of the physical experiment, and not from modeling error in Abaqus.

Axial force

The moment resistance from the cases with combined axial force and bending shows good agreement between experimental results and numerical simulations. However, also here the initial stiffness shows some discrepancy between simulation and experiment, especially for the case with compressive axial force. This can to a large extent be ascribed to the same factors as discussed previously.

As seen in Figures 3.13b and 3.15b, the maximum axial force in the simulation of joint EP10-T and EP20BP20-C, show an error of 3 % and 8 %, respectively, compared to their respective physical experiment. This implies that the approach for applying combined bending and axial force agree relatively well with the experiment. It is worth noting that the amplitude of the geometric imperfection affects the resistance of joint EP20BP-C, where larger imperfection implies lower resistance. This is also a source of error between the simulation and the physical experiment.

Rotational capacity

The obtained rotational capacity can be considered adequate for an analysis conducted without material calibration. The approach used in this thesis is uncertain, but for these experimental configurations, it gives a good estimate of the rotational capacity of the joints. In Figure 3.16, the fracture propagation from the physical experiment and the numerical simulation of joint EP10 is shown. The cracks initiated at the toe of the welds close to the bolts, before the cracks grew in the direction of the beam flange. It can be seen that the simulation is able to capture the correct failure mode of the joint, and is in that regard an accurate representation of the physical experiment. However, using this approach in other experiments with other failure modes might not yield the same acceptable results.

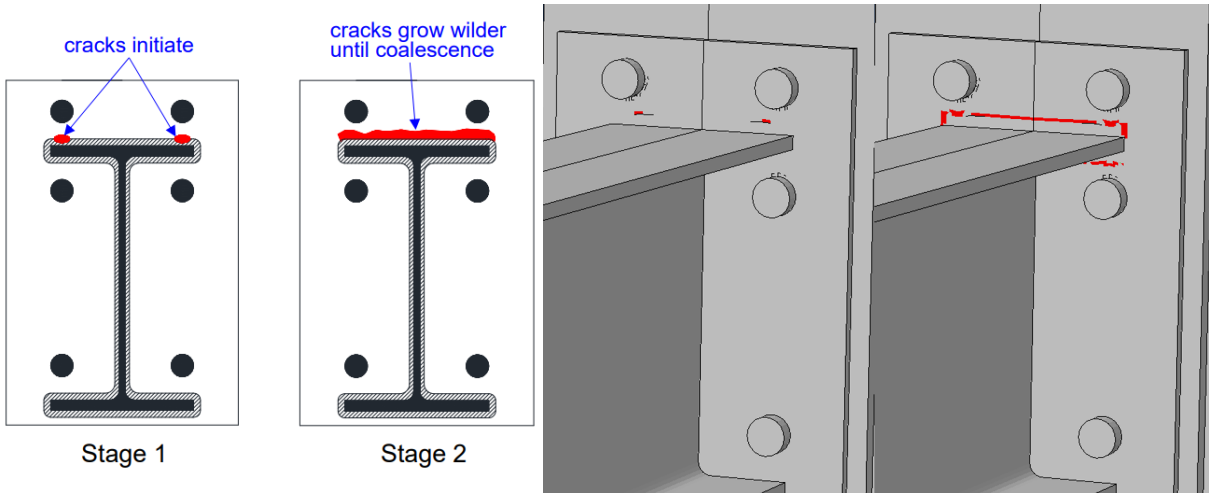

(a) Crack growth in physical experiment [29]

(b) Contour plot of elements exhibiting zero stresses (cracks) in Abaqus at fracture initiation and failure of the joint.

Figure 3.16: Failure mode and crack growth of joint EP10

3.4 Verification

In order to compare the results from numerical simulations in Abaqus to IDEA StatiCa, it was chosen to adopt a similar material model in Abaqus as in IDEA StatiCa (shown in Figure 3.8). The material model has the same yield plateau slope as in IDEA StatiCa, but with the added "ductile damage" material model to simulate material failure. The onset of damage is assumed to occur similarly as for the material model described in Section 3.2.2. It is important to acknowledge that this approach is not meant to simulate the actual behavior of the material. The intent is to establish a numerical model that is comparable to the model in IDEA StatiCa, while also being somewhat true to real-world behavior. If a progressive damage material model is not applied, the moment level would be constantly increasing, with no clearly defined moment resistance. By applying a material model with "ductile damage", it is possible to obtain quantities that can be compared to IDEA StatiCa.

The manual calculations based on NS-EN 1993-1-8 [3], Sokol et al., [25] and Beg et al. [26] were performed in Maple and are presented in Appendix D for the joint configuration EP10-T. The capacity and stiffness of each component, and the resulting moment resistance and initial stiffness, are listed in Table 3.2. The deformation capacity of each relevant component, and the resulting total rotational capacity, are shown in Table 3.3.

Table 3.2: Calculations for joint EP10-T according to NS-EN 1993-1-8

	Component	**Capacity row 1 [kN]**	**Capacity row 2 [kN]**	**Capacity group [kN]**	**Stiffness coefficient[1] [mm]**
Shear	Column web in shear	-	-	965.5	4.72 mm
Tension	Column web in tension	848.9	848.9	956.0	5.71
	Column flange in bending	403.0	403.0	703.3	4.75
	End-plate in bending	**184.8**	**267.0**	**451.8**	4.06/1.52
	Beam web in tension	-	-	906.4	∞
	Bolts in tension	-	-	1017	14.1
Compression	Column web in compression	-	-	571.9	5.95
	Beam flange in compression	-	-	1242	∞
Joint	Moment resistance	118.8 kNm			
	Initial stiffness	24100 kNm/rad			

[1] Stiffness coefficient per row in tension. See Appendix D for full calculation.

Table 3.3: Deformation capacity of joint EP10 and EP10-T after [26]

Component	**Deformation capacity**
Column web in shear	40.42 mm
Column web in tension	24.42 mm
Column flange T-stub	20.74 mm
End-plate T-stub	12.42 mm
Column web in compression	5.13 mm
Rotational capacity	51.3 mrad

For joint EP10, the moment-rotation curves from numerical simulations in IDEA StatiCa and Abaqus, and calculations according to Eurocode 3 are shown in Figure 3.17. The moment-rotation curve from the Abaqus simulation with the "real" material model (described in Section 3.2.2) is also included in the figure, to emphasize the difference between the material models. Based on the mesh convergence study, the maximum element size in IDEA StatiCa was chosen to be 6 mm. Additionally, the result from a model with a maximum element size equal to 18 mm is plotted in the same figure. To investigate the effect of the plastic strain limit in IDEA StatiCa, analyses with limit plastic strain of 5 %, 10 %, 20 %, and 30 % were carried out, and the results are plotted in Figure 3.17 as well.

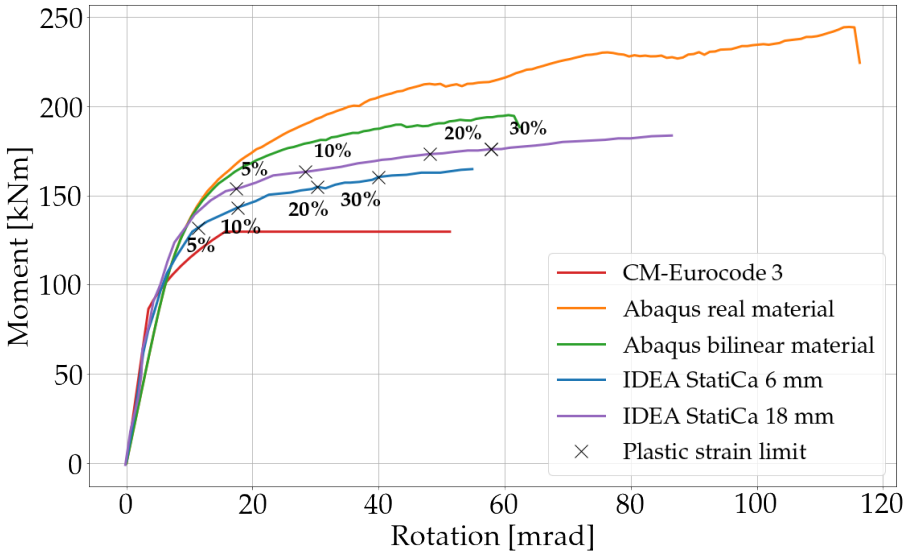

Figure 3.17: Moment-rotation curves for verification of EP10

"Abaqus real material" is described in Section 3.2.2, while "Abaqus bilinear material" is the idealized material model resembling IDEA StatiCa's material model. "IDEA StatiCa 6 mm" and "IDEA StatiCa 18 mm" are the results from IDEA StatiCa with element sizes 6 mm and 18 mm, respectively. The 'X' on the curves marks the point where the plastic strain in the plates reaches 5, 10, 20, and 30 %, respectively. "CM-Eurocode 3" are the results from calculations based on the component method, which is applied in Eurocode 3.

In the subsequent IDEA StatiCa analyses, a maximum element size of 6 mm, and a limit of plastic strain equal to 20 % were adopted. The moment-rotation curves for the joint EP10-T and EP20BP20-C are shown in Figures 3.18a and 3.18b, respectively. The analysis results from Abaqus were obtained from a model where the bilinear material model was applied.

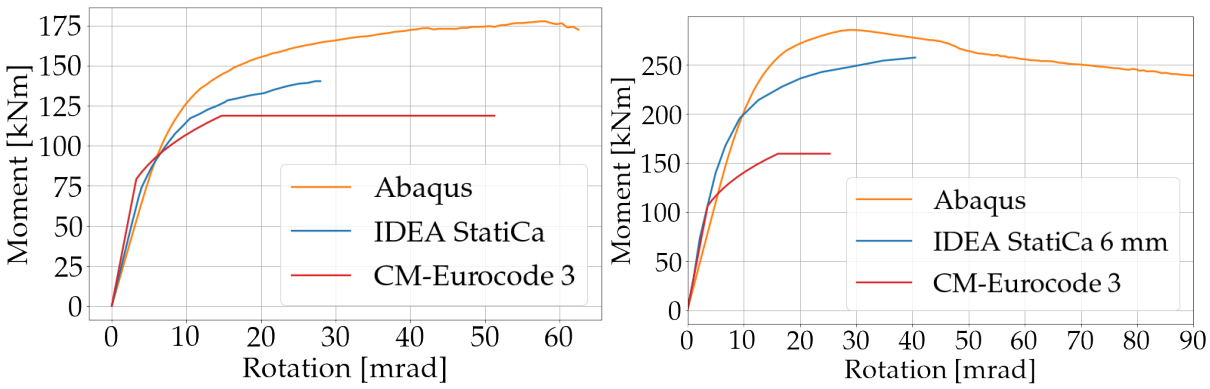

(a) EP10-T **(b)** EP20BP20-C

Figure 3.18: Moment-rotation curves for combined bending and axial force

3.4.1 Discussion of verification

The moment-rotation curves from the verification demonstrate that the moment resistance determined from the analyses in IDEA StatiCa is lower than the resistance determined from Abaqus, but higher than the resistance according to the component method and Eurocode 3. From an engineering point of view, this is not problematic. While the design in IDEA StatiCa results in structures with conservative predictions of resistance, it also allows for the possibility of less material use than when designing according to Eurocode 3. The initial stiffness, on the other hand, agrees quite well for the three methods. The rotational capacity is underestimated by IDEA StatiCa for joint EP10 and EP10-T when applying a limit of plastic strain equal to 20 %. For joint EP20BP, however, the rotational capacity is overestimated by IDEA StatiCa. The cause of the discrepancies, and other key takeaways from these results, are discussed in the following paragraphs.

Material model

In an attempt to replicate the model in IDEA StatiCa, the Abaqus model adopted the same bilinear material model as IDEA StatiCa. Preliminary analyses in Abaqus showed that limiting the resistance to a defined plastic strain resulted in overly conservative predictions of resistance. For example, limiting the moment resistance to a plastic strain of 20 % would, for the case of the "real" material model in Figure 3.17, result in a moment resistance of 201 kNm, i.e. a 17 % underestimation. The "ductile damage" material model was therefore incorporated to obtain a model that is somewhat true to real-world behavior, while simultaneously being comparable to the model in IDEA StatiCa. While this material model makes it possible to obtain a clearly defined moment resistance, it fails to accurately predict the rotational capacity when applying the simplified bilinear material law. The damage evolution adopted from Pavlovic et al. [31] yields relatively accurate results only when the complete piecewise linear material model from prEN 1993-1-14 [20] is adopted. Nonetheless, applying this material model is advantageous as it enables obtaining a clearly defined moment resistance.

Applying the simplified bilinear material model from IDEA StatiCa in Abaqus, as opposed to the material model from prEN 1993-1-14, results in a significant decrease in moment resistance. Applying a more realistic material model in IDEA StatiCa would therefore presumably yield results closer to that obtained from physical experiments. However, in a design phase where only the characteristic yield stress of the steel is known, conservative predictions of structural resistance are generally more important than accurate predictions.

Additionally, the moment-rotation curves from Abaqus presented in Figure 3.17 demonstrate that the simplified material model adopted in IDEA StatiCa is not the only source of discrepancy; employing the bilinear material model in Abaqus, instead of the "real" material model (from prEN 1993-1-14 [20]), reduces the discrepancy between IDEA StatiCa and Abaqus, but does not eliminate it.

Limit of plastic strain

One of the main parameters that must be established prior to an analysis, is the limit of plastic strain. As seen in Figure 3.17, this parameter has a significant influence on the rotational capacity. Nonetheless, applying a limit of plastic strain equal to 20 % yields conservative predictions of rotational capacity for the joints where bending of the end-plate was the governing failure mode (joint EP10 and EP10-T). The influence of the limit of plastic strain on the moment resistance is less significant. This is because the joint has started to yield, and increasing the deformation

will not significantly increase the force level. Setting the limit of the plastic strain equal to 5 %, which is in accordance with NS-EN 1993-1-5, will in this case yield highly conservative results, as the joint has not fully entered the yielding plateau. If measured values of the ultimate strain are available, it is possible to apply a higher limit in the analyses. For this reason, a limit of 20 % was applied in the subsequent analyses.

Mesh density

Another factor to consider when conducting analyses in IDEA StatiCa is the mesh density. Figure 3.17 illustrates that the mesh size influences the resulting moment resistance. When using an element size equal to 18 mm, the moment resistance was overestimated by 9-16 % (depending on the applied limit of plastic strain) compared to a model with an element size of 6 mm. The mesh dependency will also be dependent on the governing failure mode, as some failure modes exhibit a higher degree of mesh sensitivity. It is therefore wise to conduct a simplified mesh convergence study, to examine whether the mesh size has a significant effect on the resulting resistance, especially if the design moment is close to the calculated moment resistance. The default element size of 20 mm should not be assumed to yield accurate and conservative results for all structures and failure modes.

Buckling and geometric imperfections

The moment resistance of joint EP20BP20-C predicted by IDEA StatiCa is lower than that obtained from Abaqus. However, IDEA StatiCa fails to capture the correct failure mode. According to IDEA StatiCa, the plastic strain in the web of the column due to compressive force is the governing failure mode. Contrarily, in the physical experiment and the Abaqus simulation, the governing failure mode is buckling of the column web. In Abaqus, the maximum plastic strain when the moment resistance is reached (i.e. the extreme point on the moment-rotation curve) is under 10 %, which implies that buckling occurs for strains well below the ultimate strain. Since IDEA StatiCa fails to capture buckling of the column web, it also overestimates the rotational capacity for joint EP20BP20-C. To explore the effect of geometric imperfections on the joint, a simulation of the same joint, but without geometric imperfections applied, was carried out in Abaqus. The resulting moment-rotation curve from this simulation is also shown in Figure 3.15a. This demonstrates that excluding geometric imperfections will overestimate the moment resistance by 23 %.

As mentioned in Section 2.1.5, IDEA StatiCa employs a geometrically linear analysis without geometric imperfections. To consider the possibility of buckling, the software offers buckling analysis. However, it is uncertain what buckling factor constitutes a joint not susceptible to buckling. For a plastic analysis, NS-EN 1993-1-1 [1] states that geometrically linear analysis (first-order) can be performed if the critical load is more than 15 times the design load. Otherwise, the increase in load effects from the deformation of the joint must be taken into account through a geometrically nonlinear analysis (second-order). This condition is applicable for a global analysis, presumably with bar and beam elements. The theory manual for IDEA StatiCa [15], on the other hand, states that plate buckling in joints does not need to be considered if the buckling factor is higher than 3 when applying the design loads. For joints with a buckling factor lower than 3, the theory manual refers to NS-EN 1993-1-5 [2], which proposes the "reduced stress method" for determination of the resistance of plates susceptible to buckling. This includes calculating the plate slenderness, λ_p, which is given by the following equation:

$$\lambda_p = \sqrt{\frac{\alpha_{ult}}{\alpha_{cr}}} \tag{3.7}$$

where α_{ult} is the minimum load amplifier for the design loads to reach the characteristic value of resistance of the most critical point of the plate, and α_{cr} is the minimum load amplifier for the design loads to reach the elastic critical load (i.e. the lowest buckling factor). The slenderness is used to calculate the reduction factor, ρ, which reduces the resistance of the joint accordingly (ρ is given in Annex B of NS-EN 1993-1-5). The buckling factor obtained in IDEA StatiCa when applying the limit load is equal to 5.26. However, this buckling factor does not result in a reduction in resistance, even though the failure mode of this joint is proven to be buckling of the column web. The reduction factor for the component column web in compression according to NS-EN 1993-1-8 [3] is for the joint EP20BP20-C equal to 0.84. This implies that the "reduced stress method" in NS-EN 1993-1-5 does not capture the same reduction in resistance due to buckling, as the expression in NS-EN 1993-1-8 does.

When conducting a buckling analysis in Abaqus with the limit load of the post-buckling analysis (which includes geometric imperfections), a buckling factor of 4.9 is obtained. This further illustrates that even joints with a buckling factor higher than 3 might have their resistance limited by plate buckling. Figures 3.19a and 3.19b show the first buckling shape with the corresponding buckling factor obtained from the analyses in Abaqus and IDEA StatiCa, respectively. The discrepancy between the buckling factors is mainly due to different magnitudes of applied loads. The buckling shapes, on the other hand, agree well.

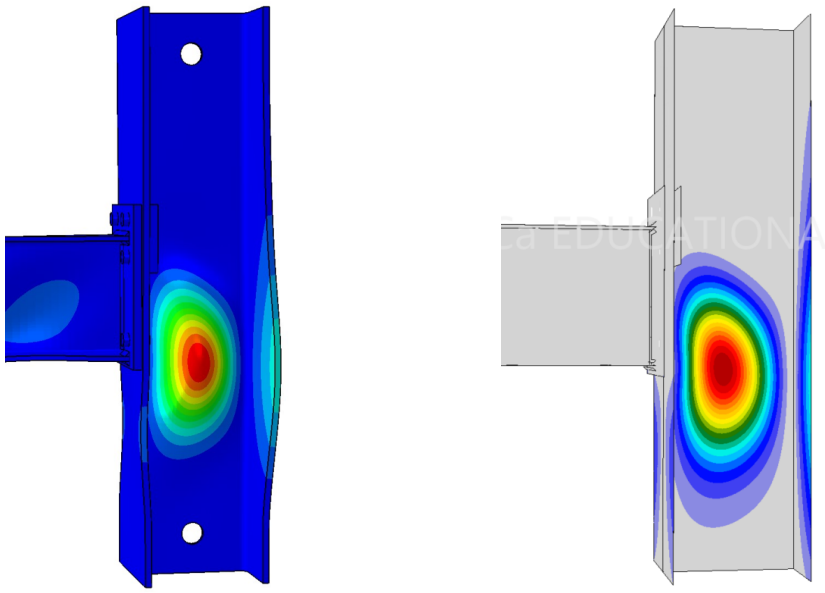

(a) Abaqus: 4.9 **(b)** IDEA StatiCa: 5.26

Figure 3.19: Buckling shapes and respective buckling factors for joint EP20BP20-C when applying the limit load

Geometric nonlinearity

For all the joints considered, IDEA StatiCa underestimates the moment resistance compared to the analysis results obtained from Abaqus. Determining the cause of the underestimation is not straightforward, as the theory manual for IDEA StatiCa is rather limited. IDEA Statica's use of plate elements and spring elements - as opposed to solid elements - is presumably not the cause of the discrepancy, as other authors have proven that bolted beam-to-column joints can accurately be simulated with models discretized with plate elements [40]. The underestimation might be caused by the solution method implemented in the software. IDEA StatiCa employs a

geometrically linear analysis, meaning that the stiffness is not a function of the displacements. While this implies shorter computation time, it also implies that the *geometric stiffness* is neglected. To accurately analyze certain structures, such as cables, it is absolutely necessary to include geometric nonlinearity as the stiffness is highly dependent on the deformation. Other structures, such as bolted joints, are possible to analyze without including geometric nonlinearity. As discussed in Section 3.4.1, neglecting geometric nonlinearity implies that buckling cannot be reproduced, which might overestimate the resistance. However, when neglecting geometric stiffness, the resistance might also be underestimated. When the joint is loaded, the bending stresses in the end-plate will partly be replaced by membrane stresses as the opening between the end-plate and the column give rise to membrane forces in the end-plate. When neglecting geometric nonlinearity, the end-plate will only experience bending stresses, as the deformation does not influence how the loads are carried. This is illustrated in Figure 3.20. Since the end-plate section has lower resistance in pure bending than in tension, the resistance of the joint will be reduced by not including geometric nonlinearity. Similar effects might occur for other components as well, and the neglect of geometric nonlinearity might be a factor contributing to the underestimation of the resistance.

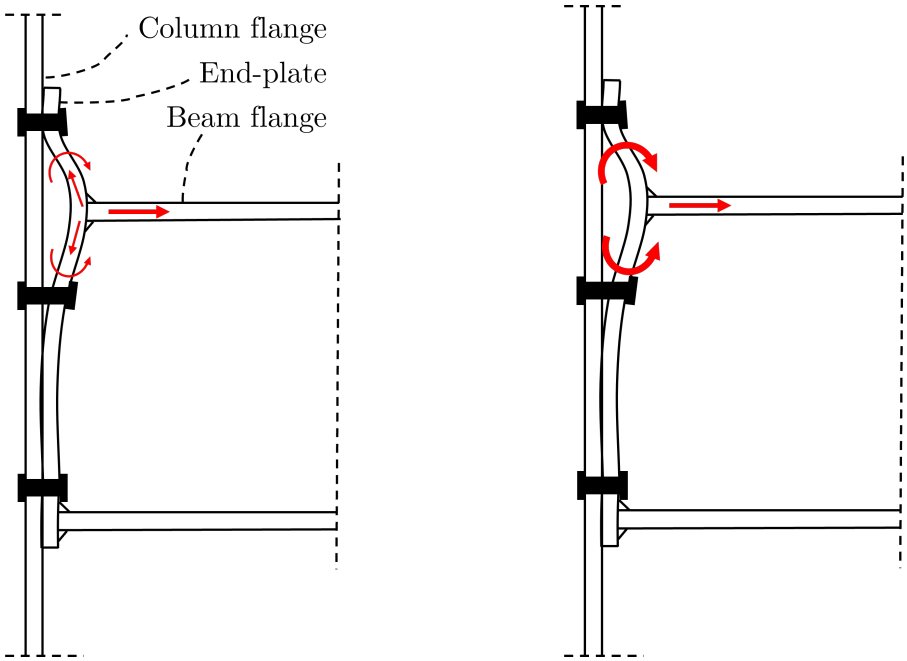

(a) Geometrically nonlinear analysis

(b) Geometrically linear analysis

Figure 3.20: Load bearing in tension zone of end-plate

Component method

The manual calculations based on the component method from Eurocode 3 yield a lower moment resistance than both IDEA StatiCa and Abaqus. However, the capacity formulas in Eurocode 3 are based on a series of simplifications and conservative assumptions, and will in general underestimate the resistance of most structures. For these joint configurations, the underestimation is especially significant. The fact that IDEA StatiCa overestimates the resistance compared to Eurocode 3 can therefore be assumed to be unproblematic. The expressions for rotational capacity by Beg et al. [26] yield conservative predictions compared to the numerical results obtained from Abaqus when bending of the end-plate is the governing failure mode (EP10 and

EP10-T). When buckling of the column web is the governing failure mode (EP20BP20-C), the expressions yield relatively accurate predictions of rotational capacity.

3.5 Parametric study

To further explore how IDEA StatiCa captures the behavior of major axis bolted joints, a parametric study is carried out. The parameters that are explored are level of axial force, end-plate thickness, column flange thickness, bolt diameter, and weld throat size. The base model for the parametric study is similar to the joint EP10, described in Section 3.1, but with certain changes in geometry or load conditions. The geometrical parameters of the joint will be varied, but if nothing else is specified in the following parametric study, the model has an end-plate thickness of 15 mm, column flange thickness of 15.4 mm, M24 bolts, and flange weld throat thickness equal to 8 mm. The analysis results obtained from IDEA StatiCa are compared to the results obtained from Abaqus analyses and manual calculations based on Eurocode 3.

Since IDEA StatiCa is primarily a design tool, it is not intended to reproduce the behavior of joints exactly. To ensure that the discrepancies between IDEA StatiCa and Abaqus are not mainly due to different material models, it is chosen to carry out the analyses in Abaqus with the same bilinear material model as described in Section 3.4. The purpose of this study is therefore to uncover to what extent IDEA StatiCa captures the same failure mode as Eurocode 3 and Abaqus, and whether IDEA StatiCa yields conservative predictions of resistance and stiffness. The analyses carried out in Abaqus are therefore not meant to reproduce the physical behavior of the joint. Instead, the model in Abaqus should be considered as a more accurate reproduction of the same idealized model adopted in IDEA StatiCa.

Section 3.4 shows that the rotational capacity calculated in IDEA StatiCa is highly dependent on the chosen limit of plastic strain. While the simplified material model applied in Abaqus makes it possible to obtain a clearly defined moment resistance, it fails to accurately predict the rotational capacity. The rotational capacity is the joint characteristic that is hardest to determine from simulations and calculations, and it is usually also the least important quantity to determine in a design process. It was therefore deemed less relevant to compare the rotational capacities, and it is chosen to only compare moment resistance and initial stiffness in the parametric study.

In the parametric study, the absolute value of moment resistance and initial stiffness is compared instead of the full moment-rotation curves. This permits easier comparison between the calculation methods, and determining the absolute value of resistance and stiffness is in general more important for an engineer than obtaining the whole moment-rotation curve. The initial stiffness from the Abaqus simulations is defined as the ratio between the moment and rotation at 2/3 of the moment resistance, i.e. the *secant stiffness* at 2/3 of the moment resistance. This is illustrated in Figure 3.21, and is consistent with how IDEA StatiCa determines the initial stiffness. Eurocode 3, on the other hand, assumes that the behavior of the joint is linear-elastic up to 2/3 of the moment resistance.

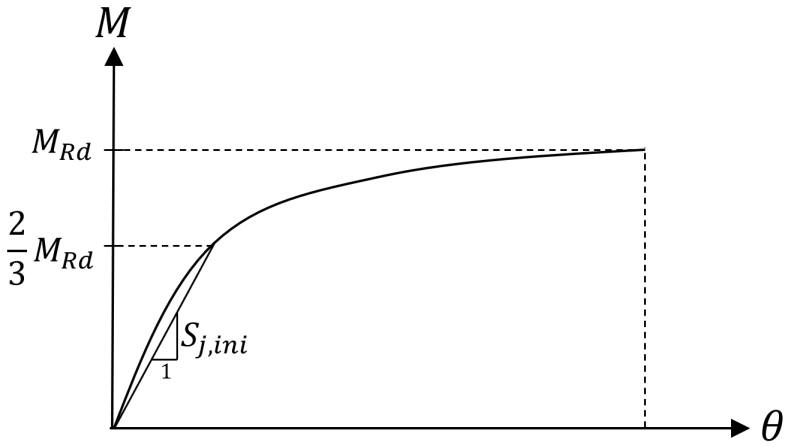

Figure 3.21: Determination of initial stiffness in IDEA StatiCa and Abaqus

In Abaqus, the joints were in general modeled without the utilization of symmetry, i.e. the whole joint was modeled. This was done as the failure mode was uncertain, and utilizing symmetry prevents buckling of the column web from occurring. The exception was the joints with a 10 mm end-plate loaded in tension, as the failure mode is proven to be bending of the end-plate. These joints were in Abaqus modeled with the utilization of symmetry, as shown in Figure 3.4.

3.5.1 Axial force

The ratio between applied moment and normal force in the beam is the first parameter to be explored. Seven different M/N-ratios applied to joints with two different end-plate thicknesses (10 mm and 15 mm) were analyzed and calculated. The approach for applying axial force was similar to the one explained in Section 3.3.2, but with a different angle for the load arm. However, it proved difficult to maintain a constant eccentricity, $e = M/N$, during the load application in Abaqus. As the simulation was deformation-controlled, and not load-controlled, the stiffness of the joint and length of the load arm determines how the eccentricity changes throughout the load application. It was therefore chosen to calculate the eccentricity acting at failure in the Abaqus simulation, and apply this in IDEA StatiCa and the manual calculations. Whether the bending moment and axial force are applied proportionally or not will affect the initial stiffness to some degree, but not the moment resistance (assuming the joint does not fail from axial force or moment acting alone).

The resulting moment resistance and initial stiffness of the joints with 10 mm and 15 mm end-plate are shown in Figures 3.22 and 3.23, respectively. Two sets of analyses were carried out in IDEA StatiCa: one with a limit of plastic strain equal to 5 %, and one with a limit of plastic strain equal to 20 %. In the plot for the moment resistance, the governing failure mode from simulations and calculations are illustrated as well. The failure mode "beam flange in tension" is the exceedance of the tensile capacity of the beam flange. This implies that the resistance of the joint is in fact limited by the beam's cross-sectional capacity, and the joint is a "full strength joint" (according to the terminology in NS-EN 1993-1-8). The failure occurs where the beam is connected to the end-plate, as the moment is largest here.

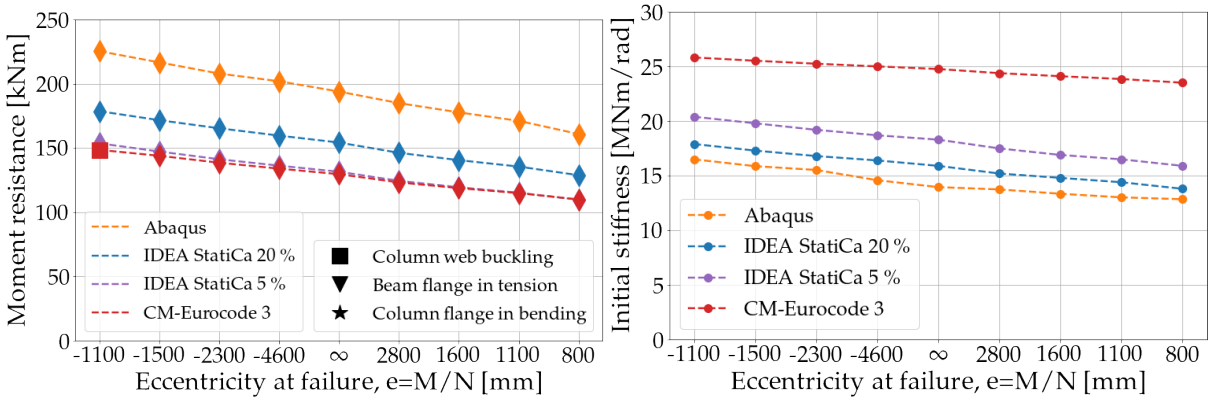

(a) Moment resistance **(b)** Initial sitffness

Figure 3.22: Parametric study with varying axial force (10 mm end-plate)

"IDEA StatiCa 20 %" and "IDEA StatiCa 5 %" are the results from analyses carried out in IDEA StatiCa with a limit of plastic strain equal to 20 % and 5 %, respectively. Eccentricity $e = \infty$ implies that no axial force acts on the joint.

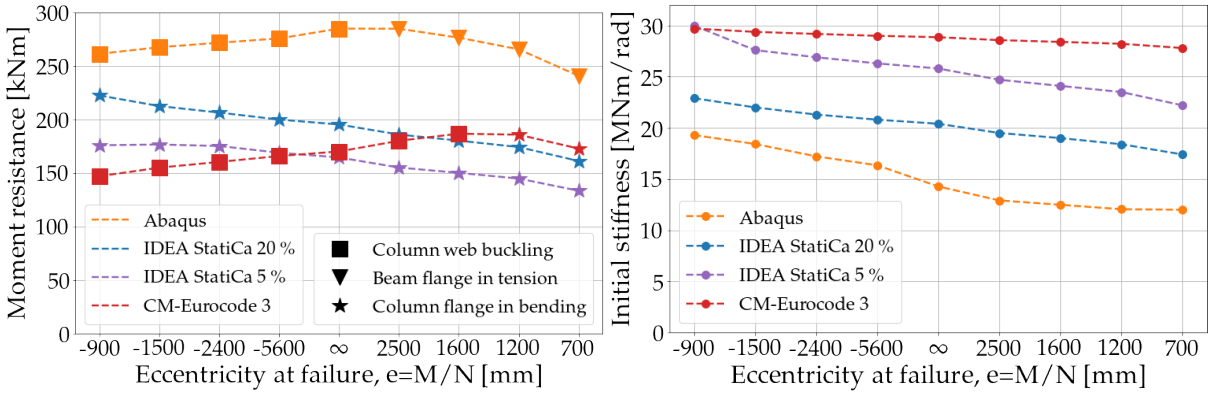

(a) Moment resistance **(b)** Initial sitffness

Figure 3.23: Parametric study with varying axial force (15 mm end-plate)

3.5.2 End-plate thickness

To further explore IDEA StatiCa, a parametric study with varying end-plate thickness is carried out. A total of five analyses with end-plate thickness equal to 10 mm, 12.5 mm, 15 mm, 17.5 mm, and 20 mm were carried out. The joint configuration is otherwise identical to joint EP10 (Table 3.1). For the remaining simulations and calculations, bending is the only load effect acting on the joints, and the analyses in IDEA StatiCa are carried out with a limit of plastic strain equal to 20 %. The resulting resistance and initial stiffness from simulations and calculations are shown in Figures 3.24a and 3.24b, respectively.

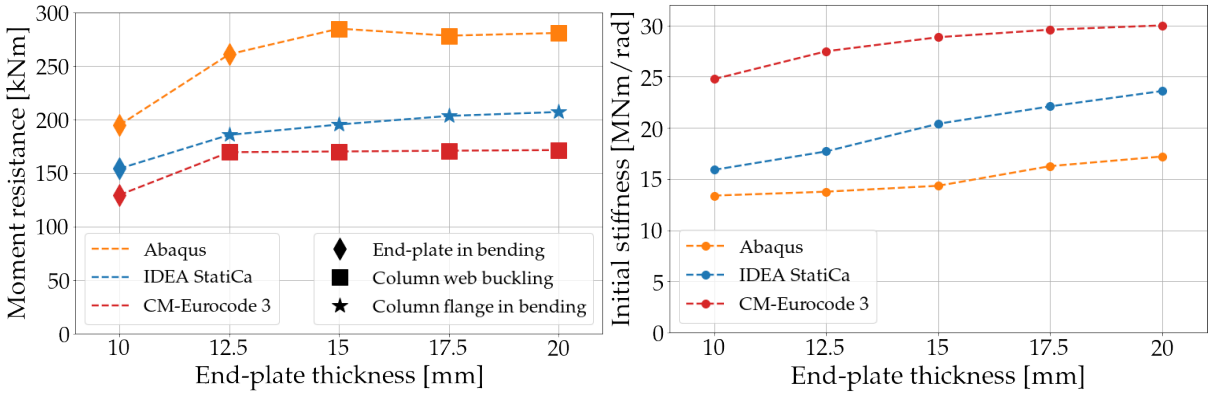

(a) Moment resistance **(b)** Initial sitffness

Figure 3.24: Parametric study with varying end-plate thickness

3.5.3 Column flange thickness

The next parameter to consider is the thickness of the column flange. A total of four analyses with column flange thicknesses equal to 15.5 mm, 14.5 mm, 13.5 mm, and 12.5 mm were carried out. The resulting moment resistance and initial stiffness from simulations and calculations are shown in Figures 3.25a and 3.25b, respectively.

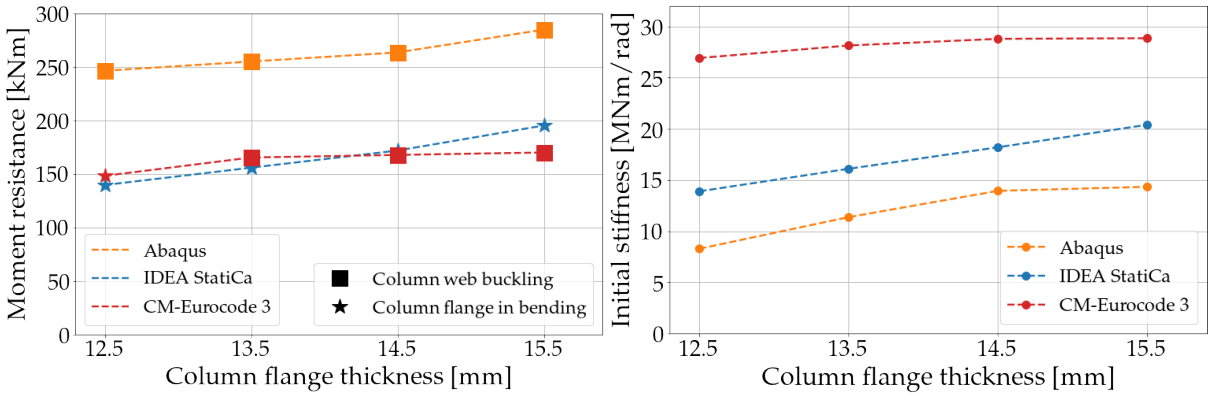

(a) Moment resistance **(b)** Initial sitffness

Figure 3.25: Parametric study with varying column flange thickness

The failure mode in Abaqus is a combination of column web buckling and yielding of column flange. This is why the resistance is lower for smaller column flange thickness.

3.5.4 Bolt diameter

The next parameter of interest is the bolt dimension. Two additional analyses with bolt diameters of 16 mm and 20 mm were carried out. The resulting moment resistance and initial stiffness from simulations and calculations are shown in Figures 3.26a and 3.26b, respectively.

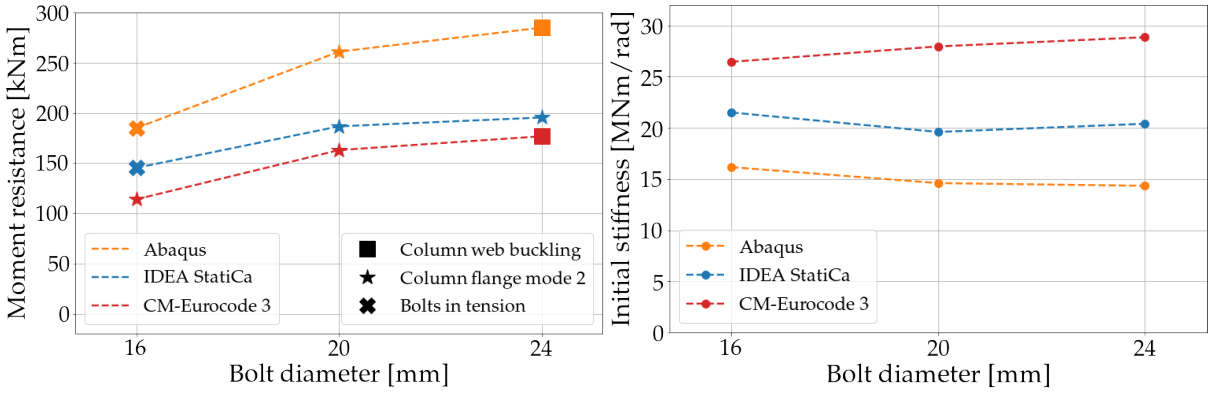

(a) Moment resistance **(b)** Initial sitffness

Figure 3.26: Parametric study with varying bolt dimensions

"Column flange mode 2" is the failure mode involving bolt failure with yielding of the column flange [3]. "Bolt in tension" is a pure fracture of the bolts, corresponding to mode 1 [3].

3.5.5 Weld throat thickness

The next and final joint parameter to explore in the parametric study of the major axis joint is the throat thickness of the flange weld. Two more analyses with flange weld throat thickness equal to 6 mm and 4 mm were carried out. The throat thickness of the web weld was kept constant at 5 mm. The results are shown in Figures 3.27a and 3.27b for the moment resistance and initial stiffness, respectively.

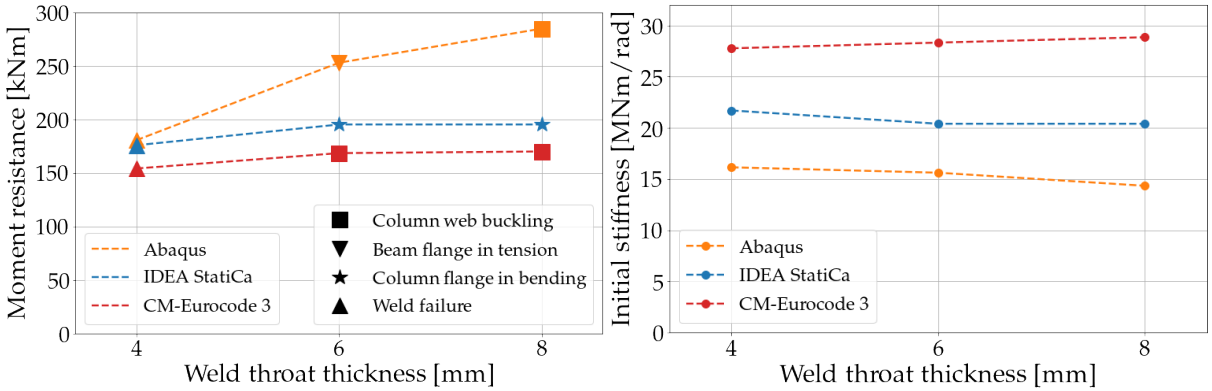

(a) Moment resistance **(b)** Initial sitffness

Figure 3.27: Parametric study with varying weld throat thickness

3.5.6 Discussion of parametric study

Moment resistance

The parametric study demonstrates that, when applying a limit of plastic strain equal to 20 %, IDEA StatiCa in most cases overestimates the moment resistance compared to Eurocode 3. On the other hand, applying a limit of plastic strain equal to 5 % yields a moment resistance much closer to, and in some cases smaller than, the moment resistance predicted by Eurocode 3. This is illustrated in Figures 3.22a and 3.23a. Nonetheless, the moment resistance obtained from IDEA StatiCa is in all cases smaller than the resistance obtained from analyses in Abaqus, and can therefore be considered safe compared to real-world behavior. This demonstrates that

applying a limit of plastic strain equal to 20 % is conservative, despite the moment resistance, in general, being overestimated compared to Eurocode 3.

The observant reader will notice a curious relationship in Figure 3.24a. According to the simulations carried out in Abaqus, a smaller resistance is obtained for a joint with end-plate thickness equal to 17.5 mm and 20 mm, than for a joint with a 15 mm end-plate. The fact that Abaqus predicts a reduction in resistance when buckling of the column web is the failure mode is likely caused by how the geometric imperfections are included in the analysis. Increased end-plate thickness implies that the compressive force from the beam flange is distributed over a larger area of the web. The buckling shape used to introduce geometric imperfections, which is shown in Figure 3.19a, will therefore extend over a larger area. The increase in the area affected by geometric imperfections is presumably the source of the reduction in resistance. However, the reduction is negligible, and this phenomenon will not be further considered.

Initial stiffness

When it comes to the prediction of initial stiffness, the situation is different. While IDEA StatiCa yields higher estimates for initial stiffness than Abaqus, the initial stiffness determined according to Eurocode 3 is in general significantly larger than that obtained from both Abaqus and IDEA StatiCa. However, the initial stiffness from analyses, which is defined as the secant stiffness at 2/3 of the moment resistance (Figure 3.21), is expected to show a large deviation compared to the initial stiffness determined according to Eurocode 3. Eurocode 3 assumes linear behavior up to 2/3 of the moment resistance, while in reality, the moment-rotation curve will exhibit curvature before reaching this point. Eurocode 3 will therefore, in general, overestimate the initial stiffness compared to that obtained from analyses. Furthermore, applying a limit of plastic strain equal to 5 % in IDEA StatiCa yields higher initial stiffness than when applying a limit equal to 20 % (Figures 3.22b and 3.23b). This demonstrates that the procedure for defining initial stiffness can yield somewhat misleading results.

When considering the moment-rotation curves in Section 3.4, it seems as if the initial stiffness determined from analyses and according to Eurocode 3 agree well. The deviation between the numerical analyses and the manual calculations arises mainly from the definition of initial stiffness in IDEA StatiCa. Part of the deviation between IDEA StatiCa and Abaqus can also be ascribed to the method of defining the initial stiffness, as higher post-yielding resistance (i.e. the increase in the moment after yielding has initiated) results in a lower prediction of initial stiffness. This can be seen in Figure 3.26b, where the initial stiffness according to Abaqus and IDEA StatiCa is higher for a joint with a bolt diameter equal to 16 mm, than for a joint with 20 mm bolts. A similar situation can be seen in Figure 3.27b, where smaller welds yield higher initial stiffness. In both cases, the increase in initial stiffness is caused by a decrease in post-yielding capacity. To avoid these somewhat misleading results, the initial stiffness could be defined as the slope at the very beginning of the moment-rotation curve. This would presumably reduce the deviation in initial stiffness, but this approach was not adopted as this is not in line with how IDEA StatiCa determines initial stiffness. Furthermore, joints are normally subjected to a combination of permanent and variable loads. The exhibited stiffness of a joint already subjected to permanent loads is not equal to the initial slope of the moment-rotation curve. Defining the rotational stiffness as the secant stiffness at 2/3 of the moment resistance is therefore arguably more appropriate.

Failure mode

Determining the governing failure mode of a joint is useful, as it can confirm that the finite element model is an accurate representation of the physical problem. Additionally, determining the correct failure mode can be important in a design process, as it makes it possible to determine what part of a joint needs to be strengthened in order to increase the joint resistance. Figures 3.22a, 3.23a, 3.24a, 3.25, 3.26a, and 3.27a demonstrate that the three calculation methods more often than not disagree on what the governing failure mode is. IDEA StatiCa frequently disagrees with both Eurocode 3 and Abaqus on what the critical component is. In most cases, this will be unproblematic, as IDEA StatiCa's predictions of moment resistance are lower than that obtained from Abaqus. Additionally, the difference in the components' resistance is often small, making it difficult to capture the correct failure mode. What is most problematic is that IDEA StatiCa fails to capture buckling of the column web. This is because IDEA StatiCa does not include geometric imperfections or nonlinearity in the analysis, as discussed in Section 3.4.1. This implies that IDEA StatiCa's prediction of moment resistance for the joint with a 15 mm end-plate increases for larger levels of compressive axial force in the beam. However, according to Eurocode 3 and Abaqus, buckling of the column web is the critical component, and the moment resistance is therefore decreasing with increasing levels of compressive axial force. This is shown in Figure 3.23a, and illustrates the implications of failing to capture the failure mode buckling of the column web. Even though it is not the case in this parametric study, IDEA StatiCa might overestimate the resistance for even higher levels of compressive axial force, or for other joint configurations.

The fact that Eurocode 3 occasionally disagrees with the analyses in Abaqus on what the governing failure mode is, can be expected. The capacity formulas provided in Eurocode 3 will in general yield conservative predictions of resistance, and sometimes predict the incorrect critical component. In many cases, the formulas are so conservative that the joint resistance is in fact limited by the cross-sectional capacity of the beam, and not by a component in the joint. For other joint configurations, the failure is caused by a combination of a compressive and a tensile failure mode. It should be noted that the geometric imperfections in the Abaqus simulations are a source of error. The amplitude of the applied imperfection is chosen according to NS-EN 1993-1-5 [2], but the procedure for introducing imperfection, and the geometric shape of the imperfection, is not necessarily realistic. However, it is presumably unproblematic that Eurocode 3 predicts the incorrect failure mode, since it in any case yields conservative predictions of resistance, as discussed in Section 3.4.1.

4 Minor axis bending of bolted beam-to-column joints

The main focus of this thesis is bolted beam-to-column joints subjected to major axis bending, as this is the most significant load effect and the most common joint configuration. However, minor axis joints are often necessary for some structures, as discussed in Sections 2.3.2 and 2.3.3. To fully explore IDEA StatiCa's possibilities and limitations when it comes to bolted beam-to-column joints, two minor axis joint configurations - one beam minor axis joint and one column minor axis joint - will be analyzed, validated, and verified similarly as in Chapter 3. The two joint configurations will be addressed separately, but in parallel, as they share some similarities. For the convenience of the reader, the illustrations of the two joint configurations are presented again in Figure 4.1.

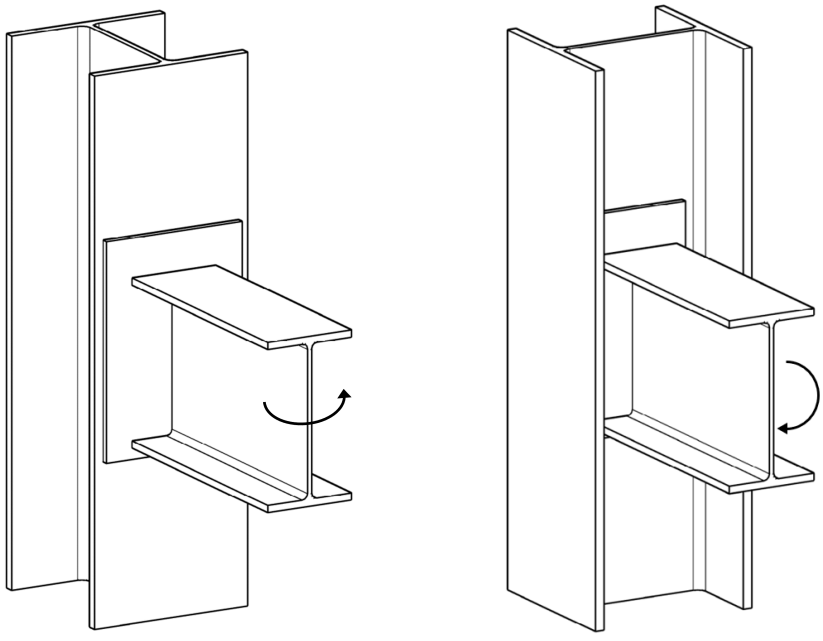

(a) Beam minor axis joint **(b)** Column minor axis joint

Figure 4.1: Different bolted minor axis beam-to-column joint configurations

This chapter is organized similarly as Chapter 3. The chapter's five sections cover the physical experiments used as basis for validation, explanation of calculation models, validation of numerical models to physical model, verification of IDEA StatiCa, and a parametric study. The procedure for establishing numerical models is similar to that explained in Chapter 3.

4.1 Experiments

In addition to experiments on major axis bolted joints, Zhu et al. [29] also conducted experiments where the beam was subjected to bending about its weak axis (beam minor axis joint). The geometry and experimental setup were similar to the major axis experiments (Figure 3.1a), except for the loading direction, which was perpendicular to the loading direction in the major axis joint. The test setup for this joint configuration is shown in Figure 4.2a.

Costa et al. [41] conducted several experiments on bolted beam-to-column joints, including experiments where the beam was bolted to the column web. The column was subsequently subjected to bending about its minor axis (column minor axis joint). The experimental setup for this joint configuration is shown in Figure 4.2b. The beam was welded to a 20 mm thick end-plate, which was bolted to the column web using six M24 bolts of grade 8.8. However, the diameter of the shank is secondary to the diameter of the nut and head. The governing failure mode was a flexural mechanism on the column web, which is highly dependent on the nut and head diameter. As this is not provided in the article, it was assumed to be equal to 36 mm, which corresponds to the key width for M24 bolts according to [42]. The profiles were made of S355 steel, but tensile tests of the profiles were performed, and the measured values were adopted in the simulations. For bolts, the characteristic material properties were adopted in the simulations. Further information about geometry and setup can be found in [41].

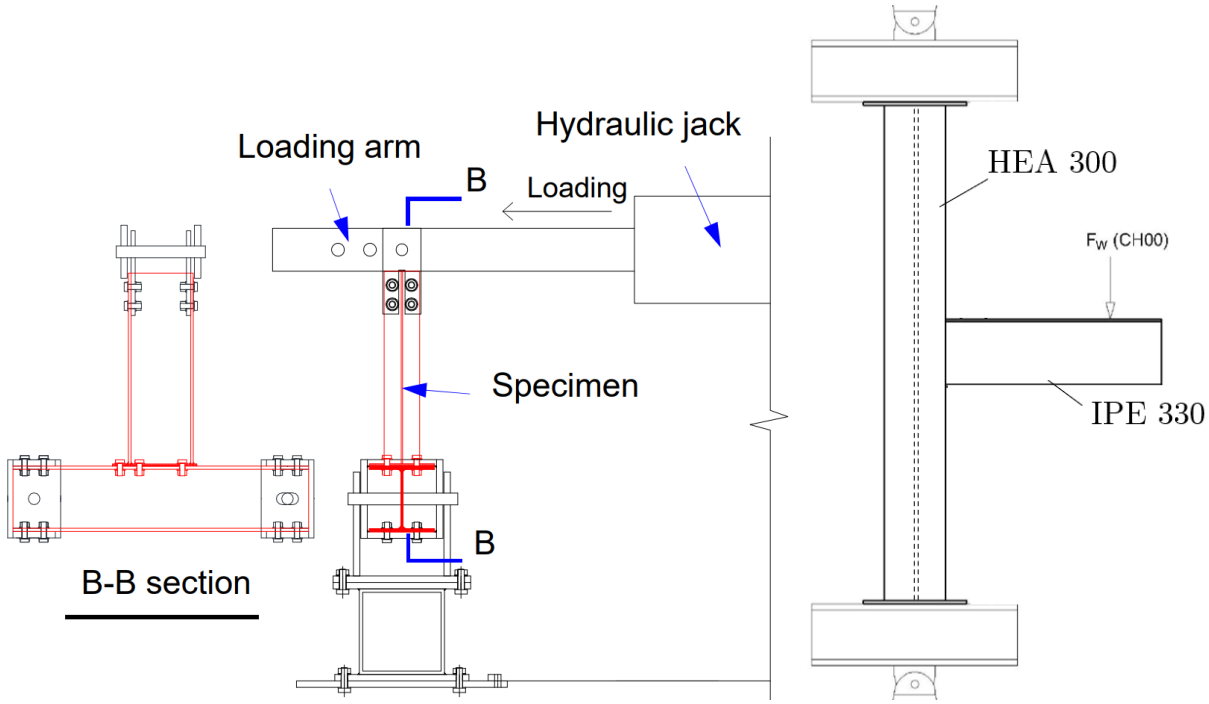

(a) Beam minor axis joint [29] **(b)** Column minor axis joint [41]

Figure 4.2: Minor axis joint experimental setups

4.2 Calculation models

The approach for establishing a finite element model, and the simplifications and assumptions adopted in the manual calculations, are largely similar to Chapter 3. Only the differences will therefore be briefly addressed in the following.

IDEA StatiCa

The models in IDEA StatiCa were easily created, and the same choices for mesh size and plastic limit strain as previously were applied in this chapter as well. Apart from load conditions and geometry, the model in IDEA StatiCa is similar to the model described in Section 3.2.1.

Abaqus

When assembling a finite element model of a beam minor axis joint in Abaqus, it is necessary to model the whole joint. The deformation is unsymmetrical, and a reduced model can therefore not be utilized. The column was restrained against deformation out-of-plane at the two ends, and the beam was restrained at the end against vertical deformation, as shown in Figure 4.3a. For the case of the column minor axis joint, the deformation is symmetrical, which can be utilized by modeling only half the joint. The assembled models of the beam minor axis joint modeled completely, and the column minor axis joint modeled with symmetry boundary conditions, can be seen in Figures 4.3a and 4.3b, respectively. Both analyses were conducted with deformation control, and a prescribed deformation was applied to the end of the beam, as shown in Figure 4.3.

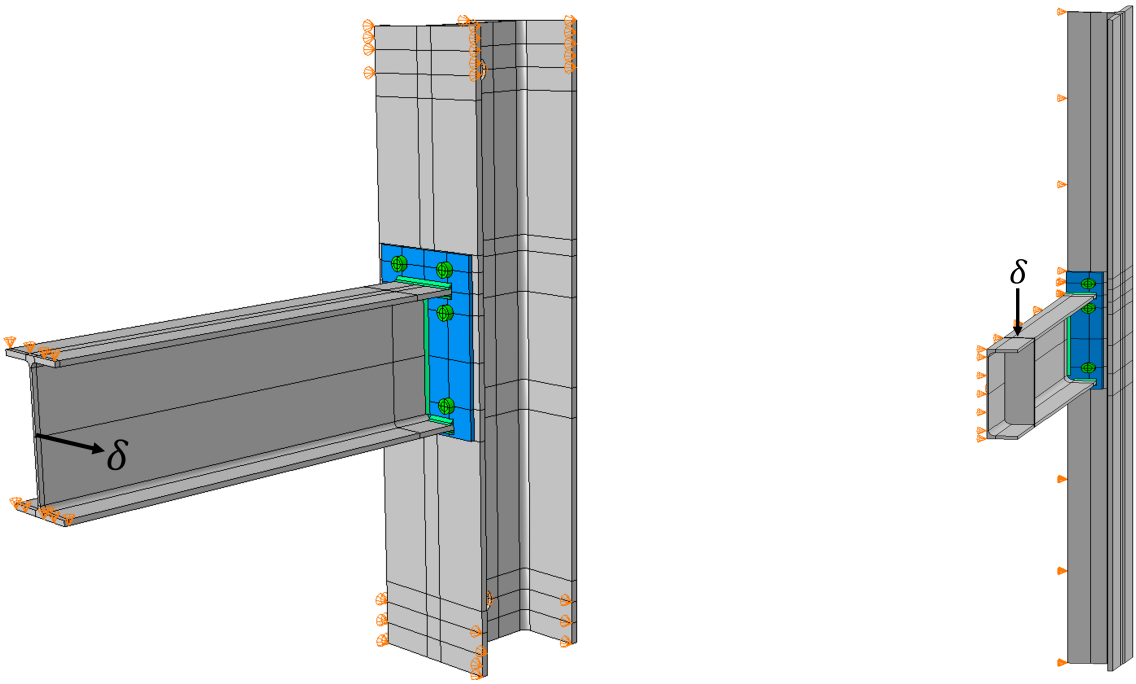

(a) Beam minor axis joint with boundary conditions

(b) Column minor axis joint with symmetry boundary condition

Figure 4.3: Finite element model assemblies of minor axis joints in Abaqus

The mesh for the beam minor axis joint was the same as shown in Section 3.2.2. For the column minor axis joint, the model was discretized similarly to the other models, i.e. four elements over the thickness, refined mesh where stress concentrations are expected to occur, and courser mesh elsewhere. The applied material model was the same as described in Section 3.2.2. The moment-rotation curves for both joints were obtained with the same approach as in their respective physical experiment. For the beam minor axis joint, the approach is described in Section 3.2.2, while for the column minor axis joint, the approach can be found in [41].

Component method

The results from the simulation of the column minor axis joint will also be compared to manual calculations according to Gomes et al. [27] and Neves et al. [28]. In the calculations, material factors were set equal to 1.0, and measured values for the yield stress of the sections, and characteristic material properties for bolts, were adopted. Manual calculations were not carried out for the beam minor axis joints, as discussed in Section 2.3.2.

4.3 Validation

The resulting moment-rotation curves from the experiment and the simulations of the beam minor axis joint and the column minor axis joint are presented in Figures 4.4a and 4.4b, respectively. The deformed shape at the end of the analysis for the beam minor axis joint is shown in Figure 4.5a, while the deformed shape after failure for the column minor axis joint is shown in Figure 4.5b.

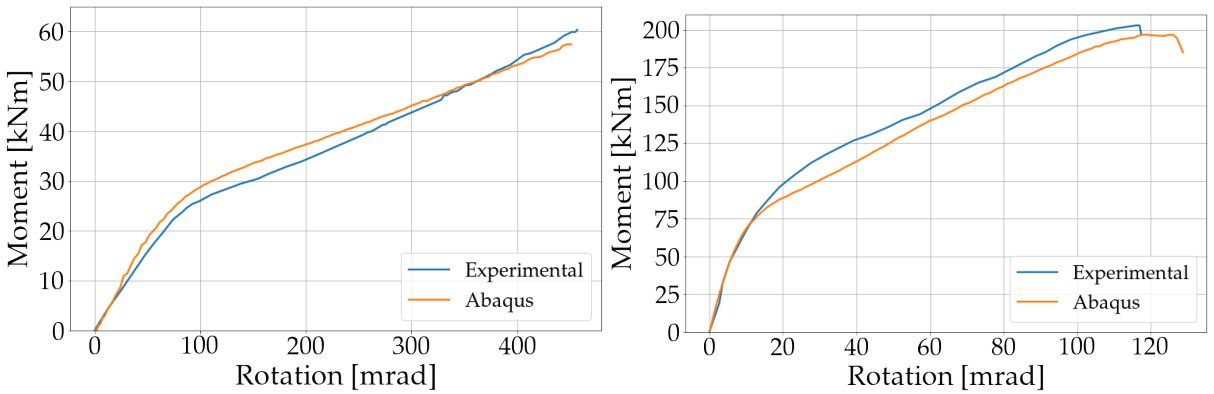

(a) Beam minor axis joint **(b)** Column minor axis joint

Figure 4.4: Moment-rotation curves for validation of minor axis joints

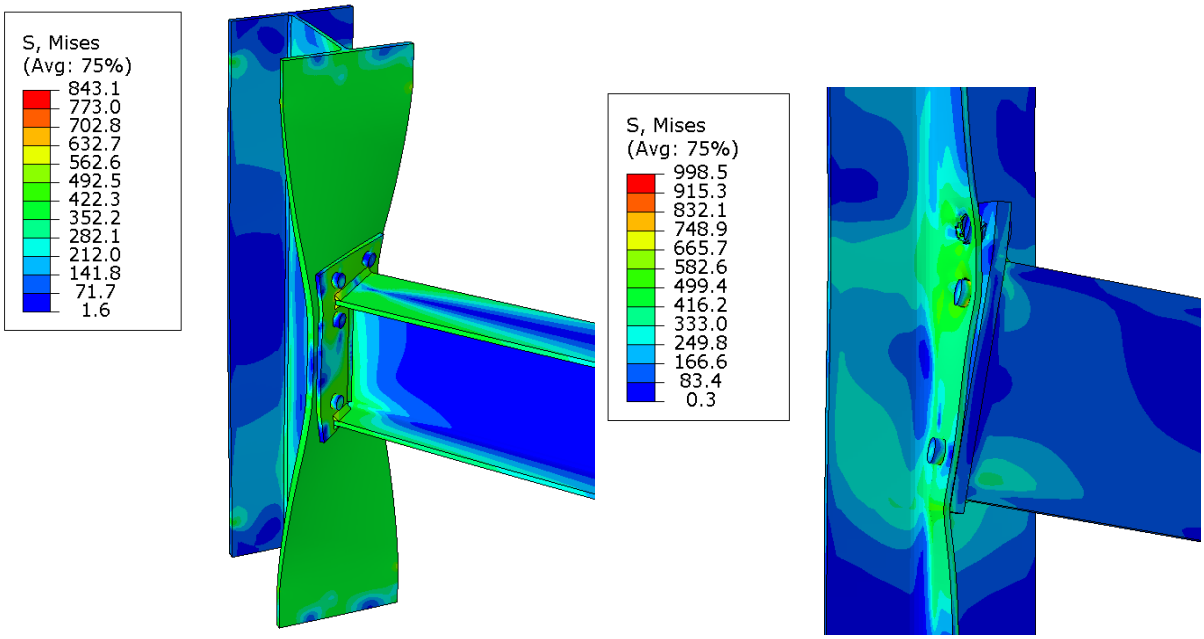

(a) Beam minor axis joint (end of analysis) **(b)** Column minor axis joint (post-failure)

Figure 4.5: Von-Mises stresses plotted on the deformed shape of the minor axis joints

4.3.1 Discussion of validation

Beam minor axis joint

From the moment-rotation curves of the beam minor axis joint (Figure 4.4a), it can be seen that the numerical solution agrees well with the experimental. For this joint and load configuration, it is not possible to obtain a clearly defined moment resistance or rotational capacity, as the steel will neither fracture nor buckle. Since the joint exhibits highly flexible behavior, the acceptable level of deformation will be the limiting factor and not the moment resistance. Despite this, the numerical model appears to be an accurate representation of the physical joint.

Column minor axis joint

For the column minor axis joint, the moment-rotation curve from the numerical solution shows some deviation compared to the experimental results. Some errors can be ascribed to the same factors discussed in Section 3.3.4. Additionally, the size of the head and the nut will greatly influence the ultimate resistance, as the failure is caused by contact between the bolt head/nut and the column web. This was also demonstrated in preliminary analyses. Since the geometry of the bolt was unavailable, some assumptions and simplifications were made when modeling the bolts. The bolts were modeled as one part, and it was assumed that the head and nut were circular with a diameter of 36 mm. These simplifications will affect the ultimate resistance of the whole joint. Despite this, the numerical solution captured the same failure mode as the physical experiment [41], and the numerical model can be considered an adequate reproduction of the physical joint.

4.4 Verification

To verify IDEA StatiCa numerically against Abaqus, IDEA StatiCa's bilinear material model was adopted in Abaqus. As no suitable expressions for resistance or initial stiffness exist for the beam minor axis joint, the analysis results will not be compared to manual calculations. For the case of the column minor axis joint, the analysis results are compared to the expression provided by Gomes et al. [27] and Neves et al. [28]. The calculations were performed in Maple, and are presented in Appendix E. The resulting moment-rotation curves for the beam and the column minor axis joint are presented in Figures 4.6a and 4.6b, respectively.

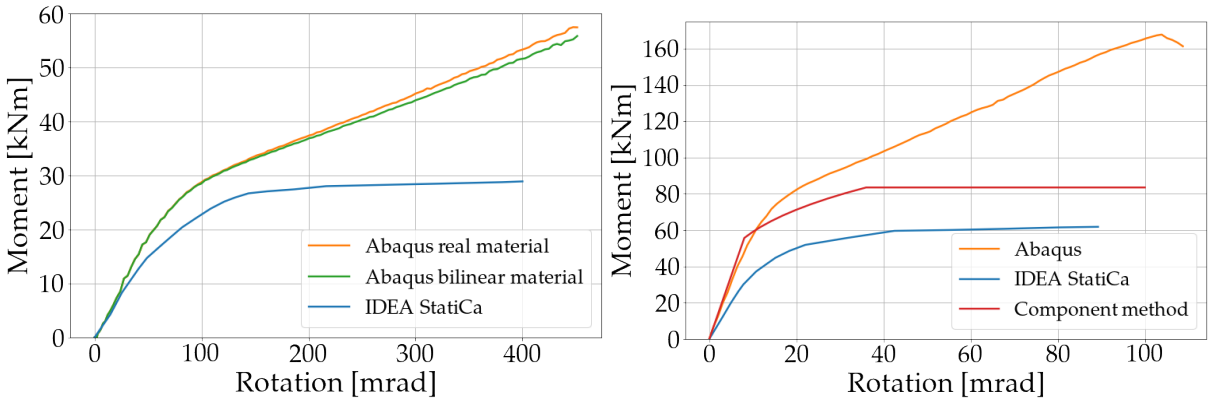

(a) Beam minor axis joint

(b) Column minor axis joint

Figure 4.6: Moment-rotation curves for verification of minor axis joints

4.5 Parametric study

As in Chapter 3, a parametric study is carried out to investigate the versatility of IDEA StatiCa. Four more joint configurations are analyzed for both the beam and column minor axis joint, and the results from the parametric study are presented in the following.

4.5.1 Beam minor axis joint

For this joint configuration, the column is the parameter with the greatest impact on the joint behavior. A total of five joints with different columns were analyzed. The moment-rotation curves from IDEA StatiCa and Abaqus for all five joints are shown in Figure 4.7. For this joint configuration, the deformation will in general be the limiting factor. The exceptions are the two joints with the stiffest columns (310 UC 137 and 310 UC 158), which according to the Abaqus analyses fail due to tearing of the beam flange. To obtain conservative and comparable predictions of moment resistance and initial stiffness also for the joints which do not exhibit failure, it is decided to limit the moment resistance to a rotation of 150 mrad (8.6 °). This implies that the moment resistance is limited by either the moment corresponding to a rotation of 150 mrad, or the actual ultimate moment if it occurs before reaching a rotation of 150 mrad. The initial stiffness is still defined as the secant stiffness at 2/3 of the moment resistance. The calculated moment resistance and initial stiffness of the beam minor axis joints are shown in Figures 4.8a and 4.8b, respectively.

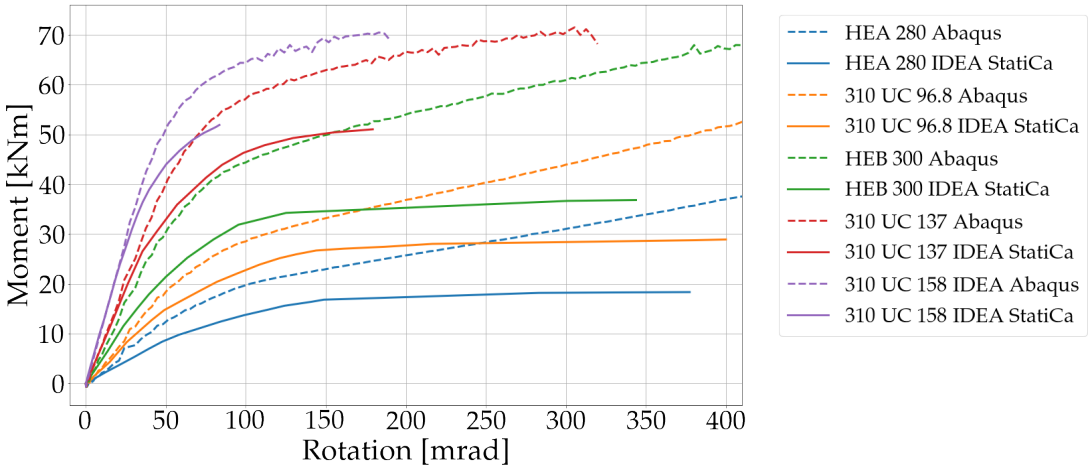

Figure 4.7: Moment-rotation curves from the parametric study of beam minor axis joint

HEA 280: $t_f = 13$ mm, $t_w = 8$ mm; 310 UC 96.8: $t_f = 15.4$ mm, $t_w = 9.9$ mm;
HEB 300: $t_f = 19$ mm, t_w=11 mm; 310 UC 137: $t_f = 21.7$ mm, $t_w = 13.8$ mm;
310 UC 158: $t_f = 25$ mm, $t_w = 15.7$ mm

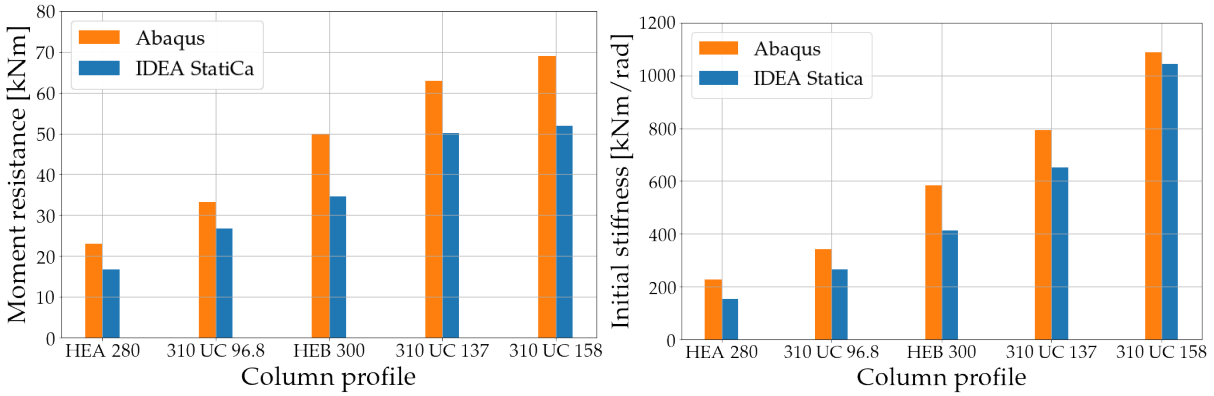

(a) Moment resistance **(b)** Initial stiffness

Figure 4.8: Parametric study of the beam minor axis joint (moment resistance defined as moment corresponding to a rotation of 150 mrad)

4.5.2 Column minor axis joint

The parameter with the greatest influence on the joint behavior is the thickness of the column web. A total of five analyses with different column web thicknesses were carried out, and the resulting moment resistance and initial stiffness from simulations and calculations are shown in Figures 4.9a and 4.9b, respectively.

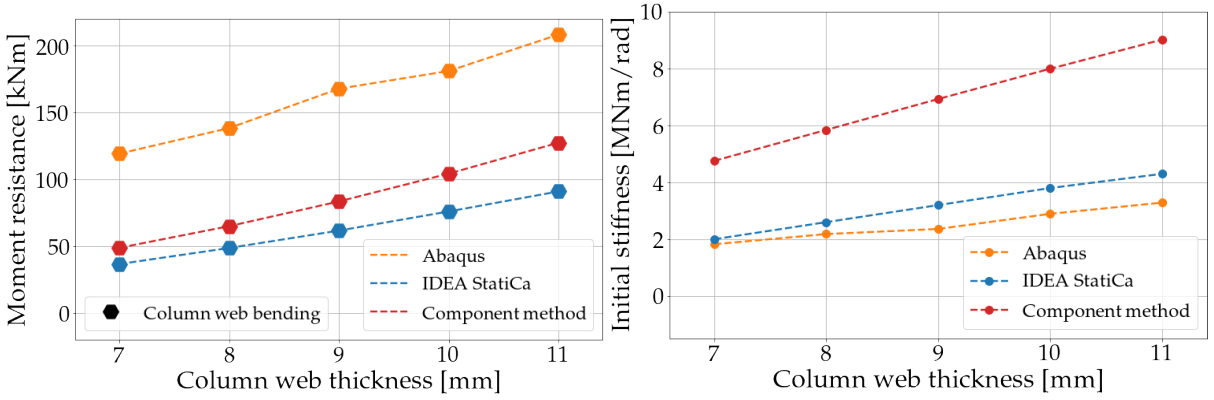

(a) Moment resistance **(b)** Initial stiffness

Figure 4.9: Parametric study of column minor axis joint

4.5.3 Discussion of verification and parametric study

Beam minor axis joint

For the joints with columns HEA 280, 310 UC 96.8, and HEB 300, the resistance is according to IDEA StatiCa limited by the plastic strain in the transition between column web and flange. For the joints with columns 310 UC 137 and 310 UC 158, the resistance is limited by the strain in the beam flanges. These failure modes are also captured in the corresponding Abaqus analyses. However, the deformation will in general be the limiting factor, as rotations surpassing 300 mrad is not realistic for most structures. Limiting the moment resistance to a rotation of 150 mrad, which was done in the parametric study, makes it possible to obtain conservative predictions of moment resistance and initial stiffness. For all the cases considered in the parametric study (Figure 4.8), the moment resistance and initial stiffness are underestimated by IDEA StatiCa.

However, considering Figure 4.7, it appears that the initial slope of the moment-rotation curves from Abaqus and IDEA StatiCa agree well. The deviation in the absolute value of initial stiffness is therefore largely caused by the difference in moment resistance, as the initial stiffness is defined as the secant stiffness at 2/3 of the resistance.

Figure 4.6a demonstrates that the numerical solutions from Abaqus are almost identical for the "real material model" and the "bilinear material model". This implies that the response of the beam minor axis joint is mainly controlled by elastic deformations. In the simulations, a yield line forms in the transition between column flange and web. However, little plastic strain is observed in the column flanges, and the elastic stresses in the flanges dominate the response of the joint.

Column minor axis joint

Column minor axis joint is the only joint configuration where the moment resistance predicted by IDEA StatiCa is lower than that predicted according to the component method. The moment resistance obtained by the analyses in Abaqus, however, is significantly larger than that predicted by both IDEA StatiCa and the component method. This implies that both IDEA StatiCa and the component method expressions yield conservative results for this joint configuration. This is seen in Figures 4.6b and 4.9a. The cause for IDEA StatiCa's underestimation of moment resistance is uncertain, but might also for this joint configuration be partially ascribed to the geometrically linear solution method.

The absolute value of initial stiffness predicted by IDEA StatiCa is marginally larger than the initial stiffness obtained from Abaqus, but the difference is insignificant. The component method's overestimation of initial stiffness, on the other hand, is more significant. This is similar to the other joint configurations explored, but the overestimation is especially significant in this case. The component method's overestimation can to a large extent be ascribed to how the initial stiffness is defined in the numerical analyses (the secant stiffness at 2/3 of the moment resistance). When comparing the moment-rotation curves in Figure 4.6b, it appears that the initial slope of the moment-rotation curves determined according to the component method and from the Abaqus simulation agree well. The deviation in the absolute value of initial stiffness is caused by the high post-yield capacity shown in the Abaqus simulations, which effectively reduces the calculated initial stiffness. From Figure 4.6b, it can also be seen that the initial slope of the moment-rotation curve from IDEA StatiCa shows some deviation compared to the initial slope from Abaqus. However, the absolute values of the initial stiffness (Figure 4.9b) agree relatively well. This is due to the low post-yield capacity in IDEA StatiCa, which effectively increases the calculated initial stiffness. It is important to acknowledge that the expressions for resistance and stiffness by Gomes et al. [27] and Neves et al. [28] are not incorporated in Eurocode 3, and the validity of the expressions is therefore uncertain.

5 Conclusion and suggestions for further work

5.1 Conclusion

IDEA StatiCa is a design tool that offers fast, simple, and versatile design of steel joints. The software has adopted several simplifications to allow for quick analyses, such as plate elements instead of solid elements, and a geometrically linear analysis instead of a nonlinear analysis. Despite its simplifications, it was found that IDEA StatiCa's prediction of moment resistance is conservative compared to the resistance obtained in Abaqus. The cause for the underestimation is assumed to mainly be the geometrically linear analysis adopted in IDEA StatiCa. Geometrically nonlinear analysis allows the bending stresses in the end-plate (and possibly elsewhere) to be partly replaced by membrane stresses when the end-plate deforms, and a higher joint resistance can therefore be achieved. This phenomenon is neglected when applying a geometrically linear analysis. Employing the recommended 5 % limit for plastic strain yields predictions of moment resistance that are closer to the resistance predicted by Eurocode 3. However, as Eurocode 3 in general yields overly conservative predictions, a higher limit of plastic strain can in many cases be applied.

Extra caution should be taken when there is potential for plate buckling in the joint, as IDEA StatiCa has included neither geometric imperfections nor geometric nonlinearity in the analysis. IDEA StatiCa offers buckling analysis for joints, but it is uncertain what buckling factor is required for a joint to not be susceptible to buckling. IDEA StatiCa's theory manual states that plate buckling does not need to be considered if the buckling factor is higher than 3 when applying the design loads. However, joints with a buckling factor well above 3 are shown to have their resistance limited by plate buckling. This recommendation is therefore uncertain. The initial stiffness predicted by IDEA StatiCa is for all cases significantly lower than that predicted by Eurocode 3. However, this discrepancy can to a large extent be ascribed to the way IDEA StatiCa defines the initial stiffness, which is the secant stiffness at 2/3 of the resistance. It can therefore be assumed that IDEA StatiCa's prediction of initial stiffness is adequate.

It is important to keep in mind the intended purpose of IDEA StatiCa. Since it is primarily a design tool, it should not be expected to produce exact predictions of structural behavior. In the design phase, it is more important to deliver conservative, and preferably quick, predictions of structural behavior. Considering the findings of this thesis, IDEA StatiCa can be considered as a reliable design tool.

5.2 Suggestions for further work

One of the consistent findings of this thesis is that IDEA StatiCa underestimates the joint's moment resistance compared to the resistance obtained in Abaqus analyses. It is assumed that a large portion of this deviation can be ascribed to the geometrically linear solution method, but this is not certain. Further exploring how a geometrically linear analysis differs from a nonlinear analysis when it comes to the prediction of structural resistance, is therefore interesting.

Several joint geometries and load conditions have been investigated, but the conclusions of this thesis are not necessarily valid for all types of joints. This thesis has explored mere drops in the vast sea of steel structures and joint design, and it is therefore encouraged to continue applying the software on other structural joints, such as beam-to-beam-splices, steel column to concrete footings, hollow section joints, or joints with several connected members.

References

[1] Standard Norge, *Eurocode 3: Design of steel structures - Part 1-1: General rules and rules for buildings*, NS-EN 1993-1-1: 2005+A1:2014+NA:2015, 2015.

[2] Standard Norge, *Eurocode 3: Design of steel structures - Part 1-5: Plated structural elements*, NS-EN 1993-1-5:2006+AC+A1:2017+A2:2019+NA:2019, 2019.

[3] Standard Norge, *Eurocode 3: Design of steel structures - Part 1-8: Design of joints*, NS-EN 1993-1-8:2005+NA:2009, 2009.

[4] C. Zhu, K. Rasmussen, S. Yan, and H. Zhang, "Experimental full-range behavior assessment of bolted moment end-plate connections," *Journal of Structural Engineering*, vol. 145, p. 04019079, 06 2019.

[5] L. Silva, L. Lima, P. Vellasco, and S. Andrade, "Behaviour of flush end-plate beam-to-column joints under bending and axial force," *Steel and Composite Structures*, vol. 4, 04 2004.

[6] F. Wald, L. Šabatka, M. Bajer, M. Kožich, M. Vild, K.Golubiatnikov, J. Kabeláč, and M. Kuříková, *Component-Based finite element design of steel connections*, 2nd ed. Czech Technical University in Prague, 2021.

[7] W. L. Oberkampf and T. G. Trucano, "Verification and validation in computational fluid dynamics," *Progress in Aerospace Sciences*, vol. 38, no. 3, pp. 209–272, 2002. [Online]. Available: https://www.sciencedirect.com/science/article/pii/S0376042102000052

[8] *Guide for the verification and validation of computational fluid dynamics simulations*, ser. AIAA guide. Reston, Va: The Institute, 1998, vol. G-077-1998.

[9] P. Roache, *Verification and Validation in Computational Science and Engineering*. Hermosa Publishers, 1998. [Online]. Available: https://books.google.no/books?id=ENRlQgAACAAJ

[10] L. Sabatka, F. Wald, J. Kabeláč, L. Gödrich, and J. Navrátil, "Component based finite element model of structural connections," *Proceedings of the 12th International Conference on Steel, Space and Composite Structures*, pp. 337–344, 01 2014.

[11] "What is the cbfem?" https://www.ideastatica.com/support-center/what-is-the-cbfem, accessed: 11.03.2022.

[12] A. Ibrahimbegovic, R. Taylor, and E. L. Wilson, "A robust quadrilateral membrane finite element with drilling degrees of freedom," *International Journal for Numerical Methods in Engineering*, vol. 30, pp. 445–457, 1990.

[13] E. N. Dvorkin, D. Pantuso, and E. A. Repetto, "A formulation of the mitc4 shell element for finite strain elasto-plastic analysis," *Computer Methods in Applied Mechanics and Engineering*, vol. 125, no. 1, pp. 17–40, 1995. [Online]. Available: https://www.sciencedirect.com/science/article/pii/004578259500767U

[14] G. Liu and S. Quek, "Chapter 2 - briefing on mechanics for solids and structures," in *The Finite Element Method (Second Edition)*, second edition ed., G. Liu and S. Quek, Eds. Oxford: Butterworth-Heinemann, 2014, pp. 13–41. [Online]. Available: https://www.sciencedirect.com/science/article/pii/B9780080983561000023

[15] "Idea statica connection theoretical background," https://www.ideastatica.com/support-center/general-theoretical-background, accessed: 11.03.2022.

[16] G. Liu and S. Quek, "Chapter 11 - modeling techniques," in *The Finite Element Method (Second Edition)*, second edition ed., G. Liu and S. Quek, Eds. Oxford: Butterworth-Heinemann, 2014, pp. 301–345. [Online]. Available: https://www.sciencedirect.com/science/article/pii/B9780080983561000114

[17] I. Huněk, "On a penalty formulation for contact-impact problems," *Computers Structures*, vol. 48, no. 2, pp. 193–203, 1993. [Online]. Available: https://www.sciencedirect.com/science/article/pii/0045794993904127

[18] K. Bell, *An Engineering Approach to Finite Element Analysis of Linear Structural Mechanics Problems*. Akademica Publishing, 2013.

[19] SIMULIA, *Abaqus user manual 6.16*, Dassault systems.

[20] Standard Norge, *Eurocode 3: Design of steel structures — Part 1-14: Design assisted by finite element analysis*, prEN 1993-1-14, 2021.

[21] P. Zoetemeijer, "A design method for the tension side of statically loaded, bolted beam-to-column connections," *HERON, 20 (1), 1974*, 1974.

[22] J. Witteveen, J. W. Stark, F. S. Bijlaard, and P. Zoetemeijer, "Welded and bolted beam-to-column connections," *Journal of the Structural Division*, vol. 108, no. 2, pp. 433–455, 1982.

[23] W. F. Chen and D. E. Newlin, "Column web strength in beam-to-column connections," *Journal of the Structural Division*, vol. 99, no. 9, pp. 1978–1984, 1973.

[24] K. Weynand, J.-P. Jaspart, and M. Steenhuis, "- the stiffness model of revised annex j of eurocode 3," in *Connections in Steel Structures III*, R. Bjorhovde, A. Colson, and R. Zandonini, Eds. Oxford: Pergamon, 1996, pp. 441–452. [Online]. Available: https://www.sciencedirect.com/science/article/pii/B9780080428215501000

[25] Z. Sokol, F. Wald, V. Delabre, J.-P. Muzeau, and M. Svarc, "Design of end plate joints subject to moment and normal force," *Eurosteel Coimbra*, vol. 2002, pp. 1219–1228, 2002.

[26] D. Beg, E. Zupančič, and I. Vayas, "On the rotation capacity of moment connections," *Journal of Constructional Steel Research*, vol. 60, no. 3, pp. 601–620, 2004, eurosteel 2002 Third European Conference on Steel Structures. [Online]. Available: https://www.sciencedirect.com/science/article/pii/S0143974X03001329

[27] F. Gomes, J.-P. Jaspart, and R. Maquoi, "Moment capacity of beam-to-column minor-axis

joints," in *Proceedings of the IABSE Colloquium on Semi-Rigid Structural Connections*, 1996, pp. 319–326.

[28] L. C. Neves, L. S. da Silva, and P. Vellasco, "A model for predicting the stiffness of beam to concrete filled column and minor axis joints under static monotonic loading," in *Proceedings of the 4th European Conference on Steel and Composite Structures, Maastricht, The Netherlands*, 2005, pp. 8–10.

[29] C. Zhu, K. Rasmussen, S. Yan, and H. Zhang, "Experimental full-range behavior assessment of bolted moment end-plate connections," *Journal of Structural Engineering*, vol. 145, 2019.

[30] Standard Norge, *Execution of steel structures and aluminium structures - Part 2: Technical requirements for steel structures*, NS-EN 1090-2:2018, 2018.

[31] M. Pavlović, Z. Marković, M. Veljković, and D. Buđevac, "Bolted shear connectors vs. headed studs behaviour in push-out tests," *Journal of Constructional Steel Research*, vol. 88, pp. 134–149, 2013. [Online]. Available: https://www.sciencedirect.com/science/article/pii/S0143974X13001314

[32] J. R. Rice and D. M. Tracey, "On the ductile enlargement of voids in triaxial stress fields," *Journal of the Mechanics and Physics of Solids*, vol. 17, no. 3, pp. 201–217, 1969.

[33] F. Yang and M. Veljkovic, "Damage model calibration for s275 and s690 steels," *ce/papers*, vol. 3, pp. 262–271, 12 2019.

[34] SIMULIA, *Abaqus user manual v6.6*, Dassault systems.

[35] H. Demirci, S. Bhattacharya, D. Karamitros, N. Alexander, and R. Singh, "Finite element model of buried pipelines crossing strike-slip faults by abaqus/explicit," 06 2018.

[36] Y. Özkılıç, "A new replaceable fuse for moment resisting frames: Replaceable bolted reduced beam section connections," *Steel and Composite Structures*, vol. 35, pp. 353–370, 05 2020.

[37] P. K. Larsen, *Dimensjonering av stålkonstruksjoner*, 2nd ed. Fagbokforlaget, 2010.

[38] B. Young, "Residual stresses in hot rolled members," *IABSE reports of the working commissions = Rapports des commissions de travail AIPC = IVBH Berichte der Arbeitskommissionen*, 1975.

[39] Y. Özkılıç, "A comparative study on yield line mechanisms for four bolted extended end-plated connection," *Challenge Journal of Structural Mechanics*, vol. 7, pp. 93–106, 07 2021.

[40] E. Hegre and H. E. M. Hauge, "Modelling of joints in large-scale analyses of steel structures," Master's thesis, Norwegian University of Science and Technology, 2021.

[41] R. Costa, J. Valdez, S. Oliveira, L. Simões da Silva, and E. Bayo, "Experimental behaviour of 3d end-plate beam-to-column bolted steel joints," *Engineering Structures*, vol. 188, pp. 277–289, 2019. [Online]. Available: https://www.sciencedirect.com/science/article/pii/S0141029618331146

[42] Standard Norge, *Hexagon head bolts - Product grades A and B*, NS-EN ISO 4014:2011, 2011.

Appendix

A Resistance and stiffness for column minor axis joint

Moment resistance

Gomes et al. [27] considered several failure mechanisms, which are listed below with their respective capacity formula:

- **Local failure:**

  (i) Flexural mechanisms:

$$F_{pl} = \frac{4\pi m_{pl}}{1 - \frac{b}{L}} \left(\sqrt{1 - \frac{b}{L}} + \frac{2c}{\pi L} \right) k \tag{A.1}$$

  where b, c and L are defined in figure A.1, m_{pl} is the plastic moment capaicty of the web, d_m is the mean diameter of the bolt head or nut, and k is given by:

$$k = \begin{cases} 0.7 + 0.6(b+c)/L & \text{if } (b+c)/L \leq 0.5 \\ 1 & \text{if } (b+c)/L > 0.5 \end{cases} \tag{A.2}$$

  (ii) Punching shear mechanisms:

$$F_{punch} = n\pi d_m \nu_{pl} \tag{A.3}$$

  where $\nu_{pl} = t_w f_y / sqrt(3)$

  (iii) Combined flexural and punching shear mechanisms

$$F_{Q2} = 4m_{pl} \left[\frac{\pi \sqrt{L(a+x)} + 2c}{a+x} + \frac{1.5cx + x^2}{\sqrt{3} t_w (a+x)} \right] k \tag{A.4}$$

  where

$$\begin{cases} x = 0 & \text{if } b \leq b_m \\ x = -a + \sqrt{a^2 - 1.5ac + \frac{\sqrt{3} t_w}{2} [\pi \sqrt{L(a+x_0)} + 4c]} & \text{if } b > b_m \end{cases} \tag{A.5}$$

$$x_0 = L \left[\left(\frac{t}{L} \right)^{\frac{2}{3}} + 0.23 \frac{c}{L} \left(\frac{t}{L} \right)^{\frac{1}{3}} \right] \frac{b - b_m}{L - b_m} \tag{A.6}$$

$$b_m = L \left[1 - 0.82 \frac{t_w^2}{c^2} \left(1 + \sqrt{1 + 2.8 \frac{c^2}{t_w L}} \right)^2 \right] \tag{A.7}$$

$$a = L - b \tag{A.8}$$

- **Global failure:**

$$F_{global} = \frac{F_{Q2}}{2} + m_{pl} \left(\frac{2b}{h} + \pi + 2\rho \right) \tag{A.9}$$

where

$$\rho = \begin{cases} 1 & \text{for } \frac{h}{L-b} \leq 1 \\ \frac{h}{L-b} & \text{for } 1 < \frac{h}{L-b} \leq 10 \\ 10 & \text{for } \frac{h}{L-b} \geq 10 \end{cases} \tag{A.10}$$

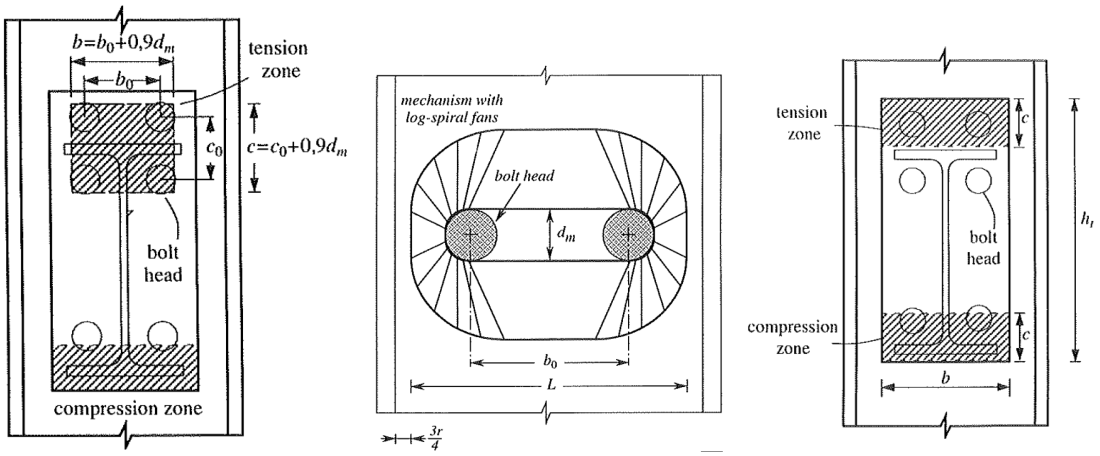

Figure A.1: Definition of parameters from [27]

From these expressions, the moment capacity of the column web is taken as $M_{pl} = h{\cdot}min(F_{local}, F_{global})$, where h is the distance between the centers of compression and tension zones. The dimension of the compressive zone can be assumed to be equal to the dimensions of the tensile zone.

Rotational stiffness

Neves et al. [28] derived an expression for the stiffness of the column web in bending, which is presented here. The bending stiffness of the column web in the case where the flanges are fixed against rotation are given by:

$$S_i = \frac{Et_{wc}^3}{L^2} 16 \frac{\alpha + (1-\beta)tan\theta}{(1-\beta)^3 + \frac{10.4(k_1 - k_2\beta)}{\mu^2}} \tag{A.11}$$

where $L = h_c - 2t_f - r$, $\alpha = c/L$, $\beta = b/L$, $\mu = L/t_{wc}$, $k_1 = 1.5$, $k_2 = 1.6$ and θ is given by:

$$\theta = \begin{cases} 35 - 10\beta & \text{if } \beta < 0.7 \\ 49 - 30\beta & \text{if } \beta \geq 0.7 \end{cases} \tag{A.12}$$

This equation is valid for the case where the column flanges are restrained against rotations. If no major-axis beams are present, this is not the case and the stiffness must be modified by multiplying with the factor, k, given as:

$$k_{red} = \frac{(\mu/\beta)^{1.25}}{230} \tag{A.13}$$

If $\mu/\beta \geq 70$, then no reduction in stiffness is needed. When considering the total stiffness of the joint, the deformation of the joint will be dominated by the column web. The total stiffness can therefore be approximated by equation A.14.

$$S_{j,ini} = Sh_1\left(h_1 - \frac{h_1 + h_2}{\frac{S_3}{S} + 2}\right) + Sh_2\left(h_2 - \frac{h_1 + h_2}{\frac{S_3}{S} + 2}\right) \tag{A.14}$$

where $S_1 = S_2 = S$ (equation A.14), S_3 is the stiffness of the compression zone, and h_1 and h_2 are shown in figure A.2

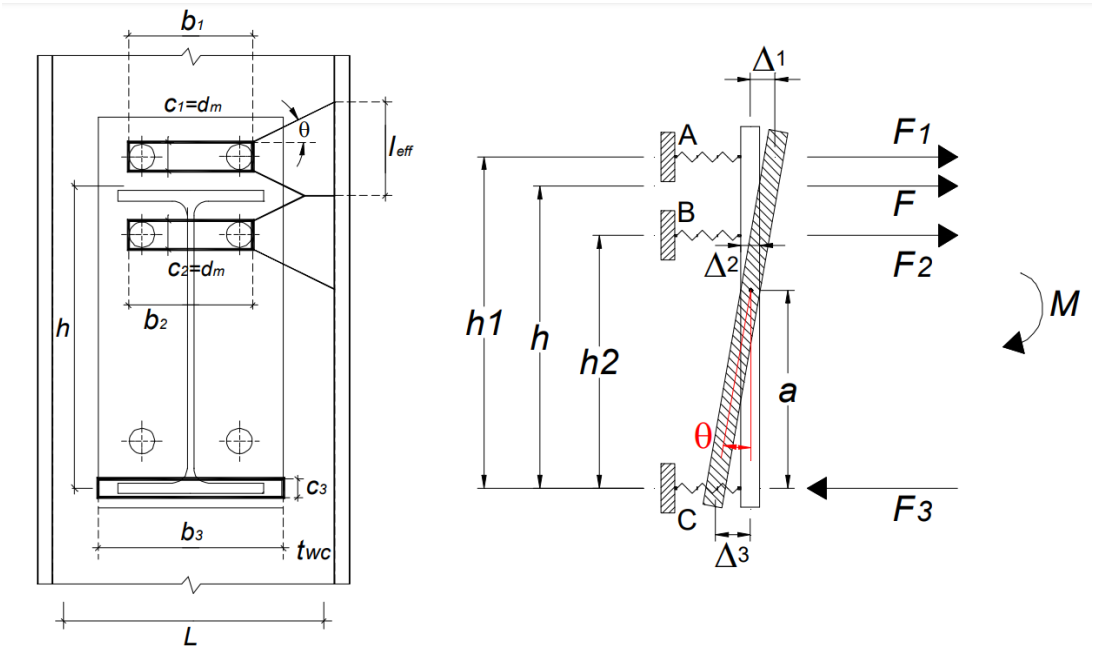

Figure A.2: Parameters from [28]

B Mesh convergence IDEA Statica

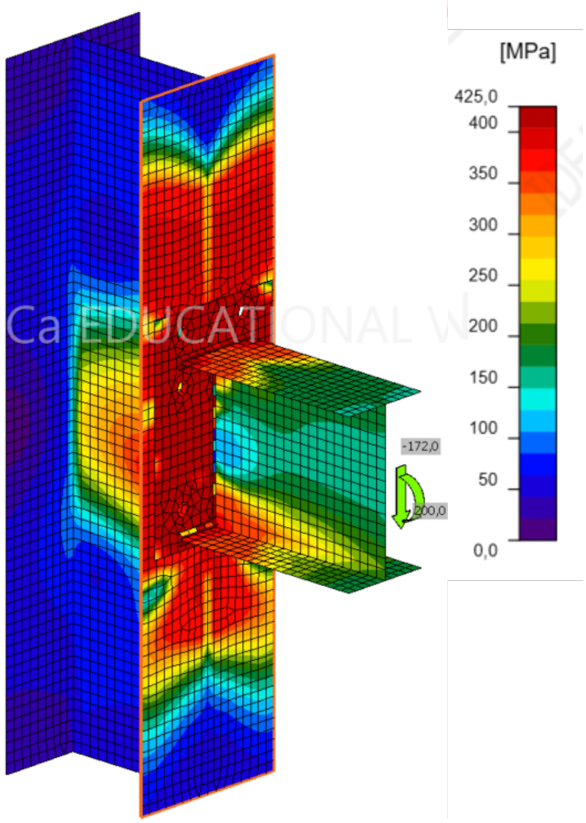

Figure B.1: Equivalent stresses with mesh size 18 mm

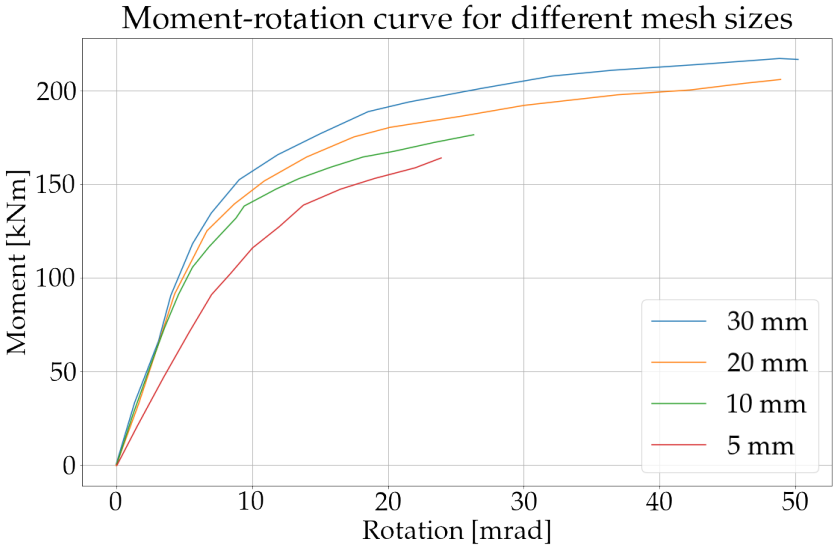

Figure B.2: Moment-rotation curve with different mesh sizes

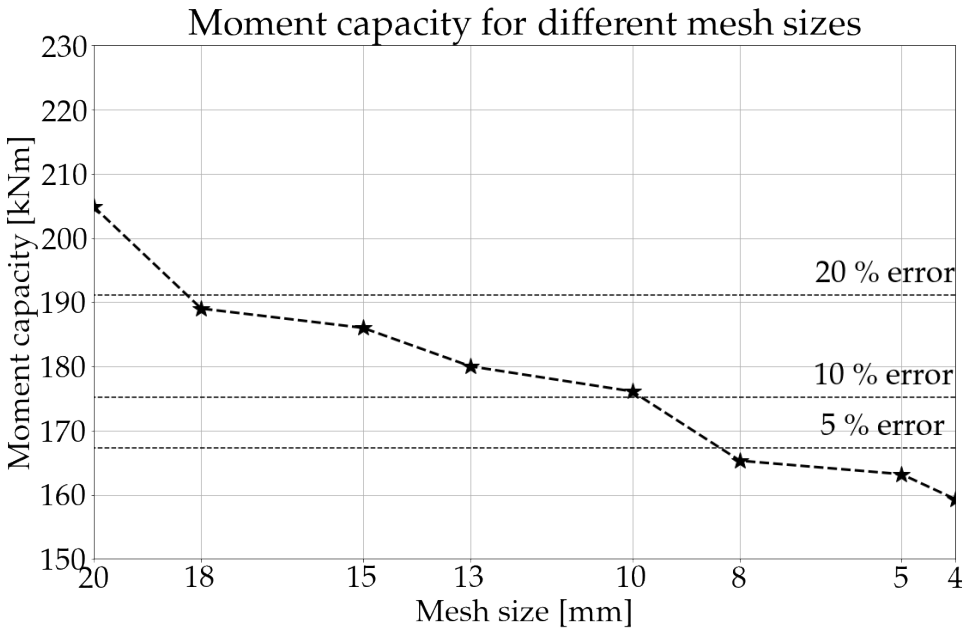

Figure B.3: Moment capacity with different mesh sizes

C Determination of axial force in Abaqus simulation

The angle of the beam is given by:

$$\theta_t = tan^{-1}(\frac{\delta_{2,1}}{L}) \tag{C.1}$$

The angle between the load-arm and the horizontal plane is given by:

$$\theta_l = tan^{-1}(\frac{b + \delta_{2,2} - \delta_{1,2}}{a + \delta_{2,1} - \delta_{1,1}}) \tag{C.2}$$

The axial force in the beam is then given as:

$$F_A = sin(\theta_l \theta_t) F \tag{C.3}$$

The moment in centerline of the column can be calculated as:

$$M_j = M \frac{L}{L_i} \tag{C.4}$$

where M is the moment calculated by the integrated section output.

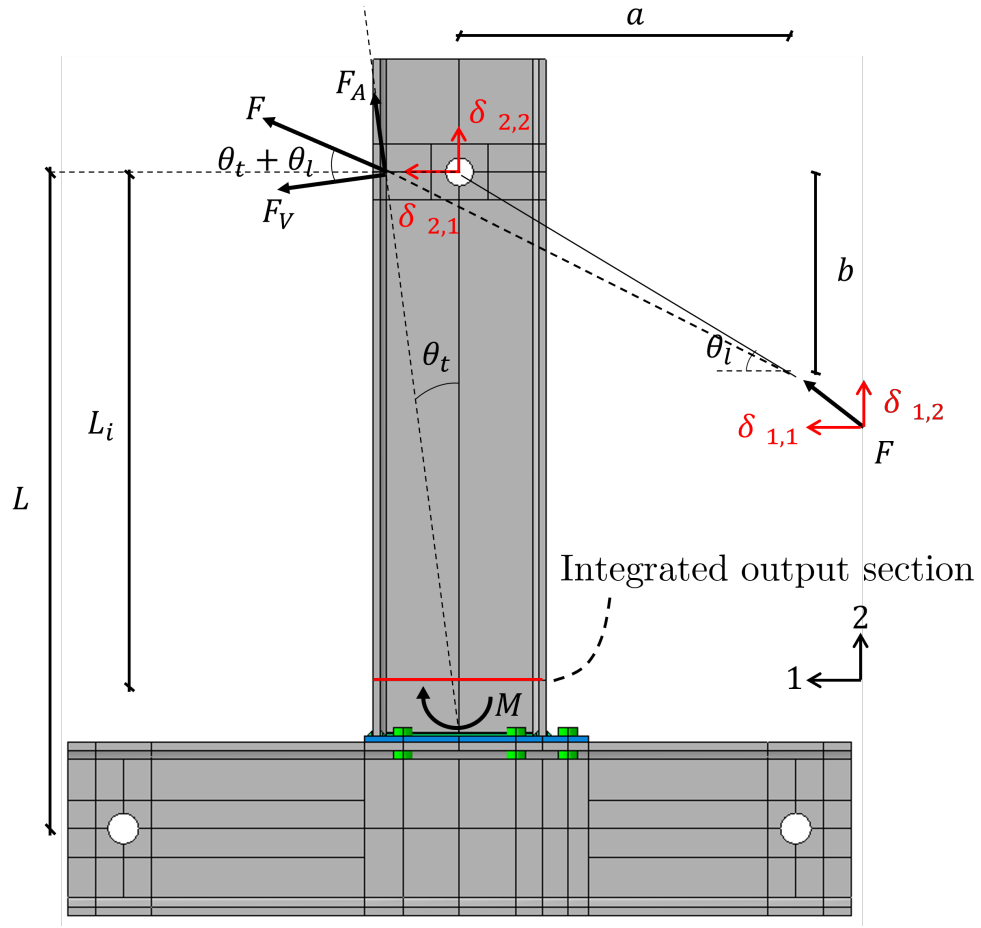

Figure C.1: Axial force calculation

D Manual calculations for major axis joint

Capacity and stiffness calculations for joint EP10-T according to Eurocode 3, Sokol et al., and Beg et al.

Input

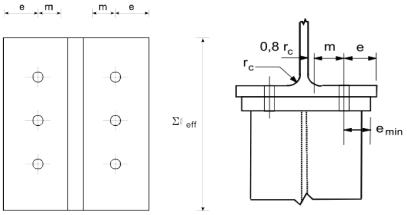

General	$E := 210000$:	pi := 3.1415926 :	$\beta_w := 0.9$:	$f_u := 510$:
Beam	$t_{fb} := 11.8$:	$t_{wb} := 6.7$:	$h_b := 307.2$:	$b_b := 166$:
	$r_b := 11.4$:	$f_{ybf} := 353$:	$f_{ybw} := 353$:	$S_y := 729 \cdot 10^3$:
Column	$t_{fc} := 15.4$:	$t_{wc} := 9.9$:	$h_c := 308$:	$b_c := 305$:
	$r_c := 16.5$:	$f_{ycf} := 382$:	$f_{ycw} := 382$:	$A_c := 12.4 \cdot 10^3$:
Endplate	$t_p := 10$:	$f_{yp} := 425$:	$L_b := t_p + t_{fc} + 2 \cdot 3 + 0.5 \cdot (18 + 12.5)$ $L_b := 46.65$ **(1.1)**	$f_{up} := 567$ $f_{up} := 567$ **(1.2)**
	$b_p := 270$:	$f_{uc} := 498$:	$f_{ubeam} := 505$:	
Bolt	$A_s := 353$:	$f_{ub} := 800$:	$n_b := 2$:	$k_2 := 0.9$:
Material factors	$\gamma_{M0} := 1.0$:	$\gamma_{M2} := 1.0$:	$\gamma_{M1} := 1.0$:	$c := 140$:
Weld	$a_w := 5$:	$a_f := 8$:		
Geometry joint column	$m := 0.5 \cdot (c - t_{wc}) - 0.8 \cdot r_c$ $m := 51.85$ **(1.3)**	$e := 82.5$:	$e_{min} := 65$:	$p := 2 \cdot 45 + t_{fb}$:
	$n := \min(e_{min}, 1.25 \cdot m)$ $n := 64.8125$ **(1.4)**	$e_1 := \infty$:		
Geometry joint endplate	$m_{ep} := 0.5 \cdot (c - t_{wb}) - 0.8 \cdot a_w \cdot 2^{0.5}$ 60.99 **(1.5)**	$e_x := 36$:	$w := c$:	$p := 92$:
	$m_x := 0.5(92 - t_{fb}) - 0.8 \cdot a_f \cdot 2^{0.5}$ $m_x := 31.04903320$ **(1.6)**	$n_x := \min(e_x, 1.25 \cdot m_x)$ $n_x := 36$ **(1.7)**	$m_2 := m_x$:	
Bolt positions	$h_1 := h_b - t_{fb} + \frac{92}{2}$ $h_1 := 341.4$ **(1.8)**	$h_2 := h_b - t_{fb} - \frac{92}{2}$ $h_2 := 249.4$ **(1.9)**		
	$ecc := 1616$ mm :	$h_f := h_b - t_{fb}$ $h_f := 295.4$ **(1.10)**	$L_{col} := 1200$:	
Joint stiffness	$\beta := 1$:			
	$Mode_{ep} := 1$:	$Mode_f := 1$:		

Capacity calculations (all references to Eurocode 3 part 1-8)

Note: The shear force is assumed to be taken by the lower bolts, which is oversized for taking shear

Column flange in bending §6.2.6.4

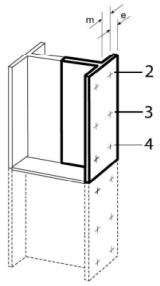

$Inner := 0$:

	Row considered individually		Row considered as a part of group	
	$l_{eff,cp,si}$:	$l_{eff,nc,si}$:	$l_{eff,cp,gr}$:	$l_{eff,nc,gr}$:
Inner row	$I1 := 2 \cdot \mathrm{pi} \cdot m$ $I1 := 325.7831526$ **(2.1)**	$I2 := 4\,m + 1.25e$ $I2 := 310.525$ **(2.2)**	$I3 := 2 \cdot p$ $I3 := 184$ **(2.3)**	$I4 := p$ $I4 := 92$ **(2.4)**
Outer row	$Y1 := \min(2 \cdot \mathrm{pi} \cdot m, \mathrm{pi} \cdot m + 2 \cdot e_1)$ $Y1 := 325.7831526$ **(2.5)**	$Y2 := \min(4 \cdot m + 1.25 \cdot e, 2 \cdot m + 0.625 \cdot e + e_1)$ $Y2 := 310.525$ **(2.6)**	$Y3 := \min(\mathrm{pi} \cdot m + p, 2 \cdot e_1 + p)$ $Y3 := 254.8915763$ **(2.7)**	$Y4 := \min(2 \cdot m + 0.625 \cdot e + 0.5 \cdot p, e_1 + 0.5 \cdot p)$ $Y4 := 201.2625$ **(2.8)**
$l_{eff,1,si}$	**if** $Inner = 1$ **then** $l_{eff,1,si} := \min(I1, I2)$ **else** $l_{eff,1,si} := \min(Y1, Y2)$ **end if** $l_{eff,1,si} := 310.525$ **(2.9)**		**if** $Inner = 1$ **then** $l_{eff,1,gr} := \min(I3, I4)$ **else** $l_{eff,1,gr} := \min(Y3, Y4)$ **end if** $l_{eff,1,gr} := 201.2625$ **(2.10)**	
$l_{eff,2,si}$	**if** $Inner = 1$ **then** $l_{eff,2,si} := I2$ **else** $l_{eff,2,si} := Y2$ **end if** $l_{eff,2,si} := 310.525$ **(2.11)**		**if** $Inner = 1$ **then** $l_{eff,2,gr} := I4$ **else** $l_{eff,2,gr} := Y4$ **end if** $l_{eff,2,gr} := 201.2625$ **(2.12)**	

Rows considered individually

$$M_{pl,1,Rd} := \frac{0.25 \cdot l_{eff,1,si} \cdot t_{fc}^{2} \cdot f_{ycf}}{\gamma_{M0}} \qquad M_{pl,1,Rd} := 7.033012410 \times 10^{6} \qquad \textbf{(2.13)}$$

$$M_{pl,2,Rd} := \frac{0.25 \cdot l_{eff,2,si} \cdot t_{fc}^{2} \cdot f_{ycf}}{\gamma_{M0}} \qquad M_{pl,2,Rd} := 7.033012410 \times 10^{6} \qquad \textbf{(2.14)}$$

$$F_{t,Rd} := \frac{k_2 \cdot f_{ub} \cdot A_s}{\gamma_{M2}} \qquad F_{t,Rd} := 254160.0000 \qquad \textbf{(2.15)}$$

$$L_{bprime} := \frac{8.8 \cdot m^3 \cdot A_s \cdot n_b}{t_{fb}^{3} \cdot l_{eff,1,si}} :$$

Fracture mode	With prying forces	Without prying forces
Mode 1	$F_{t,1,Rd} := \frac{4 \cdot M_{pl,1,Rd}}{m}$ $F_{t,1,Rd} := 542566.0488$ **(2.16)**	$F_{t,12,Rd} := \frac{2 \cdot M_{pl,1,Rd}}{m}$:
Mode 2	$F_{t,2,Rd} := \frac{2 \cdot M_{pl,2,Rd} + n \cdot 2 \cdot F_{t,Rd}}{m + n}$ $F_{t,2,Rd} := 402970.2331$ **(2.17)**	
Mode 3	$F_{t,3,Rd} := 2 \cdot F_{t,Rd}$ $F_{t,3,Rd} := 508320.0000$ **(2.18)**	

if $L_b < L_{bprime}$ **then** $F_{t,Rd,si,flens} := \min(F_{t,1,Rd}, F_{t,2,Rd}, F_{t,3,Rd})$ N **else** $F_{t,Rd,si,flens} := \min(F_{t,12,Rd}, F_{t,3,Rd})$ N **end if**

$F_{t,Rd,si,flens} := 402970.2331$ N **(2.19)**

Rows considered as part of a group

$$M_{pl,1,Rd} := \frac{0.25 \cdot 2 \cdot l_{eff,1,gr} \cdot t_{fc}^{2} \cdot f_{ycf}}{\gamma_{M0}}$$

$$M_{pl,1,Rd} := 9.116700170 \times 10^{6} \quad \textbf{(2.20)}$$

$$M_{pl,2,Rd} := \frac{0.25 \cdot 2 \cdot l_{eff,2,gr} \cdot t_{fc}^{2} \cdot f_{ycf}}{\gamma_{M0}}$$

$$M_{pl,2,Rd} := 9.116700170 \times 10^{6} \quad \textbf{(2.21)}$$

$$F_{t,Rd} := \frac{k_2 \cdot f_{ub} \cdot A_s}{\gamma_{M2}}$$

$$F_{t,Rd} := 254160.0000 \quad \textbf{(2.22)}$$

$$L_{bprime} := \frac{8.8 \cdot m^3 \cdot A_s \cdot n_b}{t_{fc}^{3} \cdot 2 \cdot l_{eff,1,si}} :$$

Fracture mode	With prying forces	Without prying forces
Mode 1	$F_{t,1,Rd} := \frac{4 \cdot M_{pl,1,Rd}}{m}$ $F_{t,1,Rd} := 703313.4172$ **(2.23)**	$F_{t,12,Rd} := \frac{2 \cdot M_{pl,1,Rd}}{m}$:
Mode 2	$F_{t,2,Rd} := \frac{2 \cdot M_{pl,2,Rd} + n \cdot 4 \cdot F_{t,Rd}}{m + n}$ $F_{t,2,Rd} := 721091.8705$ **(2.24)**	
Mode 3	$F_{t,3,Rd} := 4 \cdot F_{t,Rd}$ $F_{t,3,Rd} := 1.016640000 \times 10^{6}$ **(2.25)**	

if $L_b < L_{bprime}$ **then** $F_{t,Rd,gr,flens} := \min(F_{t,1,Rd}, F_{t,2,Rd}, F_{t,3,Rd})$ N **else** $F_{t,Rd,gr,flens} := \min(F_{t,12,Rd}, F_{t,3,Rd})$ N **end if**

$$F_{t,Rd,gr,flens} := 703313.4172 \text{ N} \quad \textbf{(2.26)}$$

Endplate in bending §6.2.6.5

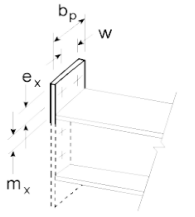

Row outside beam flange (row 1)

$$l_{eff,cp,1} := \min(2 \cdot \pi \cdot m_x, \pi \cdot m_x + w, \pi \cdot m_x + 2 \cdot e_{min})$$

$$l_{eff,cp,1} := 195.0868259 \quad \textbf{(2.27)}$$

$$l_{eff,nc,1} := \min(4 \cdot m_x + 1.25 \cdot e_x, e + 2 \cdot m_x + 0.625 \cdot e_x, 0.5 \cdot b_p, 0.5 \cdot w + 2 \cdot m_x + 0.625 \cdot e_x)$$

$$l_{eff,nc,1} := 135.0 \quad \textbf{(2.28)}$$

$$l_{eff,1,ep1} := \min(l_{eff,cp,1}, l_{eff,nc,1})$$

$$l_{eff,1,ep1} := 135.0 \quad \textbf{(2.29)}$$

$$l_{eff,2,ep1} := l_{eff,nc,1}$$

$$l_{eff,2,ep1} := 135.0 \quad \textbf{(2.30)}$$

$$M_{pl,1,Rd} := \frac{0.25 \cdot f_{yp} \cdot t_p^{2} \cdot l_{eff,1,ep1}}{\gamma_{M0}}$$

1434375.00 **(2.31)**

$$M_{pl,2,Rd} := \frac{0.25 \cdot f_{yp} \cdot t_p^{2} \cdot l_{eff,2,ep1}}{\gamma_{M0}}$$

1434375.00 **(2.32)**

Fracture mode	With prying forces	Without prying forces
Mode 1	$F_{t,1,Rd} := \frac{4 \cdot M_{pl,1,Rd}}{m_x}$ $F_{t,1,Rd} := 184788.3624$ **(2.33)**	$F_{t,12,Rd} := \frac{2 \cdot M_{pl,1,Rd}}{m}$ $F_{t,12,Rd} := 55327.86886$ **(2.34)**
Mode 2	$F_{t,2,Rd} := \frac{2 \cdot M_{pl,2,Rd} + n_x \cdot 2 \cdot F_{t,Rd}}{m_x + n_x}$ $F_{t,2,Rd} := 315713.2771$ **(2.35)**	
Mode 3	$F_{t,3,Rd} := 2 \cdot F_{t,Rd}$ $F_{t,3,Rd} := 508320.0000$ **(2.36)**	

if $L_b < L_{bprime}$ **then** $F_{t,Rd,1,ep} := \min(F_{t,1,Rd}, F_{t,2,Rd}, F_{t,3,Rd})$ N **else** $F_{t,Rd,1,ep} := \min(F_{t,12,Rd}, F_{t,3,Rd})$ N **end if**

$F_{t,Rd,1,ep} := 184788.3624$ N **(2.37)**

Row inside beam flange (row 2)

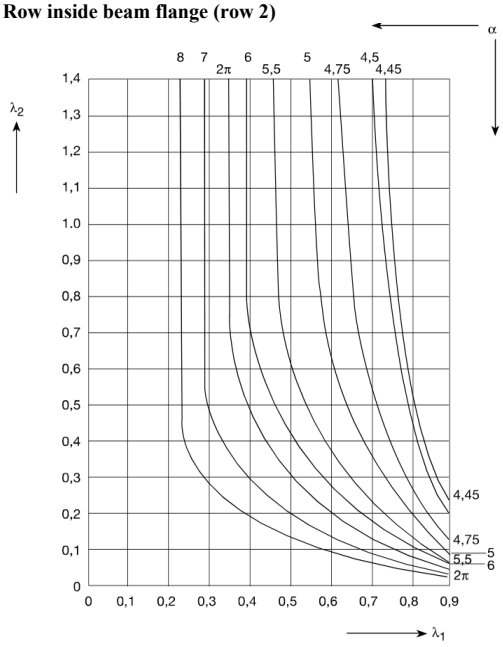

$lam1 := \frac{m_{ep}}{(m_{ep} + e_{min})}$ 0.48 **(2.38)**

$lam2 := \frac{m_2}{(m_{ep} + e_{min})}$ 0.246 **(2.39)**

$alfa := 7$ $alfa := 7$ **(2.40)**

$l_{eff,cp,2} := 2 \cdot \text{pi} \cdot m_{ep}$ $l_{eff,cp,2} := 383.2312306$ **(2.41)**

$l_{eff,nc,2} := alfa \cdot m_{ep}$ $l_{eff,nc,2} := 426.9520202$ **(2.42)**

$l_{eff,1,ep2} := \min(l_{eff,cp,2}, l_{eff,nc,2})$ $l_{eff,1,ep2} := 383.2312306$ **(2.43)**

$l_{eff,2,ep2} := l_{eff,nc,2}$ $l_{eff,2,ep2} := 426.9520202$ **(2.44)**

$M_{pl,1,Rd} := \frac{0.25 \cdot f_{yp} \cdot t_p^{\,2} \cdot l_{eff,1,ep2}}{\gamma_{M0}}$ 4071831.82 **(2.45)**	$M_{pl,2,Rd} := \frac{0.25 \cdot f_{yp} \cdot t_p^{\,2} \cdot l_{eff,2,ep2}}{\gamma_{M0}}$ 4536365.22 **(2.46)**	$F_{t,Rd} := \frac{k_2 \cdot f_{ub} \cdot A_s}{\gamma_{M2}}$:

Fracture mode	With prying forces	Without prying forces
Mode 1	$F_{t,1,Rd} := \frac{4 \cdot M_{pl,1,Rd}}{m_{ep}}$ $F_{t,1,Rd} := 267035.3709$ **(2.47)**	$F_{T,12,Rd} := \frac{2 \cdot M_{pl,1,Rd}}{m_x}$ 262283.97 **(2.48)**
Mode 2	$F_{t,2,Rd} := \frac{2 \cdot M_{pl,2,Rd} + n_x \cdot 2 \cdot F_{t,Rd}}{m_{ep} + n_x}$ 282208.0903 **(2.49)**	
Mode 3	$F_{t,3,Rd} := 2 \cdot F_{t,Rd}$ $F_{t,3,Rd} := 508320.0000$ **(2.50)**	

if $L_b < L_{bprime}$ **then** $F_{t,Rd,2,ep} := \min(F_{t,1,Rd}, F_{t,2,Rd}, F_{t,3,Rd})$ N **else** $F_{t,Rd,2,ep} := \min(F_{t,12,Rd}, F_{t,3,Rd})$ N **end if**

$F_{t,Rd,2,ep} := 267035.3709$ N **(2.51)**

Shear in column web §6.2.6.1

$A_{vc} := A_c - 2 \cdot b_c \cdot t_{fc} + (t_{wc} + 2 \cdot r_c) \cdot t_{fc}$

$A_{vc} := 3666.66$ **(2.52)**

$V_{wp,Rd} := \frac{0.9 \cdot f_{ycw} \cdot A_{vc}}{3^{0.5} \cdot \gamma_{M0}}$ N

$V_{wp,Rd} := 727806.4258$ N **(2.53)**

Column web in compression §6.2.6.2

$s_p := t_p + 5.8$

$s_p := 15.8$ **(2.54)**

$b_{eff,c,wc} := t_{fb} + 2^{1.5} \cdot a_f + 5 \cdot (t_{fc} + r_c) + s_p$

$b_{eff,c,wc} := 209.7274170$ **(2.55)**

$\sigma_{com,Ed} := 0$:

$k_{wc} := 1.0$:

$d_{wc} := h_c - 2 \cdot (t_{fc} + r_c)$

$d_{wc} := 244.2$ **(2.56)**

$\lambda_p := 0.932 \cdot \mathrm{sqrt}\left(b_{eff,c,wc} \cdot d_{wc} \cdot \frac{f_{ycw}}{E \cdot t_{wc}^{\,2}} \right)$

$\lambda_p := 0.9086637144$ **(2.57)**

$\omega_1 := \frac{1}{\left(1 + 1.3 \left(\frac{b_{eff,c,wc} \cdot t_{wc}}{A_{vc}} \right)^2 \right)^{0.5}}$

$\omega_1 := 0.8401128182$ **(2.58)**

$\rho_1 := \min\left(1, \frac{(\lambda_p - 0.2)}{\lambda_p^{\,2}}\right)$

$\rho_1 := 0.8582895497$ **(2.59)**

$F_{c,Rd,wc} := \min\left(\frac{(\omega_1 \cdot k_{wc} \cdot b_{eff,c,wc} \cdot t_{wc} \cdot f_{ycw})}{\gamma_{M0}}, \frac{(\omega_1 \cdot k_{wc} \cdot b_{eff,c,wc} \cdot t_{wc} \cdot f_{ycw} \cdot \rho_1)}{\gamma_{M1}} \right)$ N

$$F_{c,Rd,wc} := 571906.7223\ \text{N} \tag{2.60}$$

Column web in tension §6.2.6.3

Row 1 and 2 individually	$b_{eff,t,wc} := \min\left(l_{eff,1,si}, l_{eff,2,si}\right)$ $b_{eff,t,wc} := 310.525$ (2.61) $\omega_1 := \dfrac{1}{\left(1+1.3\left(\dfrac{b_{eff,t,wc}\cdot t_{wc}}{A_{vc}}\right)^2\right)^{0.5}}$ $\omega_1 := 0.7228501504$ (2.62) $F_{t,Rd,wc,1} := \dfrac{\left(\omega_1 \cdot k_{wc} \cdot b_{eff,t,wc} \cdot t_{wc} \cdot f_{ycw}\right)}{\gamma_{M0}}\ \text{N}$ $F_{t,Rd,wc,1} := 848874.3361\ \text{N}$ (2.63)
Row 1 and 2 as a group	$b_{eff,t,wc} := 2\cdot \min\left(l_{eff,1,gr}, l_{eff,2,gr}\right)$ $b_{eff,t,wc} := 402.5250$ (2.64) $\omega_1 := \dfrac{1}{\left(1+1.3\left(\dfrac{b_{eff,t,wc}\cdot t_{wc}}{A_{vc}}\right)^2\right)^{0.5}}$ $\omega_1 := 0.6280087030$ (2.65) $F_{t,Rd,wc,12} := \dfrac{\left(\omega_1 \cdot k_{wc} \cdot b_{eff,t,wc} \cdot t_{wc} \cdot f_{ycw}\right)}{\gamma_{M0}}\ \text{N}$ $F_{t,Rd,wc,12} := 955998.2088\ \text{N}$ (2.66)

Beam flange in compression §6.2.6.7

$$M_{c,Rd} := 2\cdot S_y \cdot f_{ybf}$$

$$M_{c,Rd} := 514674000 \tag{2.67}$$

$$F_{c,fb,Rd} := \frac{M_{c,Rd}}{h_b - t_{fb}}\ \text{N}$$

$$F_{c,fb,Rd} := 1.742295193 \times 10^6\ \text{N} \tag{2.68}$$

Beam web in tension §6.2.6.8

$$b_{eff,t,wb} := \min\left(l_{eff,1,ep2}, l_{eff,2,ep2}\right)$$

$$b_{eff,t,wb} := 383.2312306 \tag{2.69}$$

$$F_{t,Rd,wb} := \frac{b_{eff,t,wb}\cdot t_{wb}\cdot f_{ybw}}{\gamma_{M0}}\ \text{N}$$

$$F_{t,Rd,wb} := 906380.1835\ \text{N} \tag{2.70}$$

Capacity of weld

$$l_{wf} := b_b + b_b - 2\cdot r_b - t_{wb} + 2\cdot t_{fb}$$

$$l_{wf} := 326.1 \tag{2.71}$$

$$F_{w,fb,Rd} := \frac{l_{wf}\cdot a \cdot f_u}{\beta_w \cdot \gamma_{M2} \cdot 2^{0.5}}\ \text{N}$$

$$F_{w,fb,Rd} := 1.045330097 \times 10^6\ \text{N} \tag{2.72}$$

Total Capacity - summary

	Row 1 in tension	Row 2 in tension	Row 1 and 2 as group	Compression side	Capacity of component
Column flange in bending	$F_{t,Rd,si,flens}$ 402.97 kN **(3.1)**	$F_{t,Rd,si,flens}$ 402.97 kN **(3.2)**	$F_{t,Rd,gr,flens}$ 703.31 kN **(3.3)**		$F_{t,Rd,flens} := \min(2 \cdot F_{t,Rd,si,flens}, F_{t,Rd,gr,flens})$ 703.31 kN **(3.4)**
Endplate in bending	$F_{t,Rd,1,ep}$ 184.79 kN **(3.5)**	$F_{t,Rd,2,ep}$ 267.04 kN **(3.6)**	$F_{t,Rd,1,ep} + F_{t,Rd,2,ep}$ 451.82 kN **(3.7)**		$F_{t,Rd,ep} := F_{t,Rd,1,ep} + F_{t,Rd,2,ep}$ 451.82 kN **(3.8)**
Column web in tension	$F_{t,Rd,wc,1}$ 848.87 kN **(3.9)**	$F_{t,Rd,wc,1}$ 848.87 kN **(3.10)**	$F_{t,Rd,wc,12}$ 956.00 kN **(3.11)**		$F_{t,Rd,wc} := \min(2 \cdot F_{t,Rd,wc,1}, F_{t,Rd,wc,12})$ 956.00 kN **(3.12)**
Beam web in tension			$F_{t,Rd,wb}$ 906.38 kN **(3.13)**		$F_{t,Rd,wb}$ 906.38 kN **(3.14)**
Weld			$F_{w,fb,Rd}$ 1.05×10^3 kN **(3.15)**		$F_{w,fb,Rd}$ 1.05×10^3 kN **(3.16)**
Column web in shear				$F_{c,Rd,wp} := \frac{L_{col}}{L_{col} - h_f} \cdot V_{wp,Rd}$ 965.47 kN **(3.17)**	$F_{t,Rd,wp} := \frac{L_{col}}{L_{col} - h_f} \cdot V_{wp,Rd}$ 965.47 kN **(3.18)**
Column web in compression				$F_{c,Rd,wc}$ 571.91 kN **(3.19)**	
Beam flange in compression				$F_{c,fb,Rd}$ 1742295.19 N **(3.20)**	
Min	$F_{t,1,Rd} := \min(F_{t,Rd,si,flens}, F_{t,Rd,1,ep}, F_{t,Rd,wc,1})$ 184.79 kN **(3.21)**	$F_{t,2,Rd} := \min(F_{t,Rd,si,flens}, F_{t,Rd,2,ep}, F_{t,Rd,wc,1})$ 267.04 kN **(3.22)**	$F_{t,12,Rd} := \min(F_{t,Rd,gr,flens}, F_{t,Rd,1,ep} + F_{t,Rd,2,ep}, F_{t,Rd,wc,12}, F_{t,Rd,wb}, F_{w,fb,Rd})$ 451.82 kN **(3.23)**	$F_{c,Rd} := \min(F_{c,Rd,wc}, F_{c,Rd,wp}, F_{c,fb,Rd})$ 571.91 kN **(3.24)**	$F_{T,Rd} := \min(F_{t,Rd,flens}, F_{t,Rd,ep}, F_{t,Rd,wc}, F_{t,Rd,wb}, F_{t,Rd,wp}, F_{w,fb,Rd})$ 451.82 kN **(3.25)**

Note: The "capacity" of column web in shear is increased, since the force in flange is not equal to the shear force in the web.

$F_{t,Rd} := F_{t,Rd}\,\mathrm{N}$

$F_{t,Rd} := 254160.0000\ \mathrm{N}$ **(3.26)**

if $\left(\frac{F_{t,1,Rd}}{F_{t,Rd}}\right) > (1.9)$ **then** $F_{t,2,Rd,tot} := \min\left(F_{T,Rd} - F_{t,1,Rd}, F_{t,2,Rd}, \frac{h_2}{h_1} \cdot F_{t,1,Rd}\right)$ **else** $F_{t,2,Rd,tot} := \min(F_{T,Rd} - F_{t,1,Rd}, F_{t,2,Rd})$ **end if**

$F_{t,2,Rd,tot} := 267035.3709\ \mathrm{N}$ **(3.27)**

$F_{C,Rd} := F_{c,Rd}$

$F_{C,Rd} := 571906.7223\ \mathrm{N}$ **(3.28)**

$F_{T,Rd} := F_{t,2,Rd,tot} + F_{t,1,Rd}$

$F_{T,Rd} := 451823.7333\ \mathrm{N}$ **(3.29)**

$z := (h_b - t_{fb})\,\mathrm{mm}$

$z := 295.4\ \mathrm{mm}$ **(3.30)**

$$z_c := \left(\frac{h_b}{2} - \frac{t_{fb}}{2} \right) \text{mm}$$

$$z_c := 147.7000000 \text{ mm} \quad \textbf{(3.31)}$$

$$z_t := z - z_c$$

$$z_t := 147.7000000 \text{ mm} \quad \textbf{(3.32)}$$

$$M_{Rd,t0} := F_{T,Rd} \cdot z$$

$$M_{Rd,t0} := 1.334687308 \times 10^8 \text{ N mm} \quad \textbf{(3.33)}$$

$$M_{Rd,c0} := F_{C,Rd} \cdot z$$

$$M_{Rd,c0} := 1.689412458 \times 10^8 \text{ N mm} \quad \textbf{(3.34)}$$

Note: If the tension zone is critical, the moment arm must be changed as plastic distributiong of forces is assumed, and the bolts have a different moment arm than half the height.

$$\textbf{if } \frac{\left(\frac{M_{Rd,t0}}{1 + \frac{z_c}{ecc}} \right)}{\left(\frac{M_{Rd,c0}}{1 - \frac{z_t}{ecc}} \right)} < 1 \textbf{ then } z := \frac{\left(h_1 \cdot F_{t,1,Rd} + h_2 \cdot F_{t,2,Rd,tot} \right)}{F_{T,Rd}} \text{ mm } \textbf{end if}$$

$$z := 287.0264637 \text{ mm} \quad \textbf{(3.35)}$$

$$M_{Rd,t0} := F_{T,Rd} \cdot z$$

$$M_{Rd,t0} := 1.296853684 \times 10^8 \text{ N mm} \quad \textbf{(3.36)}$$

$$z_t := z - z_c$$

$$z_t := 139.3264637 \text{ mm} \quad \textbf{(3.37)}$$

$$M_{Rd} := \min\left(\frac{M_{Rd,t0}}{1 + \frac{z_c}{ecc}}, \frac{M_{Rd,c0}}{1 - \frac{z_t}{ecc}} \right)$$

$$1.188249449 \times 10^8 \text{ N mm} \quad \textbf{(3.38)}$$

Capacity T-stub 0.9fu

$$f_{ycf} := 0.9 \cdot f_{uc}$$

$$f_{ycf} := 448.2 \quad \textbf{(4.1)}$$

$$f_{yp} := 0.9 \cdot f_{up}$$

$$f_{yp} := 510.3 \quad \textbf{(4.2)}$$

f_{up}

567 **(4.3)**

Column flange in bending §6.2.6.4

$Inner := 0$:

	Row considered individually		Row considered as a part of group	
	$l_{eff,cp,si}$:	$l_{eff,nc,si}$:	$l_{eff,cp,gr}$:	$l_{eff,nc,gr}$:
Inner row	$I1 := 2 \cdot \pi \cdot m$ $I1 := 325.7831526$ **(4.4)**	$I2 := 4\,m + 1.25e$ $I2 := 310.525$ **(4.5)**	$I3 := 2 \cdot p$ $I3 := 184$ **(4.6)**	$I4 := p$ $I4 := 92$ **(4.7)**
Outer row	$Y1 := \min(2 \cdot \pi \cdot m, \pi \cdot m + 2 \cdot e_1)$ $Y1 := 325.7831526$ **(4.8)**	$Y2 := \min(4 \cdot m + 1.25 \cdot e, 2 \cdot m + 0.625 \cdot e + e_1)$ $Y2 := 310.525$ **(4.9)**	$Y3 := \min(\pi \cdot m + p, 2 \cdot e_1 + p)$ $Y3 := 254.8915763$ **(4.10)**	$Y4 := \min(2 \cdot m + 0.625 \cdot e + 0.5 \cdot p, e_1 + 0.5 \cdot p)$ $Y4 := 201.2625$ **(4.11)**
$l_{eff,1,si}$	**if** $Inner = 1$ **then** $l_{eff,1,si} := \min(I1, I2)$ **else** $l_{eff,1,si} := \min(Y1, Y2)$ **end if** $l_{eff,1,si} := 310.525$ **(4.12)**		**if** $Inner = 1$ **then** $l_{eff,1,gr} := \min(I3, I4)$ **else** $l_{eff,1,gr} := \min(Y3, Y4)$ **end if** $l_{eff,1,gr} := 201.2625$ **(4.13)**	
$l_{eff,2,si}$	**if** $Inner = 1$ **then** $l_{eff,2,si} := I2$ **else** $l_{eff,2,si} := Y2$ **end if** $l_{eff,2,si} := 310.525$ **(4.14)**		**if** $Inner = 1$ **then** $l_{eff,2,gr} := I4$ **else** $l_{eff,2,gr} := Y4$ **end if** $l_{eff,2,gr} := 201.2625$ **(4.15)**	

Rows considered individually

$$M_{pl,1,Rd} := \frac{0.25 \cdot l_{eff,1,si} \cdot t_{fc}^{\,2} \cdot f_{ycf}}{\gamma_{M0}} \qquad M_{pl,1,Rd} := 8.251822412 \times 10^6 \quad \textbf{(4.16)}$$

$$M_{pl,2,Rd} := \frac{0.25 \cdot l_{eff,2,si} \cdot t_{fc}^{\,2} \cdot f_{ycf}}{\gamma_{M0}} \qquad M_{pl,2,Rd} := 8.251822412 \times 10^6 \quad \textbf{(4.17)}$$

$$F_{t,Rd} := \frac{k_2 \cdot f_{ub} \cdot A_s}{\gamma_{M2}} \qquad F_{t,Rd} := 254160.0000 \quad \textbf{(4.18)}$$

$$L_{bprime} := \frac{8.8 \cdot m^3 \cdot A_s \cdot n_b}{t_{fb}^{\,3} \cdot l_{eff,1,si}} :$$

Fracture mode	With prying forces	Without prying forces
Mode 1	$F_{t,1,Rd} := \frac{4 \cdot M_{pl,1,Rd}}{m}$ $F_{t,1,Rd} := 636591.8928$ **(4.19)**	$F_{t,12,Rd} := \frac{2 \cdot M_{pl,1,Rd}}{m}$:
Mode 2	$F_{t,2,Rd} := \frac{2 \cdot M_{pl,2,Rd} + n \cdot 2 \cdot F_{t,Rd}}{m + n}$ $F_{t,2,Rd} := 423864.8651$ **(4.20)**	
Mode 3	$F_{t,3,Rd} := 2 \cdot F_{t,Rd}$ $F_{t,3,Rd} := 508320.0000$ **(4.21)**	

if $L_b < L_{bprime}$ **then** $F_{t,Rd,si,flens} := \min(F_{t,1,Rd}, F_{t,2,Rd}, F_{t,3,Rd})$ N **else** $F_{t,Rd,si,flens} := \min(F_{t,12,Rd}, F_{t,3,Rd})$ N **end if**

$F_{t,Rd,si,flens} := 423864.8651$ N **(4.22)**

Rows considered as part of a group

$$M_{pl,1,Rd} := \frac{0.25 \cdot 2 \cdot l_{eff,1,gr} \cdot t_{fc}^{\,2} \cdot f_{ycf}}{\gamma_{M0}} \qquad M_{pl,1,Rd} := 1.069660999 \times 10^7 \quad \textbf{(4.23)}$$

$$M_{pl,2,Rd} := \frac{0.25 \cdot 2 \cdot l_{eff,2,gr} \cdot t_{fc}^{\,2} \cdot f_{ycf}}{\gamma_{M0}} \qquad M_{pl,2,Rd} := 1.069660999 \times 10^7 \quad \textbf{(4.24)}$$

$$F_{t,Rd} := \frac{k_2 \cdot f_{ub} \cdot A_s}{\gamma_{M2}} \qquad F_{t,Rd} := 254160.0000 \quad \textbf{(4.25)}$$

$$L_{bprime} := \frac{8.8 \cdot m^3 \cdot A_s \cdot n_b}{t_{fc}^{\,3} \cdot 2 \cdot l_{eff,1,si}} :$$

Fracture mode	With prying forces	Without prying forces
Mode 1	$F_{t,1,Rd} := \frac{4 \cdot M_{pl,1,Rd}}{m}$ $F_{t,1,Rd} := 825196.5276$ **(4.26)**	$F_{t,12,Rd} := \frac{2 \cdot M_{pl,1,Rd}}{m}$:
Mode 2	$F_{t,2,Rd} := \frac{2 \cdot M_{pl,2,Rd} + n \cdot 4 \cdot F_{t,Rd}}{m + n}$ $F_{t,2,Rd} := 748177.0062$ **(4.27)**	
Mode 3	$F_{t,3,Rd} := 4 \cdot F_{t,Rd}$ $F_{t,3,Rd} := 1.016640000 \times 10^{6}$ **(4.28)**	

if $L_b < L_{bprime}$ **then** $F_{t,Rd,gr,flens} := \min(F_{t,1,Rd}, F_{t,2,Rd}, F_{t,3,Rd})$ N **else** $F_{t,Rd,gr,flens} := \min(F_{t,12,Rd}, F_{t,3,Rd})$ N **end if**

$F_{t,Rd,gr,flens} := 748177.0062$ N **(4.29)**

Endplate in bending §6.2.6.5

Row outside beam flange (row 1)

$l_{eff,cp,1} := \min(2 \cdot \pi \cdot m_x, \pi \cdot m_x + w, \pi \cdot m_x + 2 \cdot e_{min})$

$l_{eff,cp,1} := 195.0868259$ **(4.30)**

$l_{eff,nc,1} := \min(4 \cdot m_x + 1.25 \cdot e_x, e + 2 \cdot m_x + 0.625 \cdot e_x, 0.5 \cdot b_p, 0.5 \cdot w \cdot 2 \cdot m_x + 0.625 \cdot e_x)$

$l_{eff,nc,1} := 135.0$ **(4.31)**

$l_{eff,1,ep1} := \min(l_{eff,cp,1}, l_{eff,nc,1})$

$l_{eff,1,ep1} := 135.0$ **(4.32)**

$l_{eff,2,ep1} := l_{eff,nc,1}$

$l_{eff,2,ep1} := 135.0$ **(4.33)**

$M_{pl,1,Rd} := \frac{0.25 \cdot f_{yp} \cdot t_p^{2} \cdot l_{eff,1,ep1}}{\gamma_{M0}}$ 1722262.50 **(4.34)**	$M_{pl,2,Rd} := \frac{0.25 \cdot f_{yp} \cdot t_p^{2} \cdot l_{eff,2,ep1}}{\gamma_{M0}}$ 1722262.50 **(4.35)**

Fracture mode	With prying forces	Without prying forces
Mode 1	$F_{t,1,Rd} := \frac{4 \cdot M_{pl,1,Rd}}{m_x}$ $F_{t,1,Rd} := 221876.4738$ **(4.36)**	$F_{t,12,Rd} := \frac{2 \cdot M_{pl,1,Rd}}{m}$ $F_{t,12,Rd} := 66432.49758$ **(4.37)**
Mode 2	$F_{t,2,Rd} := \frac{2 \cdot M_{pl,2,Rd} + n_x \cdot 2 \cdot F_{t,Rd}}{m_x + n_x}$ $F_{t,2,Rd} := 324300.6493$ **(4.38)**	
Mode 3	$F_{t,3,Rd} := 2 \cdot F_{t,Rd}$ $F_{t,3,Rd} := 508320.0000$ **(4.39)**	

if $L_b < L_{bprime}$ **then** $F_{t,Rd,1,ep} := \min(F_{t,1,Rd}, F_{t,2,Rd}, F_{t,3,Rd})$ N **else** $F_{t,Rd,1,ep} := \min(F_{t,12,Rd}, F_{t,3,Rd})$ N **end if**

$F_{t,Rd,1,ep} := 221876.4738$ N **(4.40)**

Row inside beam flange (row 2)

$l_{eff,cp,2} := 2 \cdot \pi \cdot m_{ep}$

$l_{eff,cp,2} := 383.2312306$ **(4.41)**

$l_{eff,nc,2} := alfa \cdot m_{ep}$

$l_{eff,nc,2} := 426.9520202$ **(4.42)**

$l_{eff,1,ep2} := \min(l_{eff,cp,2}, l_{eff,nc,2})$

$l_{eff,1,ep2} := 383.2312306$ **(4.43)**

$l_{eff,2,ep2} := l_{eff,nc,2}$

$l_{eff,2,ep2} := 426.9520202$ **(4.44)**

$M_{pl,1,Rd} := \frac{0.25 \cdot f_{yp} \cdot t_p^2 \cdot l_{eff,1,ep2}}{\gamma_{M0}}$

4889072.42 **(4.45)**

$M_{pl,2,Rd} := \frac{0.25 \cdot f_{yp} \cdot t_p^2 \cdot l_{eff,2,ep2}}{\gamma_{M0}}$

5446840.40 **(4.46)**

$F_{t,Rd} := \frac{k_2 \cdot f_{ub} \cdot A_s}{\gamma_{M2}}$:

Fracture mode	With prying forces	Without prying forces
Mode 1	$F_{t,1,Rd} := \frac{4 \cdot M_{pl,1,Rd}}{m_{ep}}$ $F_{t,1,Rd} := 320630.9407$ **(4.47)**	$F_{T,12,Rd} := \frac{2 \cdot M_{pl,1,Rd}}{m_x}$ 314925.90 **(4.48)**
Mode 2	$F_{t,2,Rd} := \frac{2 \cdot M_{pl,2,Rd} + n_x \cdot 2 \cdot F_{t,Rd}}{m_{ep} + n_x}$ 300982.1011 **(4.49)**	
Mode 3	$F_{t,3,Rd} := 2 \cdot F_{t,Rd}$ $F_{t,3,Rd} := 508320.0000$ **(4.50)**	

if $L_b < L_{bprime}$ **then** $F_{t,Rd,2,ep} := \min(F_{t,1,Rd}, F_{t,2,Rd}, F_{t,3,Rd})$ N **else** $F_{t,Rd,2,ep} := \min(F_{t,12,Rd}, F_{t,3,Rd})$ N **end if**

$F_{t,Rd,2,ep} := 300982.1011$ N **(4.51)**

Total Capacity

	Row 1 in tension	Row 2 in tension	Row 1 and 2 as group	Capacity of component
Column flange in bending	$F_{t,Rd,si,flens}$ 423.86 kN **(4.52)**	$F_{t,Rd,si,flens}$ 423.86 kN **(4.53)**	$F_{t,Rd,gr,flens}$ 748.18 kN **(4.54)**	$F_{t,Rd,flens} := \min(2 \cdot F_{t,Rd,si,flens}, F_{t,Rd,gr,flens})$ 748.18 kN **(4.55)**
Endplate in bending	$F_{t,Rd,1,ep}$ 221.88 kN **(4.56)**	$F_{t,Rd,2,ep}$ 300.98 kN **(4.57)**	$F_{t,Rd,1,ep} + F_{t,Rd,2,ep}$ 522.86 kN **(4.58)**	$F_{t,Rd,ep} := F_{t,Rd,1,ep} + F_{t,Rd,2,ep}$ 522.86 kN **(4.59)**

Stiffness

$A_{vc} := A_c - 2 \cdot b_c \cdot t_{fc} + (t_{wc} + 2 \cdot r_c) \cdot t_{fc}$

$A_{vc} := 3666.66$ **(5.1)**

$z := h_b - t_{fb}$

$z := 295.4$ **(5.2)**

$s_p := t_p + 5.8$

$s_p := 15.8$ **(5.3)**

$b_{eff,c,wc} := t_{fb} + 2^{1.5} \cdot a_f + 5 \cdot (t_{fc} + r_c) + s_p$

$b_{eff,c,wc} := 209.7274170$ **(5.4)**

$d_c := h_c - 2 \cdot (t_{fc} + r_c)$

$d_c := 244.2$ **(5.5)**

$b_{eff,t,wc} := 201.2625$

$$b_{eff,t,wc} := 201.2625 \quad (5.6)$$

$l_{eff,ep1} := 135.0$

$$l_{eff,ep1} := 135.0 \quad (5.7)$$

$l_{eff,ep2} := 383.2312306$

$$l_{eff,ep2} := 383.2312306 \quad (5.8)$$

$$k_1 := \frac{0.38 \cdot A_{vc}}{\beta \cdot z}$$

$$k_1 := 4.716759648 \quad (5.9)$$

$$k_2 := \frac{0.7 \cdot b_{eff,c,wc} \cdot t_{wc}}{d_c}$$

$$k_2 := 5.951723995 \quad (5.10)$$

$$k_3 := \frac{0.7 \cdot b_{eff,t,wc} \cdot t_{wc}}{d_c}$$

$$k_3 := 5.711503379 \quad (5.11)$$

$$k_4 := \frac{0.9 \cdot b_{eff,t,wc} \cdot t_{fc}^3}{m^3}$$

$$k_4 := 4.745929175 \quad (5.12)$$

$$k_{5,1} := \frac{0.9 \cdot l_{eff,ep1} \cdot t_p^3}{m_x^3}$$

$$k_{5,1} := 4.059121329 \quad (5.13)$$

$$k_{5,2} := \frac{0.9 \cdot l_{eff,ep2} \cdot t_p^3}{m_{ep}^3}$$

$$k_{5,2} := 1.520058508 \quad (5.14)$$

$$k_{10} := \frac{1.6 \cdot A_s}{L_b}$$

$$k_{10} := 12.10718114 \quad (5.15)$$

Equivalent stiffness after "Dimensjonering av stålkonstruksjoner" by Per Kr. Larsen

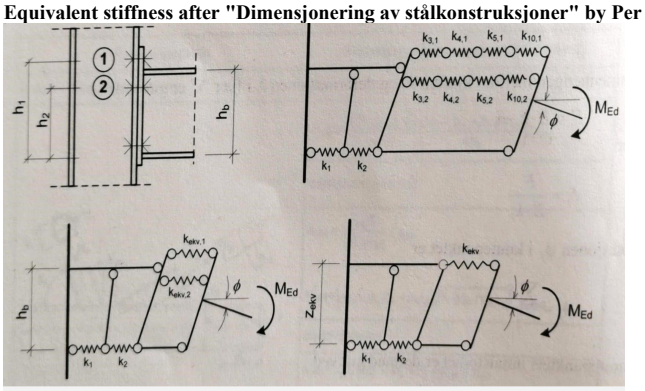

$$k_{ekv,1} := \frac{1}{\frac{1}{k_3} + \frac{1}{k_4} + \frac{1}{k_{5,1}} + \frac{1}{k_{10}}}$$

$$k_{ekv,1} := 1.399097461 \quad (5.16)$$

$$k_{ekv,2} := \frac{1}{\frac{1}{k_3} + \frac{1}{k_4} + \frac{1}{k_{5,2}} + \frac{1}{k_{10}}}$$

$$k_{ekv,2} := 0.8878966790 \quad (5.17)$$

$$z_{ekv} := \frac{\left(h_1^2 \cdot k_{ekv,1} + h_2^2 \cdot k_{ekv,2}\right)}{h_1 \cdot k_{ekv,1} + h_2 \cdot k_{ekv,2}}$$

$$z_{ekv} := 312.2585227 \quad \textbf{(5.18)}$$

$$k_{ekv} := \frac{\left(h_1 \cdot k_{ekv,1} + h_2 \cdot k_{ekv,2}\right)}{z_{ekv}}$$

$$k_{ekv} := 2.238828580 \quad \textbf{(5.19)}$$

$$k_t := \frac{1}{\frac{1}{k_{ekv}} + \frac{1}{2 \cdot k_1}}$$

$$k_t := 1.809407399 \quad \textbf{(5.20)}$$

$$k_c := \frac{1}{\frac{1}{2 \cdot k_1} + \frac{1}{k_2}}$$

$$k_c := 3.649321762 \quad \textbf{(5.21)}$$

$$z_c := \frac{h_f}{2}$$

$$z_c := 147.7000000 \quad \textbf{(5.22)}$$

$$z_t := z_{ekv} - z_c$$

$$z_t := 164.5585227 \quad \textbf{(5.23)}$$

$$e_0 := \frac{\left(z_c \cdot k_c - z_t \cdot k_t\right)}{k_c + k_t} \text{ mm}$$

$$e_0 := 44.19552767 \text{ mm} \quad \textbf{(5.24)}$$

Initial stiffness according to EC3:

$$S_{j,ini} := \frac{E \cdot z_{ekv}^2}{\frac{1}{k_1} + \frac{1}{k_2} + \frac{1}{k_{ekv}}}$$

$$S_{j,ini} := 2.476879439 \times 10^{10} \quad \textbf{(5.25)}$$

Initial stiffness according to Sokol et al., which takes into account the eccentricity:

$$S_{j,ini,e} := \frac{S_{j,ini} \cdot ecc}{ecc + e_0}$$

$$S_{j,ini,e} := 2.410943233 \times 10^{10} \quad \textbf{(5.26)}$$

Rotation Capacity after Beg. et al.

$$f_{yc} := f_{ycw}$$

$$f_{yc} := 382 \quad \textbf{(6.1)}$$

$$N := 0$$

$$N := 0 \quad \textbf{(6.2)}$$

$$N_{pl} := A_c \cdot f_{yc}$$

$$N_{pl} := 4.7368000 \times 10^6 \quad \textbf{(6.3)}$$

$$k := 1$$

$$k := 1 \quad \textbf{(6.4)}$$

$$n_a := \frac{N}{N_{pl}}$$

$$n_a := 0. \quad \textbf{(6.5)}$$

Column web in compression

$$eps := \left(\frac{235}{f_{yc}}\right)^{0.5}$$

$$0.78 \quad \textbf{(6.6)}$$

$$\left(\frac{d_c}{t_{wc} \cdot eps}\right)$$

$$31.44909956 \quad \textbf{(6.7)}$$

$$eps_{u,\,cwc} := \frac{2.1}{100}$$

$$eps_{u,cwc} := 0.02100000000 \quad \textbf{(6.8)}$$

$$\delta_{u,\,cwc} := eps_{u,\,cwc} \cdot d_c$$

$$\delta_{u,cwc} := 5.128200000 \quad \textbf{(6.9)}$$

Column web in tension

$$eps_{u,\,cwt} := 0.1 \cdot \left(\frac{\left(4 - 3 \cdot n_a^{\,2}\right)^{0.5} - n_a}{2} \right)^2$$

$$eps_{u,cwt} := 0.1000000000 \quad \textbf{(6.10)}$$

$$\delta_{u,\,cwt} := eps_{u,\,cwt} \cdot d_c$$

$$\delta_{u,cwt} := 24.42000000 \quad \textbf{(6.11)}$$

Column web in shear

$$\gamma_u := 0.155$$

$$\gamma_u := 0.155 \quad \textbf{(6.12)}$$

End plate in bending

$$\left(0.4 \cdot \min\left(m_{ep}, m_x\right), 0.1 \cdot L_b \cdot \left(1 + \frac{k \cdot m_x}{n}\right), 0.1\, L_b\right)$$

$$12.41961328,\ 6.899811802,\ 4.665 \quad \textbf{(6.13)}$$

$$\textbf{if } Mode_{ep} = 1 \textbf{ then } \delta_{u,\,T,\,ep} := 0.4 \cdot \min\left(m_{ep}, m_x\right) \textbf{ elif } Mode_{ep} = 2 \textbf{ then } \delta_{u,\,T,\,ep} := 0.1 \cdot L_b \cdot \left(1 + \frac{k \cdot m_{ep}}{n}\right) \textbf{ else } \delta_{u,\,T,\,ep} := 0.1\, L_b \textbf{ end if}$$

$$\delta_{u,T,ep} := 12.41961328 \quad \textbf{(6.14)}$$

Column flange in bending

$$\left(0.4 \cdot m, 0.1 \cdot L_b \cdot \left(1 + \frac{k \cdot m}{n}\right), 0.1\, L_b\right)$$

$$20.740,\ 8.397000000,\ 4.665 \quad \textbf{(6.15)}$$

$$\textbf{if } Mode_f = 1 \textbf{ then } \delta_{u,\,T,\,f} := 0.4 \cdot m \textbf{ elif } Mode_f = 2 \textbf{ then } \delta_{u,T,f} := 0.1 \cdot L_b \cdot \left(1 + \frac{k \cdot m}{n}\right) \textbf{ else } \delta_{u,T,f} := 0.1\, L_b \textbf{ end if}$$

$$\delta_{u,T,f} := 20.740 \quad \textbf{(6.16)}$$

Note: the 'k' in the expression for deformation capacity of og mode is ∈[1,5], and k=1 is assumed as this is conservative.

Combined

Note: Stiffnesses of end plate and column flange must be reevaluated in such a way that their equivalent spring is located in the beam flange.

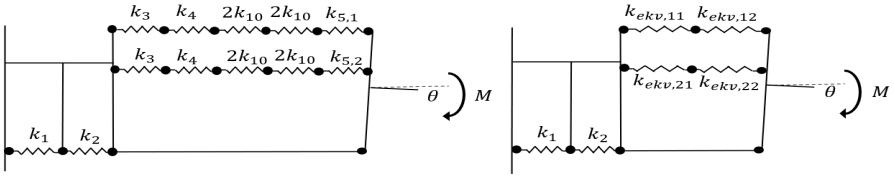

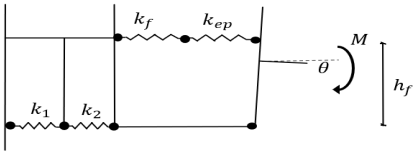

$$k_{ekv,\,11} := \frac{1}{\frac{1}{k_3} + \frac{1}{k_4} + \frac{1}{2 \cdot k_{10}}}$$

$$k_{ekv,11} := 2.341427140 \quad \textbf{(6.17)}$$

$$k_{ekv,\,12} := \frac{1}{\frac{1}{k_{5,\,1}} + \frac{1}{2 \cdot k_{10}}}$$

$$k_{ekv,12} := 3.476368026 \quad \textbf{(6.18)}$$

$$k_{ekv,\,21} := k_{ekv,\,11}$$

$$k_{ekv,21} := 2.341427140 \quad \textbf{(6.19)}$$

$$k_{ekv,22} := \frac{1}{\frac{1}{k_{5,2}} + \frac{1}{2 \cdot k_{10}}}$$

$k_{ekv,22} := 1.430273007$ **(6.20)**

$$z_{ekv,1} := \frac{\left(h_1^2 \cdot k_{ekv,11} + h_2^2 \cdot k_{ekv,21}\right)}{h_1 \cdot k_{ekv,11} + h_2 \cdot k_{ekv,21}}$$

$z_{ekv,1} := 302.5631686$ **(6.21)**

$$z_{ekv,2} := \frac{\left(h_1^2 \cdot k_{ekv,12} + h_2^2 \cdot k_{ekv,22}\right)}{h_1 \cdot k_{ekv,12} + h_2 \cdot k_{ekv,22}}$$

$z_{ekv,2} := 320.1389489$ **(6.22)**

$$k_{ekv,1} := \frac{\left(h_1 \cdot k_{ekv,11} + h_2 \cdot k_{ekv,21}\right)}{z_{ekv,1}}$$

$k_{ekv,1} := 4.571987927$ **(6.23)**

$$k_{ekv,2} := \frac{\left(h_1 \cdot k_{ekv,12} + h_2 \cdot k_{ekv,22}\right)}{z_{ekv,2}}$$

$k_{ekv,2} := 4.821475604$ **(6.24)**

$z_{ekv} := z$

$z_{ekv} := 295.4$ **(6.25)**

$$k_{ekv,1,z} := \frac{k_{ekv,1} \cdot z_{ekv,1}^2}{z_{ekv}^2}$$

$k_{ekv,1,z} := 4.796409034$ **(6.26)**

$$k_{ekv,2,z} := \frac{k_{ekv,2} \cdot z_{ekv,2}^2}{z_{ekv}^2}$$

$k_{ekv,2,z} := 5.662862558$ **(6.27)**

$$k_{ekv} := \frac{1}{\frac{1}{k_{ekv,1,z}} + \frac{1}{k_{ekv,2,z}}}$$

$k_{ekv} := 2.596873491$ **(6.28)**

$$S_{j,ini,alternative} := \frac{E \cdot z_{ekv}^2}{\frac{1}{k_1} + \frac{1}{k_2} + \frac{1}{k_{ekv}}}$$

$S_{j,ini,alternative} := 2.395069578 \times 10^{10}$ **(6.29)**

As seen, the stiffness of the joint is almost unchanged, but this allows for retrieving the stiffness of end plate T-stub and column flange T-stub

$k_f := k_{ekv,1,z}$

$k_f := 4.796409034$ **(6.30)**

$k_{ep} := k_{ekv,2,z}$

$k_{ep} := 5.662862558$ **(6.31)**

Summary

M_{Rd} $1.188249449 \times 10^{8}$ N mm **(7.1)**		$S_{j,ini,e}$ $2.410943233 \times 10^{10}$ **(7.2)**	
	Capacity	**Stiffness coefficient incl E-modul**	**Fracture deformation**
Column web in compression	$F_{c,Rd,wc}$ 571906.7223 N **(7.3)**	$k_2 \cdot E$ $1.249862039 \times 10^{6}$ **(7.4)**	$\delta_{u,cwc}$ 5.128200000 **(7.5)**
Column web in tension	$F_{t,Rd,wc}$ 956.00 kN **(7.6)**	$k_3 \cdot E$ $1.199415710 \times 10^{6}$ **(7.7)**	$\delta_{u,cwt}$ 24.42000000 **(7.8)**
Column web in shear	$F_{c,Rd,wp}$ 965.47 kN **(7.9)**	$k_1 \cdot E$ 990519.5261 **(7.10)**	$\gamma_u \cdot z_{ekv}$ 45.7870 **(7.11)**
End plate in bending	$F_{t,Rd,ep}$ 522858.5749 N **(7.12)**	$k_{ep} \cdot E$ $1.189201137 \times 10^{6}$ **(7.13)**	$\delta_{u,T,ep}$ 12.41961328 **(7.14)**
Column flange in bending	$F_{t,Rd,flens}$ 748177.0062 N **(7.15)**	$k_f \cdot E$ $1.007245897 \times 10^{6}$ **(7.16)**	$\delta_{u,T,f}$ 20.740 **(7.17)**

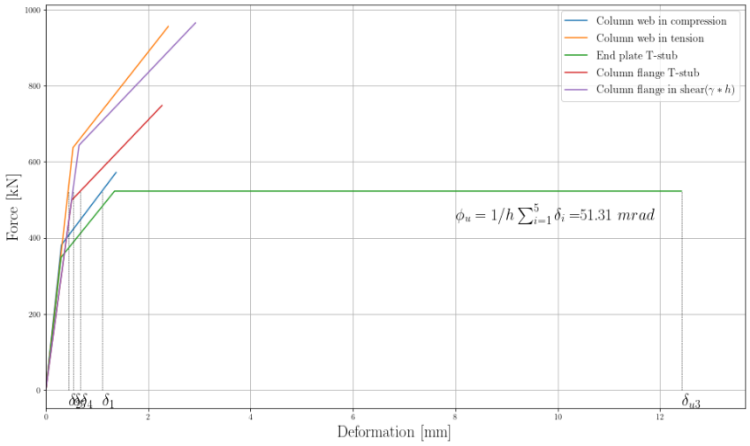

E Manual calculations for column minor axis joint

Resistance and stiffness calculations according to Gomes et al. and Neves et al.

Input

$h := 430$:	$b_0 := 120$:	$c_0 := 90$	$t_p := 20$:
$d_m := 36$:	pi := 3.1415 :	$h_c := 290$:	$b_c := 300$:
$r_c := 27$:	$t_{fc} := 14$:	$t_{wc} := 8.5$:	$f_{yp} := 388$:
$f_{yc} := 388$:	$h_b := 330$:	$E := 210000$:	$t_{fb} := 11.5$:
	$h_1 := h - 20 - \frac{t_{fb}}{2} - 40$ $h_1 := 364.2500000$ **(1.1)**	$h_2 := h - 20 - \frac{t_{fb}}{2} - 130$ $h_2 := 274.2500000$ **(1.2)**	

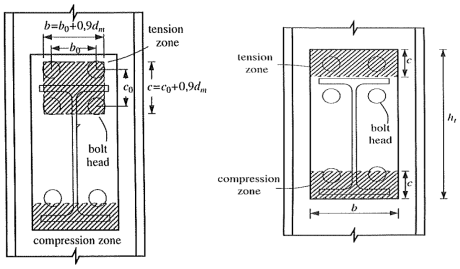

Moment resistance

$b := b_0 + 0.9 \cdot d_m$

$b := 152.4$ **(1)**

$c := c_0 + 0.9\, d_m$

$c := 122.4$ **(2)**

$L := h_c - 2 \cdot t_{fc} - 1.5\, r_c$

$L := 221.5$ **(3)**

$\frac{(b+c)}{L}$

1.240632054 **(4)**

if $\frac{(b+c)}{L} > 0.5$ **then** $k := 1$ **else** $k := 0.7 + \frac{0.6(b+c)}{L}$ **end if**

$k := 1$ **(5)**

$m_{pl} := \frac{1}{4} \cdot t_{wc}^{\,2} \cdot f_{yc}$

$m_{pl} := 7008.250000$ **(6)**

Flexural mechanism

$F_{pl} := \frac{4 \cdot \text{pi} \cdot m_{pl}}{1 - \frac{b}{L}} \cdot \left(\left(1 - \frac{b}{L} \right)^{0.5} + \frac{2 \cdot c}{\text{pi} \cdot L} \right) k$

$F_{pl} := 256984.2439$ **(7)**

Punching shear mechanism

$v_{pl} := \frac{t_{wc} f_{yc}}{30.5}$

$v_{pl} := 1904.101187$ **(8)**

$F_{punch} := 4 \cdot \text{pi} \cdot d_m \cdot v_{pl}$

$F_{punch} := 861369.6784$ **(9)**

Combined mechanism

$$b_m := L\cdot\left(1-\frac{0.82\cdot t_{wc}^{\,2}}{c^2}\cdot\left(1+\left(1+\frac{2.8\cdot c^2}{t_{wc}\cdot L}\right)^{0.5}\right)^2\right)$$

$$b_m := 191.7795675 \quad (10)$$

$$x_0 := \frac{L\cdot\left(\left(\frac{t_p}{L}\right)^{\frac{2}{3}}+\frac{0.23\cdot c}{L}\cdot\left(\frac{t_{wc}}{L}\right)^{\frac{1}{3}}\right)\cdot\left(b-b_m\right)}{L-b_m}$$

$$x_0 := -71.65082850 \quad (11)$$

$$b-b_m$$

$$-39.3795675 \quad (12)$$

$$x := 0$$

$$x := 0 \quad (13)$$

$$a := L-b$$

$$a := 69.1 \quad (14)$$

$$F_{Q2} := 4\cdot m_{pl}\cdot\left(\left(\frac{\mathrm{pi}\cdot(L\cdot(a+x))^{0.5}+2\cdot c}{a+x}\right)+\left(\frac{(1.5\cdot c\cdot x+x^2)}{3^{0.5}\cdot t_{wc}\cdot(a+x)}\right)\right)\cdot k$$

$$F_{Q2} := 256984.2438 \quad (15)$$

Global failure

Assume compression and tensile zone have same dimensions:

$$c_c := c$$

$$c_c := 122.4 \quad (16)$$

$$h_r := \left(h-\frac{c_c}{2}-\frac{t_{fb}}{2}\right)$$

$$h_r := 363.0500000 \quad (17)$$

$$\mathrm{rho} := \frac{h_r}{L-b}$$

$$\rho := 5.253979740 \quad (18)$$

$$F_{glob} := \frac{F_{Q2}}{2}+m_{pl}\cdot\left(\frac{2\cdot b}{h_r}+\mathrm{pi}+2\cdot\mathrm{rho}\right)$$

$$F_{glob} := 230034.7491 \quad (19)$$

$$F_{Rd} := \min\left(F_{glob}, F_{punch}, F_{Q2}, F_{pl}\right)\mathrm{N}$$

$$F_{Rd} := 230034.7491\ \mathrm{N} \quad (20)$$

$$M_{Rd} := h_r\cdot F_{Rd}\,\mathrm{mm}$$

$$M_{Rd} := 8.351411566\times 10^7\ \mathrm{N\ mm} \quad (21)$$

Stiffness

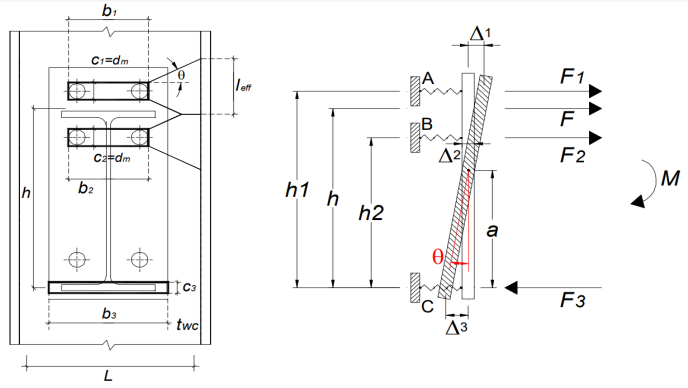

$L := h_c - 2 \cdot t_{fc} - r_c$

$L := 235$ **(22)**

$c_1 := d_m$

$c_1 := 36$ **(23)**

$b_1 := 120 + d_m$

$b_1 := 156$ **(24)**

$\alpha_1 := \frac{c_1}{L}$

0.15 **(25)**

$\beta_1 := \frac{b_1}{L}$

0.66 **(26)**

$\mu := \frac{L}{t_{wc}}$

$\mu := 27.64705882$ **(27)**

$k_1 := 1.5$

$k_1 := 1.5$ **(28)**

$k_2 := 1.6$

$k_2 := 1.6$ **(29)**

if $\beta_1 < 0.7$ **then** $\theta_1 := 35 - 10 \cdot \beta_1$ **else** $\theta_1 := 49 - 30 \cdot \beta_1$ **end if**

28.36 **(30)**

$\frac{\mu}{\beta_1}$

41.64781297 **(31)**

if $\frac{\mu}{\beta_1} < 70$ **then** $k_{red1} := \frac{\left(\frac{\mu}{\beta_1}\right)^{1.25}}{230}$ **else** $k_{red1} := 1$ **end if**

$k_{red1} := 0.4600048543$ **(32)**

$$S_1 := \frac{E \cdot t_{wc}^{\,3}}{L^2} \cdot \frac{16 \cdot (1 - \beta_1) \cdot \tan\left(\frac{\theta_1 \cdot \mathrm{pi}}{180}\right)}{(1 - \beta_1)^3 + \frac{10.4 \cdot (k_1 - k_2 \cdot \beta_1)}{\mu^2}} k_{red1}$$

$S_1 := 70971.40603$ **(33)**

$c_3 := t_{fb} + 2 \cdot t_p$

$c_3 := 51.5$ **(34)**

$b_3 := 190$

$b_3 := 190$ **(35)**

$\alpha_3 := \frac{c_3}{L}$

$\alpha_3 := 0.2191489362$ **(36)**

$$\beta_3 := \frac{b_3}{L}$$

$$0.81 \quad (37)$$

if $\beta_3 < 0.7$ **then** $\theta_3 := 35 - 10 \cdot \beta_3$ **else** $\theta_3 := 49 - 30 \cdot \beta_3$ **end if**

$$\theta_3 := \frac{1163}{47} \quad (38)$$

if $\frac{\mu}{\beta_3} < 70$ **then** $k_{red3} := \frac{\left(\frac{\mu}{\beta_3}\right)^{1.25}}{230}$ **else** $k_{red3} := 1$ **end if**

$$k_{red3} := 0.3595225714 \quad (39)$$

$$S_3 := \frac{E \cdot t_{wc}^{\ 3}}{L^2} \cdot \frac{16 \cdot (1 - \beta_3) \cdot \tan\left(\frac{\theta_3 \mathrm{pi}}{180}\right)}{(1 - \beta_3)^3 + 10.4 \cdot \frac{(k_1 - k_2 \cdot \beta_3)}{\mu^2}} k_{red3}$$

$$S_3 := 120608.9655 \quad (40)$$

$$S_j := S_1 \cdot h_1 \cdot \left(h_1 - \frac{(h_1 + h_2)}{\frac{S_3}{S_1} + 2} \right) + S_1 \cdot h_2 \cdot \left(h_2 - \frac{(h_1 + h_2)}{\frac{S_3}{S_1} + 2} \right) :$$

$(F_{glob}, F_{punch}, F_{Q2}, F_{pl})$

230034.7491, 861369.6784, 256984.2438, 256984.2439 **(41)**

M_{Rd}

8.351411566×10^7 N mm **(42)**

S_j

6.933120633×10^9 **(43)**

(Unit: Nmm/rad)

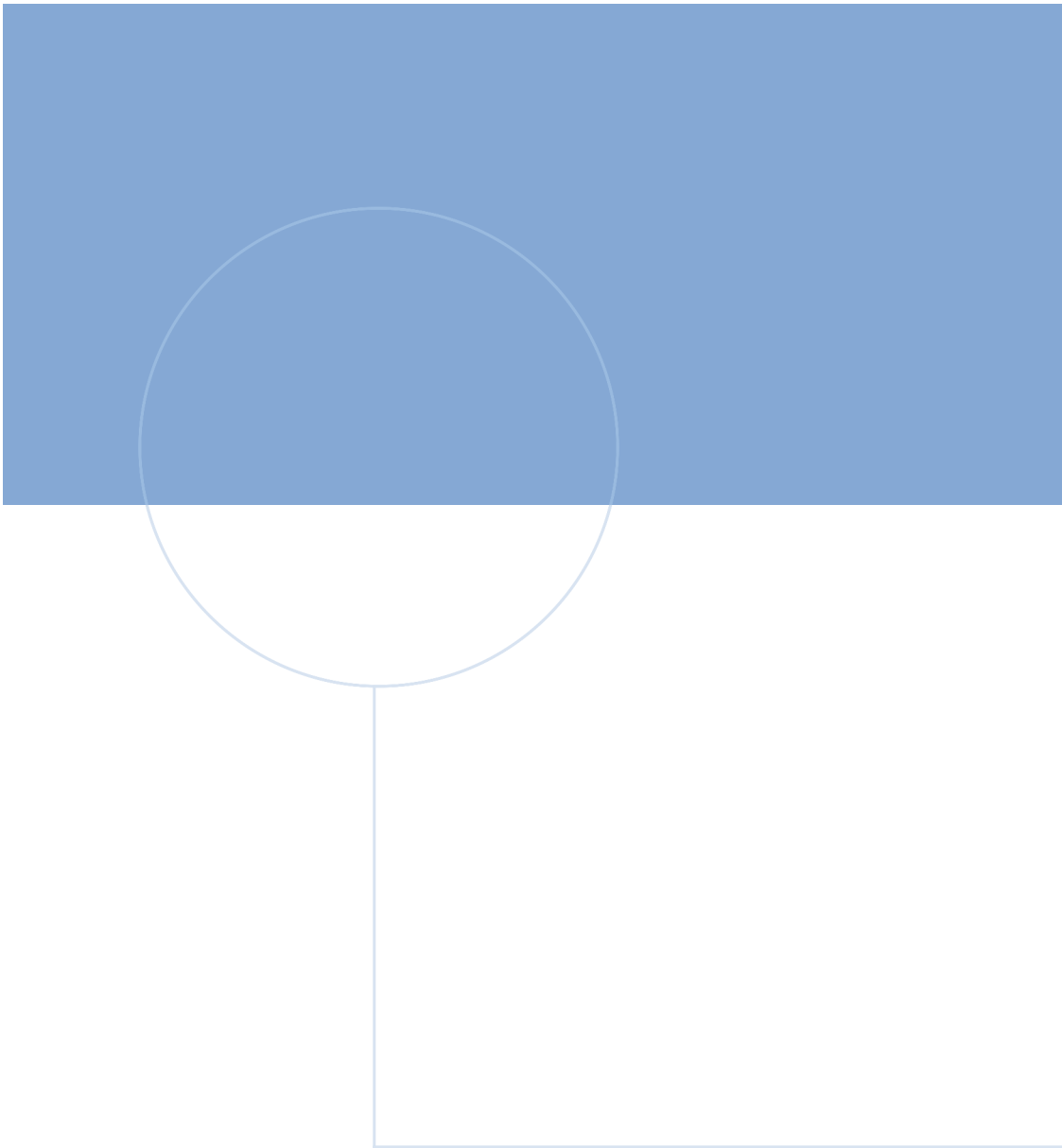

NTNU

Kunnskap for en bedre verden